PERFORMANCE OF STEEL PIPE PILE-TO-CONCRETE BENT CAP CONNECTIONS SUBJECT TO SEISMIC OR HIGH TRANSVERSE LOADING PHASE I: PRELIMINARY INVESTIGATION FHWA/MT-98-005/8117-7

Prepared by:
Ladean McKittrick, Jason Hicks,
Jerry Stephens, Dan VanLuchene, and Don Rabern

Department of Civil Engineering
Montana State University
Bozeman, Montana

Prepared for:

State of Montana
Department of Transportation
Research, Development, and Technology Transfer Program
in cooperation with the
U.S. Department of Transportation
Federal Highway Administration

June 1998

Technical Report Documentation Page

1. Report No. FHWA/MT-98-005/8117-7	2. Government Accession No.	3. Recipient's Catalog No.
4. Title and Subtitle Performance of Steel Pipe Pile-to-Concrete Bent Cap Connections Subject to Seismic or High Transverse Loading Phase I: Preliminary Investigation		5. Report Date June 1998 6. Performing Organization Code MSU G+C #290490
7. Author(s) McKittrick, L., Hicks, J., Stephens, J., VanLuchene, R., and Rabern, D.		8. Performing Organization Report No.
9. Performing Organization Name and Address Department of Civil Engineering, Montana State University Bozeman, Montana 59717		10. Work Unit No. (TRAIS) 11. Contract or Grant No. 8117
12. Sponsoring Agency Name and Address Montana Department of Transportation 2701 Prospect Avenue Helena, Montana 59620-1001		13. Type of Report and Period Covered Final, June 1997 - June 1998 14. Sponsoring Agency Code 5401

15. Supplementary Notes
Research performed in cooperation with the U.S. D.O.T., Federal Highway Administration

16. Abstract

A preliminary investigation was conducted on the behavior of steel pipe pile-to-concrete pile cap connections for bridge structures subjected to extreme seismic and ice forces. This investigation consisted of reviewing available information on the analysis, design, and performance of steel pipe pile-to-concrete pile cap connections, setting up a finite element model for analyzing the behavior of these connections, and investigating a method for experimentally testing these connections. Only limited information on the behavior of steel pipe pile-to-concrete pile cap was found during the literature search. Therefore, a finite element model was developed to study connection behavior. The model, developed in ANSYS, consisted of a typical bridge bent (comprised of steel pipe piles topped with a concrete pile cap) and superstructure. The concrete and steel were represented with 3-D brick and link elements. All materials were modeled as linear and elastic. Inelastic material behavior was studied in some detail, and issues that need to be addressed in future analyses in modeling such behaviors were identified.

The finite element model was used to study the behavior of the pipe pile-to-concrete pile cap connection in different situations. The model was loaded with a horizontally directed inertial body force of 1g to study the behavior of the connection under lateral seismic loads. Ice loads were applied as pressures acting directly on the pile cap (high water case) and on the lead pile in a bent. These pressures varied from zero to 200 psi. In general, large stresses and strains were predicted in the pile-to-pile cap connection under seismic loads. The predicted strains exceeded the elastic limit of the materials, suggesting that large deformations and significant damage may occur in the pile and cap under seismic loads. The stresses and strains predicted in the ice load analyses were significantly lower than those predicted in the seismic analyses, and only minor damage would be expected in the pile and cap under ice loads. Parametric calculations were performed to estimate the effect of deck support conditions, pile height, pile embedment, and pile reinforcement on connection response.

Performance of the finite element model was validated by comparing its results with the results of simple hand calculations and with the results of a test on a physical model of a pile and pile cap. The hand calculations were performed using a simple 2-D frame model of a typical bent. The physical test was performed on a 1/2 size model of an interior section of a typical bent.

Further calculations need to be done that realistically consider the inelastic response of the pile and cap materials under seismic loads. The objectives of such calculations would be (a) to precisely determine the vulnerability (strength and ductility) of these connections under seismic loads, (b) to develop retrofit strategies for existing connections, and (c) to develop design approaches for new connections, as necessary. A draft proposal for this work (Phase II of this project) was prepared and submitted as part of the final report for this effort.

17. Key Words bridge bents, steel piles, pile caps, seismic bridge response, Montana		18. Distribution Statement Unrestricted. This document is available through the National Technical Information Service, Springfield, VA 21161.	
19. Security Classif. (of this report) Unclassified	20. Security Classif. (of this page) Unclassified	21. No. of Pages 88	22. Price

Form DOT F 1700.7 (8-72) Reproduction of completed page authorized

Disclaimer

The opinions, findings, and conclusions expressed in this publication are those of the authors and not necessarily those of the Montana Department of Transportation or the Federal Highway Administration.

Alternate Format Statement

MDT attempts to provide reasonable accomodations for any known disability that may interfere with a person participating in any service, program, or activitiy of the department. Alternative accessible formats of this document will be provided upon request. For further information, call (406) 444-7693 or TTY (406) 444-7696.

Contents

Executive Summary **x**

Unit Conversions **xiii**

1 Introduction **1**
1.1 Objective and Scope 1

2 Literature Review **3**
2.1 UCSD Research 3
2.2 New Zealand Research 5
2.3 FE Studies 8
2.4 Pile-Cap Retrofits 9
2.5 Conclusions 10

3 FE Model **11**
3.1 Model Geometry 11
3.1.1 Deck Geometry 12
3.1.2 Pile-Cap Geometry 12
3.1.3 Pile Geometry 13
3.1.4 Footing Geometry 13
3.2 Boundary Conditions 13
3.3 Material Models 15
3.3.1 Steel Reinforcement 15
3.3.2 Concrete Behavior 17
3.3.3 Confined Concrete Behavior 18
3.3.4 Composite Action 20
3.3.5 Discussion 20
3.4 Dynamic Behavior 21
3.5 Loads 21
3.5.1 Seismic Loads 23
3.5.2 Channel (Ice) Loads 27
3.5.3 Quasi-static Ice Loads 27
3.5.4 Dynamic effects 28

4 Frame Model **30**
4.1 Geometry . . . 31
4.2 Structural Mass . . . 31
4.3 Elastic Rigidity . . . 31
4.4 Static Behavior . . . 32
4.4.1 Pile Model . . . 33
4.4.2 Deck Model . . . 36
4.5 Dynamic Behavior . . . 37
4.5.1 Model Formulation . . . 37
4.6 Harmonic Frequencies . . . 39
4.6.1 Lollipop Constraints . . . 41
4.6.2 Pinned End Constraints . . . 41
4.7 Structural Damping . . . 43
4.8 Loads . . . 44

5 Experimental Effort **46**
5.1 Description of the Model . . . 46
5.2 Test Setup . . . 48
5.3 Instrumentation . . . 48
5.4 Test Chronology . . . 49
5.5 Test Results . . . 50
5.6 FE vs. Experimental Model . . . 53
5.6.1 FE Model Specifications . . . 53
5.6.2 Elastic Response . . . 54
5.6.3 Inelastic Deformation . . . 57

6 Parametric Studies with Seismic Loads **59**
6.1 Horizontal Fixity . . . 59
6.1.1 Transverse Loading . . . 60
6.1.2 Longitudinal Loading . . . 67
6.1.3 Discussion . . . 68
6.2 Unbraced Pile Length Variations . . . 68
6.3 Pipe Embedment . . . 71
6.4 Interior-Reinforcement Patterns . . . 72

7 Responses to Ice Loads **76**
7.1 Ice Load on Cap . . . 76
7.2 Ice Load on Pile . . . 78
7.3 Discussion . . . 78

8 Summary and Conclusions **81**

9 Implementation **83**

References Cited **84**

Appendix A Experimental Model **87**

List of Figures

3.1 Overview of bridge, as modeled 12
3.2 Model Geometry 14
3.3 Stress-strain models for grade 40 and grade 60 reinforcement steel 16
3.4 Typical stress-strain responses for monotonic loading of concrete 17
3.5 Stress-strain responses for confined and unconfined concrete 19
3.6 Increased ultimate compressive strain of steel-jacketed concrete 20
3.7 Harmonic responses for the modeled bent with lollipop constraints 22
3.8 Seismic accelerations coefficients for the United States 24
3.9 Normalized seismic response spectrum 26
3.10 Load variations as a moving ice sheet buckles and/or crushes 28
3.11 Load response spectrum as a moving ice sheet buckles and/or crushes 29

4.1 Frame model for a bent 30
4.2 Free body diagram for an unbraced pile length 33
4.3 Free body diagram for one span of the deck 36
4.4 Seismic model for SDOF system 38
4.5 Comparison of displacements: Frame vs. FE model 43

5.1 Overview of detail regions studied with experimental model 47
5.2 Overview of geometry and strain gage locations 49
5.3 Recorded strain gage responses for Runs 1 and 2 51
5.4 Recorded strain gage responses for Runs 3 and 4 51
5.5 Tip displacement as a function of tip load (Run 4). 52
5.6 Overview of experimental geometry, as modeled 54
5.7 Tip displacements for the FE and experimental models 55
5.8 Strain comparison between the FE and experimental model (Run 2) 56
5.9 Strain comparison between the FE and experimental model (Run 4) 56
5.10 Stress-strain response in the pile jacket of the FE model 57

6.1 Overview of detail regions analyzed 60
6.2 Stress-strain contours for the left-exterior pile/pile-cap connection under a 1g transverse acceleration 61
6.3 Stress-strain contours for the left-interior pile/pile-cap connection under a 1g transverse acceleration with a 1 ft embedment 62

6.4 Stress-strain responses along pipe and re-bar in the center plane for a 1g transverse acceleration with an unbraced pile height (h) of 16 feet 64
6.5 Variations in vibrational parameters due to variations in unbraced pile height 69
6.6 Axial stress-strain variations due to variations in unbraced height 70
6.7 Variations in the maximum pipe stress as unbraced height is varied 71
6.8 Stress-strain contours for a 1g transverse acceleration with a pile embedment depth of 0 inches 73
6.9 Stress-strain contours for a 1g transverse acceleration with a pile embedment depth of -1.5 inches 74

7.1 Stress-strain contours for the left-interior pile/pile-cap connection under a 200 psi ice load on the pile-cap 77
7.2 Stress-strain contours for the left-exterior pile/pile-cap connection under a 200 psi ice load on the left exterior pile 79
7.3 Stress-strain contours for the left-interior pile/pile-cap connection under a 200 psi ice load on the left exterior pile 80

List of Tables

4.1 Rigidity parameters for a pipe pile 32

6.1 Pile reactions with lollipop constraints ($L = 30$ ft, $h = 16$ ft) 63
6.2 Pile reactions with pinned end constraints ($L = 30$ ft) 66
6.3 Pile reactions with pinned end constraints ($L = 60$ ft) 67

Executive Summary

In this study, a preliminary investigation was conducted on the behavior of steel pipe pile-to-concrete pile cap connections for bridge structures subjected to extreme seismic and ice forces. These connections are found in many bridges in Montana, as the steel pile/concrete pile cap system is an economically attractive support system for highway bridges. The study began with a search for existing information on the behavior of steel pile-to-pile cap connections under lateral loads. This search found only limited information concerning the specific systems used by the Montana Department of Transportation. Observations and conclusions drawn from this information include:

1) the steel casing on the pile contributes significantly to the shear and flexural capacity of the pile,

2) anchorage bars inserted through the pile jacket (transverse to the longitudinal axis of the pile) within the pile cap may be responsible for failure of the connection before the design capacity is reached,

3) significant shear reinforcement may be necessary in the connection zone in the pile cap to fully develop the flexural strength of the pile and cap,

4) for precast, prestressed concrete piles, the best connection performance is obtained when the pile is embedded in the cap, and

5) finite element analysis is a promising technique for studying pile-to-pile cap connection behavior.

Insufficient information was found, however, to allow for the confident prediction of the performance of MDT steel pile-to-concrete pile cap connections under extreme lateral loads, and the decision was made to proceed with a preliminary analytical investigation of the connection. For this purpose, a finite element model of a typical bridge bent (consisting of the steel pipe piles topped with a concrete pile cap) and superstructure was developed in ANSYS, a multi-purpose finite element program. The concrete and the steel jacket of the pile were represented using 3-D brick elements; the reinforcing steel, using 3-D link elements. In these preliminary analyses, the concrete and steel were both modeled as linear elastic materials. The inelastic behavior of these materials was reviewed in some detail, and issues that need to be addressed in future analyses in modeling their inelastic, nonlinear behavior under large deformations were identified.

The basic model described above was used to study to the behavior of the pipe pile-to-concrete pile cap connection under different situations. The model was loaded with a horizontally directed inertial body force of 1g to study the behavior of the connection under lateral seismic loads. This equivalent static force was generally representative of the demands from a seismic event with a peak ground acceleration of 0.4g. Ice loads were applied as pressures acting directly on the pile cap (high water case) and on the lead pile in a bent. These pressures varied from zero to 200 psi. In general, large stresses and strains were predicted in the pile-to-pile cap connection under all the seismic calculations performed. The most highly stressed areas were typically in the pile, immediately below the pile cap. The strains predicted in these areas exceeded the elastic limit of the materials, suggesting that large deformations and significant damage may occur under seismic loads (a plastic hinge may form at the top of the pile). The stresses and strains predicted in the ice load analyses were significantly lower in magnitude than those predicted in the seismic analyses. The maximum demands under ice loads were generally lower than the elastic limit of the materials, and thus only minor damage would be expected in the pile and cap under ice loads. Based on the magnitudes of the strains and stresses predicted in the connection under extreme seismic events, the finite element analysis performed herein would have to be done using nonlinear material models for the concrete and the steel to obtain precise results. Such analyses were beyond the scope of this study and are proposed for a follow-on phase (Phase II) of this project.

The linear elastic model developed herein was used under a variety of situations to generally predict where localized areas of high stress would occur, and in a rough sense, the relative magnitude of the associated distress. Calculations were done using different support conditions for the bridge deck (at the abutments), different pile lengths, and different depths of embedment of the steel pipe pile jacket into the body of the pile cap. The demands placed on the pile-to-pile cap connections were found to be influenced by:

1) the nature of the lateral support provided to the bridge deck by the abutments. Two models for this situation were considered. In the first model, the deck was assumed to be free to translate horizontally in the longitudinal and transverse directions at the abutments (lollipop case). In this situation, any horizontal loads applied to the deck were carried by the bridge bent as it deformed relative to the ground. In the second model, the deck was assumed to be pinned in the horizontal plane at the abutments (pinned end constraints). Following this assumption, the deck carried most (if not all) of the inertial forces generated by the deck and the bent through its connections at the abutments. The strains in the lollipop model were consistently at least an order of magnitude higher than the strains in the pinned end constraint case.

2) the unbraced height of the piles. For the lollipop model, the forces transmitted to the connection increased steadily as the pile height increased. The increase in moment at the connection was offset to some extent above a certain height by a change in the fundamental period of vibration of the structure (which resulted in a decrease in the

magnitude of the dynamic response of the bent). These various calculations indicated that a bent with lollipop constraints, an unbraced pile height of 16', acted on by a 1 g transverse spectral acceleration, provides a reasonable measure of an extreme seismic load for Montana bridges (except perhaps for bridges founded on soft soil types).

The behavior of the pile-to-pile cap connection under the loads predicted above was influenced by the depth of embedment of the steel jacket on the pile into the pile cap. Embedment led to a reduction in the peak stress in the concrete at the pile-to-pile cap interface with only a small increase in the stresses imposed on the steel jacket. Little change in behavior was observed for embedment depths greater than 12 inches. The presence of internal steel reinforcement in the pile did not make a difference in the stress-strain response of the pile-to-pile cap connection.

Before the finite element calculations described above were done, the performance of the finite element model was validated by comparing its results with the results of simple hand calculations and with the results of a test on a physical model of a pile and pile cap. The hand calculations were performed using a simple 2-D frame model of a typical bent. The internal moments and shear forces produced in the 2-D frame compared favorably with those generated by the finite element analysis. The dynamic characteristics (harmonic frequencies) of the 2-D frame and finite element models were also in close agreement. The physical test was performed on a 1/2 size model of an interior section of a typical bent. The physical model consisted of a single pile and part of the pile cap. Displacements and strains measured during the test compared favorably with the results of a finite element analysis of the test article. While the laws of similitude were not rigorously applied in developing the test article, it was designed to reasonably represent a typical pile-to-pile cap connection in which the steel jacket is embedded in the pile cap. During lateral load testing of the connection assembly, the first plastic deformation was observed in the pipe pile immediately adjacent to the pile cap. The model was not tested to failure, due to problems with the test apparatus.

While the various analyses described above are useful in grossly estimating the relative response of the steel pipe pile-to-concrete pile cap connection in various circumstances, further calculations need to be done that realistically consider the inelastic response of the pile and cap materials under seismic loads. The objectives of such calculations would be (a) to precisely determine the vulnerability (strength and ductility) of these connections under seismic loads, (b) to develop retrofit strategies for existing connections, and (c) to develop design approaches for new connections, as necessary. A draft proposal for this work (Phase II of this project) was prepared and submitted as part of the final report for this effort.

Unit Conversions

	English	Metric
Length	1 inch	2.540 cm
	1 foot	0.305 m
	1 yard	0.914 m
Area	1 inch^2	6.452 cm^2
	1 foot	0.305 m
Mass	1 lbm	0.454 kg
Force	1 lbf	4.448 N
	1 kip	4.448 kN
Pressure	1 psi	6.895 kPa
(Stress)	1 ksi	6.895 MPa

1

Introduction

Concrete filled steel pipe columns are commonly used in Montana as structural supports for multispan bridges. These pipe columns are generally driven into the ground in a linear array that is oriented transverse to the longitudinal axis of the bridge. The columns are joined with a concrete cap to form a bent or pier. While these bents are attractive from an economic perspective, the structural behavior of the pile/pile-cap connection within the bent is not well understood, and the strength and ductility of the connection under extreme loads (notably, seismic and ice loads) is uncertain.

1.1 Objective and Scope

The objective of this investigation is to study the behavior of steel pipe pile-to-concrete pile cap connections under extreme seismic and channel loads (due to ice forces acting on a bridge). This objective is being accomplished by subjecting analytical models of a typical bent and connection zone to equivalent static seismic and ice loads. The analytical effort is being supplemented by a limited experimental program designed to obtain information that can be used to validate the analytical procedures and to determine the types of inelastic behaviors the system will experience under extreme loads.

This investigation is being conducted in two phases. Phase I consists of performing a preliminary investigation of the connection behavior with the intent of:

1) locating information that is already available on the behavior of steel pipe pile-to-concrete pile cap connections,

2) developing a simple finite element model of the connection and performing some parametric calculations on its response,

3) performing some simple hand calculations with respect to the connections to assist in evaluating and interpreting the results of the finite element analysis, and

4) exploring methods for experimentally investigating the behavior of these connections.

Phase II of the project consists of performing an in-depth investigation of the steel pipe pile-to-concrete pile cap connection based on the results of the first phase of the project. The final results for Phase II of the project will include (1) a definitive assessment of the vulnerability of existing steel pipe pile-to-concrete pile cap installations to extreme seismic and ice related loads, (2) specific retrofit strategies for these installations, as appropriate, and (3) recommended detailing and design procedures for future installations.

Phase I of this project has been completed, and the results are reported herein. The literature search conducted at the beginning of this phase of the project located several experimental and analytical studies in which pile-to-pile cap connection behavior was researched. None of these studies, however, dealt with the specific steel pipe pile-to-concrete pile cap connection details used in Montana. Therefore, work continued with the development of an analysis procedure for this specific connection. A three dimensional solid model of the pile and pile cap was generated with ANSYS (1997), a multi-purpose finite element (FE) program. This basic model was subsequently used to analytically study the behavior of the pile-to-pile cap connection under different loads and for various configurations of the connection used in Montana. Notably, the connection response was analyzed for different horizontal restraint conditions at the end of the deck, unbraced pile lengths, and depths of embedment of the steel jacket into the pile cap.

The FE analyses in Phase I were all conducted using linear elastic material models. The results of these calculations were useful in locating the highly stressed regions of the modeled structures where permanent damage would likely begin, and, in a very rough sense, the extent of any such damage that would be likely to occur. Based on these calculations, the pile and pile cap are expected to experience permanent damage under some of the situations considered in Phase I of this investigation. As a consequence, non-linear damage analyses are recommended for Phase II of this investigation.

The response of the connection was also analyzed with a two dimensional frame model in Phase I of this investigation. This analysis was primarily used to validate the gross rather than the local response of the structure. The gross results obtained from this frame model were also used to interpret the results of the more sophisticated FE analysis.

A half-size model of a typical steel pile-to-pile cap connection was constructed and tested during Phase I of this investigation. This model was used to validate the FE analysis and to obtain an indication of the types of distress that the connection might experience under extreme loads. The model was tested under a quasi-static load, while measurements were recorded—for displacement, strain, and applied load. The results were compared with the response obtained from an FE analysis of the experimental system.

Finally, based on the activities described above, specific recommendations were made for Phase II of this investigation. A draft proposal was prepared for the work to be done in Phase II of the project.

2

Literature Review

A comprehensive literature search was conducted as part of this project to locate any pertinent information on the analysis, design, and general behavior of steel encased concrete pile-to-pile cap connections. The results of this search are presented herein. While valuable information was obtained during the search which will greatly aid in furthering this project, no documentation was located that dealt specifically with the behavior of a steel pipe pile-to-pile cap connection under natural loads.

The information collected was grouped into several categories. Two significant projects have been conducted at the University of California at San Diego (UCSD), and they are described in the section titled **UCSD Research** (§2.1). Similarly, **New Zealand Research** (§2.2) describes two other pile-cap related investigations that took place in New Zealand. **FE Studies** (§2.3) reports on some studies related to the development of FE modeling of pile-cap geometries. Finally, **Pile-Cap Retrofits** (§2.4), describes several options for improving the performance of existing pile-cap structures which have been determined to be inadequate in terms of their lateral load resistance under extreme loads. **Conclusions** (§2.5) concludes the literature review with a discussion of pile-to-pile cap characteristics that are still poorly understood and how they relate to the present investigation.

2.1 UCSD Research

Two major research efforts related to pile/pile-cap behavior were performed at the University of California at San Diego. The first effort focused on predicting the behavior of pile-cap connections when the piles are embedded in soft soils. The overall geometry of the structures being studied was based on as-built units from the Cypress Viaduct Replacement Project in Oakland, California (Silva, Seible & Priestley 1996). A typical unit consists of a square grid of 25 piles embedded fully into the ground and topped with a 24'-0" square concrete cap. This cap provides a footing for columns supporting the superstructure. To simplify the analysis of such a large structure, a single-pile unit was chosen to represent a "worst-case" scenario. In this case, a corner pile was selected because it is situated in a location in which two directions of soil distortion occur under lateral seismic loading. This pile, embedded in a

representative tributary portion of the pile cap, was loaded axially and laterally. Using this configuration, Silva et al. (1996) studied the geometric design and reinforcement layout of the pile cap, the cantilever length of the pile test units, and an appropriate loading scheme to simulate seismic loads on the piles.

Soil-structure interaction was studied in depth as part of this research at UCSD. The effective cantilever length of the pile varies due to different soil properties in which the pile might be embedded. To address this issue, finite element analysis was used to determine an "idealized" cantilever length to be used in designing the experimental models for a variety of soil types. Physical test models were then analyzed using a moment-curvature approach and tested with fully reversed axial and lateral load cycles to mimic a seismic event.

The first model that was successfully tested and compared with analytical representations was a round concrete-filled steel pipe pile that had two hooked reinforcing bars passing transversely through the pile and into the pile cap. No reinforcement (other than the two anchorage bars) was provided inside the pile. The assumption was made in the design that the pile cap concrete around the embedment of the steel shell did not contribute to the total moment capacity of the unit. When the unit was tested, however, the moment capacity was significantly greater than expected. This increase in capacity was attributed to the concrete around the steel shell of the embedded pile. The surrounding concrete also influenced the deformation of the pile, especially during the early stages of loading. At high load levels, however, the cover concrete in the pile cap spalled off, exposing the longitudinal and transverse reinforcing steel. It was further noted that by hooking the anchorage bars through the pipe pile, failure in the connection occurred below design loads due to bearing loads imposed by the reinforcement bars where they contacted the steel shell. In spite of the range of failure mechanisms, a moment curvature analysis method successfully modeled the total deformation of the test unit (Silva et al. 1996), implying that the moment-curvature technique is a useful tool for modeling gross inelastic deformation.

With regard to the present project, the results of the UCSD investigation can be used to, (1) evaluate cantilever lengths for the embedded piles being modeled in the analysis, (2) determine lateral loads to be used in the analysis to simulate seismic events, and (3) identify types of distress that may occur, including cover concrete problems, in the pile anchorage zone.

A second research project performed at UCSD was a Caltrans-funded project to determine the seismic response of column/cap beam tee-connections with cap prestressing (Sritharan, Priestley & Seible 1996). As part of this project, Sritharan et al. (1996) studied shear transfer mechanisms of round prestressed-concrete pile/rectangular concrete pile-cap connections. These connections are geometrically similar to those being considered in this project. Joints of this kind, which were designed prior to the 1970, failed during recent seismic events in California. When these joints were designed, the load transfer mechanisms in these joints were poorly understood, and pile-to-bent cap foundation connections were built without shear reinforcement in the joint region. However, code-mandated shear reinforcement was provided in the beam and column members themselves. It is not surprising that some of these

joints failed during seismic events, as shear forces induced within the joints were typically 4 to 6 times higher than those developed in adjacent beam or column members (Sritharan et al. 1996). When these connections were redesigned to carry these shear forces using contemporary methods, a considerable amount of joint reinforcement was required, resulting in a congestion of steel in the joint region.

To alleviate the congestion of reinforcing steel inside the pile/pile-cap connection, Sritharan et al. (1996) showed that, by varying the levels of prestressing in the bent cap, the amount of shear reinforcement required to meet current seismic design criteria could be reduced. Although the report (Sritharan et al. 1996) does not directly apply to the investigation at hand, important observations that do pertain are as follows:

1) Extreme amounts of shear reinforcement are required in reinforced concrete bent caps. The MDT as-built units lack these extreme amounts of reinforcement. Thus, the shear design approach used by MDT needs to be compared with that described in Sritharan's research project to determine why the reinforcement requirements appear to be different. In buildings, the amount of reinforcement in beam-column joints is determined from the over-strength capacity of the adjacent beams and column. Since the bent cap reinforcing in the current MDT designs may be high compared to building beam applications, the over strength moments that can create high joint shear stresses. The shear situation in MDT designs may by influenced by the embedment of the steel jacketed column in the cap.

2) In the connection, an elastic response (limited deformation) is preferred to a ductile response, since significant damage in the joint regions can lead to catastrophic failure of the entire structure. The joint design approach presented in Sritharan et al. (1996, Ch. 4) limits ductility (permanent deformation) of the joint through a rigorous reinforcement design method. The philosophy adopted by MDT may need review.

3) Post-tensioning of the concrete cap may be a viable retrofit option for as-built units judged to be seismically inadequate (See §2.4).

2.2 New Zealand Research

In New Zealand, two major research efforts were conducted on the behavior of piles and pile cap connections. On one project, Joen & Park (1990) researched prestressed-concrete pile/reinforced-concrete cap connections subjected to simulated seismic loads. On a second project, Park, Priestley & Walpole (1983) researched the behavior of steel jacketed piles, independent of the end connections.

On the subject of pile/pile-cap connections, Joen & Park (1990) state that to prevent catastrophic failure, it is preferable to design connections so that they remain undamaged during severe earthquakes. To accomplish this goal, it is often necessary to design a chosen part of the structure as an energy-dissipating mechanism, such as a plastic hinge in the

pile, to prevent damage in undesirable locations. The specific location of this plastic hinge becomes an additional design consideration. Plastic hinges in the structure above the ground surface are easier to inspect and repair than those below the ground surface. Hinge location is dependent on soil properties, which may be both uncertain and highly variable. For this reason, accurate prediction of the location of plastic hinges can be unpredictable for driven piles and it may be impossible to prevent them from occurring below the ground surface.

Joen & Park (1990) were primarily concerned with the moment-resisting connection between embedded prestressed concrete piles and the reinforced concrete bent caps. They considered three mechanisms for creating this connection: (1) embedding the pile into the cap for a length of four-fifths of the cap depth, (2) breaking back the prestressed concrete in the pile and constructing the connection to the bent cap by embedding the exposed reinforcement in the cap, and (3) providing dowel bars epoxied into the piles and embedded into the pile cap. The behavior of each type of structure was studied experimentally and analytically.

Six experimental models, representing the three connection techniques, were physically tested with interesting results. The models were subjected to combined axial and lateral loads. The main damage in all of the units was concentrated in certain regions of the piles and not in the pile caps. This result was especially interesting in the units where the pile was not embedded into the cap; the embedded reinforcement was much less than that required by the American Concrete Institute (ACI) code for full development (the New Zealand code was used for design and is similar to the ACI code for design requirements). An additional observation for the test units was the seemingly important role of utilizing spiral reinforcing in the pile anchorage zone, both in the "terminated" and in the embedded pile. The unit in which epoxied dowels were used was the most flexible, concentrating its failure point at the end of the pile adjacent to the connection interface.

Similar to the research performed at UCSD, moment-curvature relationships were used to estimate the maximum moment that could be carried at the face of the pile cap for each unit. These estimates were comparable with results obtained from experimental tests.

Of the three connections investigated, Joen & Park (1990) concluded that the best connection was obtained by embedding surface-roughened piles in the pile cap, as this practice provided a solid connection that resulted in damage in the piles adjacent to the connection and minimized the damage in the pile cap. This conclusion is especially relevant to this study. The second, less preferred, connection was that in which the concrete was broken back to expose reinforcing bars, which were then embedded into the cap. This second connection behaved similar to the first, but required more work during the construction phase. The third (dowel bar) connection was not recommended due the flexibility of the epoxied connections that led to concentrated cracking at the pile/pile-cap connection, rather than a distribution of yielding in the pile. Finally, the use of spiral reinforcement in the anchorage zone of the joint was strongly recommended both in the embedded and non-embedded piles. This reinforcement improved the bond of the pile prestressing strands to the concrete and also assisted in the transfer of forces to the surrounding concrete within the pile cap.

In the second project, Park et al. (1983) analytically and experimentally investigated the seismic performance of steel encased reinforced concrete bridge piles. Although this project focused on the piles and not on the pile/pile-cap connection, some interesting information was published regarding steel encased piles. A common design practice in New Zealand is to neglect the presence of the casing when determining a piles moment capacity. This approach provides a conservative estimate when the effects of corrosion on the casing are uncertain or there are doubts concerning the efficiency of the composite action between the fill concrete and steel casing. Another uncertainty in steel-jacketed pile design develops as a result of the difficulty in determining where plastic hinging of the pile below ground due to soil-pile interactions.

The structural response of steel-jacketed piles is characterized by a state of biaxial stress in the casing. Under axial loading and bending of the pile, normal and shear stresses are generated along with hoop stresses which result from confinement of the concrete by the steel casing (Park et al. 1983). The response is further complicated by the potential for local buckling in the steel shell on the compressive side of the pile. According to Park et al. (1983), local buckling of the casing is addressed in the New Zealand Concrete Code by specifying a minimum steel encasement thickness (t), which is determined from an equation relating pile diameter (D), steel yield strength (f_y), and the modulus of elasticity (E_s):

$$t \geq D\sqrt{\frac{f_y}{8E_s}}. \tag{2.1}$$

For standard steel-pipe cases ($E_s = 29,000$ ksi, $f_y = 36$ ksi), this estimate can be expressed as

$$\frac{D}{t} \leq \sqrt{\frac{f_y}{8E_s}} = 80. \tag{2.2}$$

Based on a moment-curvature analysis, it was determined that the model piles exhibited satisfactory seismic performance with predictable strength. Additionally, the ductility of the test units exceeded the New Zealand specifications. However, local buckling of the casing limited the ductile performance in the test units at high strains; therefore, it was concluded that values of pile diameter to thickness ratios should not exceed 72 (Park et al. 1983). For typical MDT piles, $D/t = 32$, indicating that buckling is not likely to be a significant problem with present MDT designs.

Observations also indicated that at high strains, the casing provided about 70% of the flexural strength of the unit and 95% of the shear strength. Additionally, calculated over-strength values of the units were surprisingly high due to the steel jackets. Thus, ignoring the presence of the steel jackets does not accurately predict the behavior of these pile units. Finally, by comparing the estimate for minimum steel encasement thickness (2.1) with experimental results concerning local buckling of the steel shell, the estimate was found to be conservative (Park et al. 1983).

2.3 FE Studies

Few of the articles discovered during the literature search dealt specifically with the FE analysis of pile/pile-cap connections subjected to lateral loading. Many contained information similar to that in the reports described previously (§2.1-2.2). References that did include new information pertinent to this topic are described in the following paragraphs.

The seismic performance of steel-encased concrete piles was studied in a comprehensive Doctoral Thesis submitted by Park (1987). This document is an excellent resource for determining appropriate constitutive relationships for both the confined concrete and steel tube which are in a state of triaxial stress when subjected to monotonically increasing tensile and compressive loads.

Additionally, information published by Sam & Iyer (1995*a*) describes detailed procedures and results for FE modeling of pile cap units subjected to vertical loads. Connection performance was predicted with analytical models and verified through experimental results for various reinforcement patterns. These researchers state that understanding the behavior of pile-cap connections is important due to the frequent inability to make cheap repairs if damage occurs. They believe that "a complete and satisfactory solution can only be achieved through performing a nonlinear analysis of the pile cap throughout the entire load range" (Sam & Iyer 1995*a*). Comprehensive models were assembled using eight node isoparametric brick elements to model the concrete material combined with two-noded truss elements to model the reinforcing steel. The smeared cracking model, representing accurate composite action between the steel and concrete, was utilized to model crack propagation during the analysis. The nonlinear effects of the multiaxial compressive behavior of concrete, cracking of concrete when the modulus of rupture is reached, steel reinforcement yielding at appropriate strain levels, tension stiffening, and the change in Poisson's ratio with excessive post-crack straining were considered in this study. Creep of concrete and bond slip between steel reinforcing and concrete were not considered.

In obtaining the element equations for the finite element system, the stiffness contributions of the concrete and the steel were evaluated separately and then superimposed to derive the global stiffness matrix for the structure. Constitutive relationships employed provisions to

1) weaken the compressive strength of the concrete under increasing compressive strain (termed strain softening),

2) model the post-cracking and crushing behavior of the concrete, and

3) model tensile cracking and compressive crushing conditions.

It has been observed in prior research that the ratio of lateral strain to principal compressive strain remains constant until approximately 80% of the maximum compressive stress is reached, at which point Poisson's ratio of the concrete begins to increase (Sam & Iyer 1995*a*). Utilizing this information in the finite element model and applying a vertical load

on the plan view of a pile cap unit, crack propagation predictions were graphed. The behavior achieved experimentally was matched "fairly accurately" through proper modeling techniques and proper balancing of the above factors (along with many more not listed here). Three important conclusions were drawn from this research:

1) pile caps with similar amounts of reinforcement, one having its reinforcement bunched over the pile connection and the other with uniform distribution throughout the pile, resisted nearly the same vertical load,

2) at lower vertical load levels, beam action in the pile-cap dominates the behavior, while at higher loads strut action occurs within the cap beneath the applied load, and

3) FE modeling can be an appropriate tool to model post yield behavior of reinforced concrete structures.

Sam and Iyer further studied stresses at various locations within the pile cap through its depth and across its breadth using a three-dimensional analysis. An elasticity solution was obtained using a Fourier series analysis of Galerkin's vector (Sam & Iyer 1995*b*). The ability of this approach to describe varying stress conditions throughout the joint region appears promising and should be explored in future work.

2.4 Pile-Cap Retrofits

The information gathered to date concerning the analysis and design of pile-to-pile cap connections indicates that deficiencies may be revealed in existing connections of this type in Montana. Considering the high number of these structures already built around the state, cost-effective and efficient methods of retrofit will be sought.

As previously mentioned in the Caltrans-funded project at UCSD (Sritharan et al. 1996), prestressing of the pile cap provided an efficient solution to improving the shear capacity within the joint regions. Post-tensioning could prove to be a viable means of applying this methodology to existing structures. The lack of shear reinforcement within the joint region may be an area of concern, as previously discussed. Improvement of shear transfer through the joint might be necessary. Post-tensioning operates on the same principle as prestressing, as it is a form of inducing compression within concrete members after concrete hardening has occurred. Drilling holes through existing pile caps might be possible, followed by the installation of high strength, post-tensioning rods. Jacking these cables to a pre-calculated tension force could provide the required shear capacity across the joint, thereby improving the seismic integrity of the pile/pile-cap connection.

Another viable retrofit option to improve seismic behavior of these structures might be the installation of seismic mass isolators. According to Cooper, Friedland & Buckle (1994), these isolators may be especially effective for bridges on short, stiff columns. Beneficial effects of isolation may be realized by two mechanisms. First, separating the mass of the bridge superstructure from the supporting pile bents will reduce the inertial force imposed

in the structural members, and the joint shear forces will drop. Second, elastomeric bearing installation may lengthen the period of free vibration of a structure (Mori, Carr & Moss 1996). As is well accepted in structural dynamics, maximum displacement of a structure occurs when it is excited at its natural frequency. This situation occurs when the frequency of the ground motion during an earthquake coincides (or is close to) the natural frequency of the structure. By altering the natural frequency of a bridge through the use of elastomeric bearings, maximum deflections can be greatly reduced, if the two respective periods of vibration are further separated.

Yet another option for the retrofit of seismically vulnerable structures is that of eliminating expansion joints within the structure and creating a continuous superstructure (Cooper et al. 1994). This approach not only improves seismic performance of the structure, but also reduces maintenance costs throughout its service life. An extension of this option is to positively connect approach slabs to the abutments. This option also helps to provide continuity within the superstructure and to transfer forces into the supporting ground surface. Additionally, overall stiffness of the system is increased, which limits deflections with respect to lateral loading.

2.5 Conclusions

In conducting the literature review for this project, it was discovered that that the pile/pile-cap connection has not yet been studied to any great extent, and therefore, its behavior is still not well understood under extreme loading events. However, useful information was located that will serve as a basis for further research of the pile/pile-cap connections and their behavior.

The sources reviewed gave indications of the complexity of steel encased concrete pile behavior. The effects of variations in pile embedment depth, reinforcement patterns, and cap geometry are still not adequately quantified with respect to seismic performance. Confident evaluations of the seismic performance of existing MDT pile/pile-cap connections will likely require a combination of experimental and analytical techniques.

The predominant tools for modeling pile/pile-cap components are moment curvature and FE methods. The moment curvature method lacks the thoroughness of the FE method in modeling actual stress-strain relationships in the steel and concrete, and post-crack behavior of the structure during a loading event. The work that has been done with FE models has been promising with respect to modeling inelastic responses under large deformation.

3

FE Model

FE models provide an attractive approach to studying the response of the pile/pile-cap connection. One of the primary advantages of FE models, compared with other analysis techniques, is their ability to model the geometric aspects of a structure in three dimensions (3-D) with relatively good accuracy. This geometric accuracy provides a means of modeling stress-strain responses in localized areas of a structure. In addition to the geometric advantage, commercial FE codes such as ANSYS and ABAQUS include a set of material models that provide the means for modeling nonlinear aspects of geometric and material behaviors. With the intent of considering large deformation and material non-linearities at a later date, the present development has been focused on building a model that will model initial deformation of a bridge bent with relatively good accuracy, using linear elastic material models. The same FE model can be used with non-linear material models as the project continues.

For this initial study, the FE model was developed using ANSYS (1997). The entire structure was modeled using 3-D brick elements (ANSYS Solid65 elements), except for the bars of steel reinforcement which were modeled with 3-D link elements (ANSYS Link8 elements). Both element types (3-D brick and 3-D link) model displacement with linear shape functions, while the stiffness matrix (i.e. stress) is modeled with extra quadratic-type shape functions. This section presents the details of how these elements were used to build a model of a pile bent and its associated components, along with aspects of the dynamic behavior of the completed model and loads that were considered in this investigation.

3.1 Model Geometry

Figure 3.1 shows the overall structure of the FE model and its associated components. The following subsections present an outline of the structural details of the model and its components. The primary focus of this endeavor was the pile/pile-cap connection. As a consequence, the connection and its components were modeled in detail, while the superstructure and base area were modeled in a simplified and approximate manner. The discussion begins with a description of the model geometry, continues with an explanation of the model boundary conditions, and concludes with a discussion of material models.

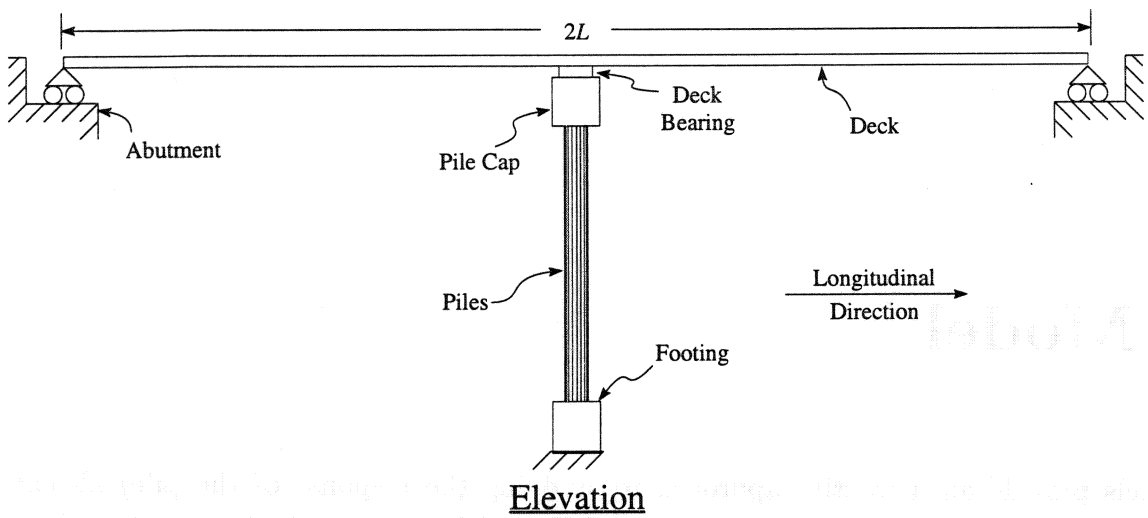

Figure 3.1: Overview of bridge, as modeled

3.1.1 Deck Geometry

To represent those loads and constraints that will be passed to a bent from the superstructure, without including a lot of unnecessary detail, the superstructure was modeled as a solid slab. The slab model consisted of a series of coarse solid elements. The slab had only one element through the thickness with element dimensions in the plane of the slab on the order of 40×40 inches. Unless otherwise specified, the slab was modeled with a total length ($2L$) equal to 720 in (60 ft). The width in all cases was 640 in (~53 ft) and the thickness was 7.5 in. A stringer system was not explicitly considered in the model. For lateral response studies, it was judged that the effect of the stringers could be lumped into the deck slab.

The dynamic and dead loads from the deck were transmitted to the bent through central nodes at the top of "soft" elastic bearings. These bearings were modeled with a steel cap that distributed the load to an underlying soft material. These bearings minimized the transmission of localized moments between the deck and the pile cap, but required the deck to translate, for the most part, in conjunction with the bent.

Each of the four bearings was modeled with a square geometry that was centered directly over each of the four piles. The sides of the bearings were 24 in long. The steel bearing cap was two inches thick, and the soft elastic base was 6 inches thick.

3.1.2 Pile-Cap Geometry

To accurately model the structural behavior of a pile/pile-cap connection, the cap itself was modeled fairly precisely based on specifications for a typical Montana bridge bent (Beaverhead River, Station 2+42.00, Bent No. 2). The modeled pile cap in the model was 528 inches (44 ft) long with cross sectional dimensions of 34 × 34 in. Common pile caps have cross-sectional dimensions of 36×36 in. The reduction in the cross-sectional dimensions was

used to accommodate the inclusion of steel reinforcement in the somewhat coarse grid used to model parts of the pile cap. Due to the relative coarseness of the finite element mesh, it was necessary to add the link elements used for the steel reinforcement to the outer faces of the pile cap. According to standard designs, the steel reinforcement is typically embedded 2" inside the exterior faces of a member. As a result, to provide a rough balance in the cross-sectional inertia, the outer faces were shifted in an inch, which left the reinforcement elements shifted out an inch from their specified positions. Circumferential reinforcement elements were spaced along the length of the pile cap at approximately 11" intervals , as shown in Figure 3.2a. Transverse reinforcement elements and end cap reinforcement elements were positioned as illustrated in Figure 3.2b. Notice that the mesh displayed in Figure 3.2a is not the finite element mesh but is instead only the mesh of modeled steel reinforcement.

3.1.3 Pile Geometry

The layout of the cross section used to model each pile is presented in Figure 3.2c. The corresponding finite element grid is shown in Figure 3.2d. As with the pile cap, each pile was modeled with reasonable accuracy. Consistent with the pile cap model, pile models were based on specifications for a typical Montana bridge bent (Beaverhead River, Station 2+42.00, Bent No. 2); the longitudinal reinforcement pattern was slightly modified, however, in that eight vertical bars were used in the model rather than the ten specified in the drawing. The symmetry of the FE grid of brick elements used to model the interior concrete did not lend itself to placement of ten vertical bars, where eight could be defined quite readily. As a result, the cross-sectional area of vertical steel reinforcement bars was 80% of that in an actual pile (Beaverhead River, Station 2+42.00, Bent No. 2).

In particular, the pile was encased with a 1/2 inch thick steel pipe that had an outer diameter of 16 inches. The internal steel reinforcement cage was constructed from 8-#10 vertical bars, modeled with link elements, spaced circumferentially at radial positions 6 inches from the pile center. The vertical reinforcing bars were joined with #4 re-bar hoops, also modeled with link elements, that were spaced at approximately 12 inch intervals along the vertical axis. These hoops were also placed at radial positions 6 inches from the pile center.

3.1.4 Footing Geometry

To model the loads and relative displacements enforced on the structure due to ground motions, and yet maintain relative simplicity, the footing was modeled with a coarse mesh.

3.2 Boundary Conditions

In this study, boundary conditions or displacement constraints were applied only to the footing and the ends of the deck. In all cases modeled, the bottom of the footing had all degrees of freedom fixed, implying that the footing was rigid at its base. Additionally, in

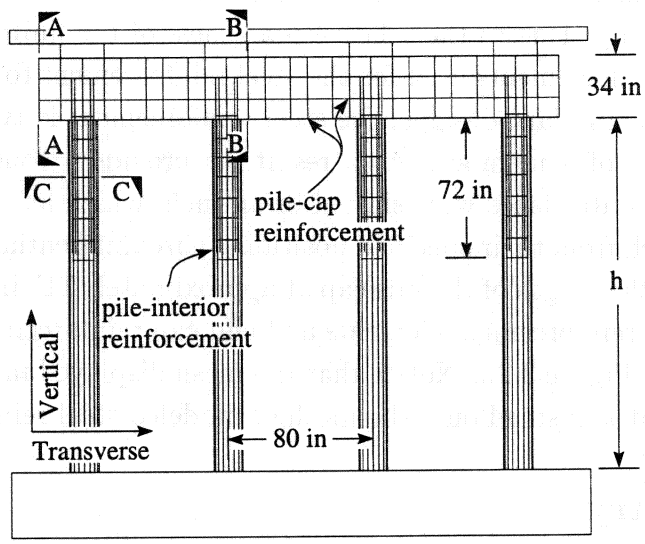

(a) Pile Bent Elevation (Longitudinal View) without FE grid

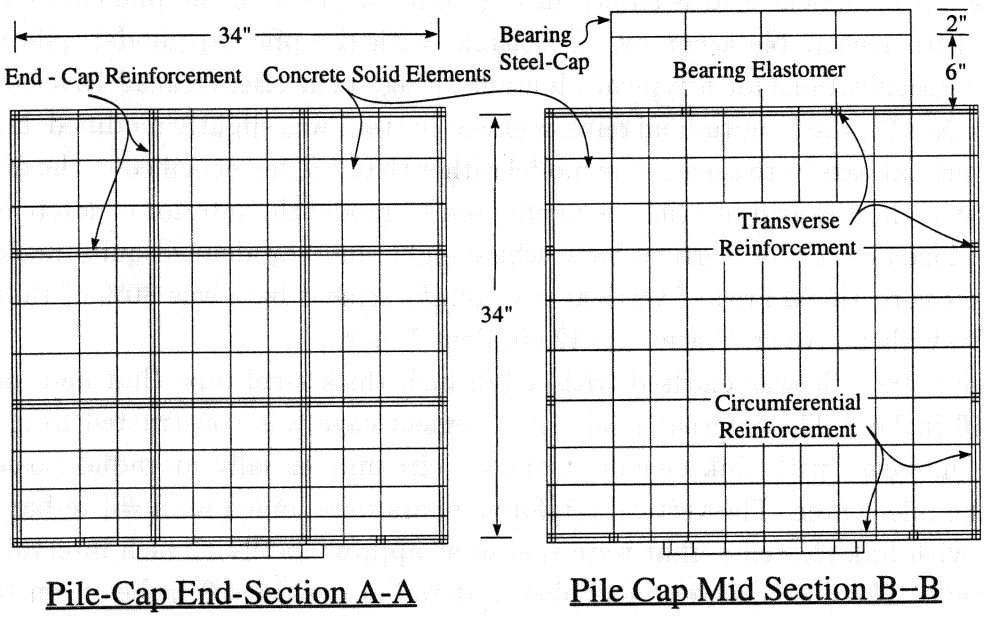

(b) Pile cap cross-sections with finite element grid patterns

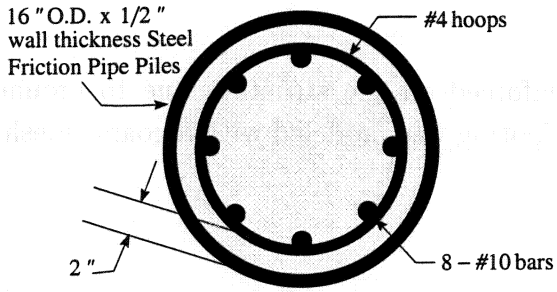

(c) Pile Cross Section

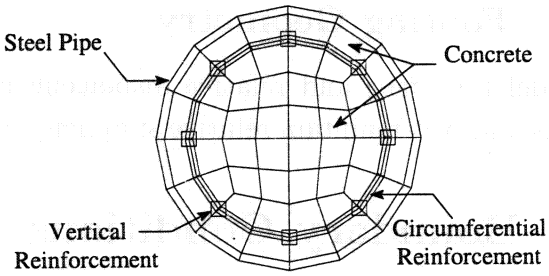

(d) Pile-Grid Section C-C

Figure 3.2: Model Geometry.

all cases modeled, the ends of the deck were constrained so that they could move only in the horizontal plane, as if they were resting on abutments. Both of these constraint sets are illustrated in Figure 3.1.

In some cases, these footing and deck constraints were the only constraints applied to the model. In these instances, all resistance to horizontal motion of the deck was provided by the bent in the center of the bridge. These constraints are referred to as *lollipop (LP) constraints*. In other cases, the deck was, in addition to the lollipop constraints, pinned in the transverse direction to the abutments at the center of each end. In these cases, resistance to transverse-horizontal motion of the deck was provided by the bent and by the pin connections at the ends of the deck. These constraints are referred to as the *pinned end (PE) constraints*. These two constraint sets, LP and PE, were used to provide approximate bounds on the realm of possible loads and associated deformation that might be imposed on the pile/pile-cap connection.

3.3 Material Models

Concrete, without reinforcement, is a complex composite material, and as a result, is rather difficult to model analytically; when steel reinforcement is added, the complexity, and hence the modeling difficulties, increase significantly.

The analyses presented in this study are based on linear elastic material models; therefore, to interpret the results, it is necessary to understand when these material models apply and when they don't. The following subsections present a short synopsis of material behaviors that are likely to influence the structural response of the bent under the loads considered and therefore serve as an aid in the interpretation of the modeled responses. Because the behavior of reinforced concrete is highly dependent on the character of the reinforcement, models for the steel reinforcement will be considered first.

3.3.1 Steel Reinforcement

Steel reinforcement is approximately linearly elastic until a given yield stress (σ_y) is reached, as shown in Figure 3.3. This behavior is followed by a perfectly plastic yield plateau up to a given strain (ε_h), where further deformation leads to a strain hardening response with a slope defined by a strain hardening modulus (E_h) until the ultimate strain (ε_u) is reached (Chen 1982, Fig. 2.24). For the present analysis, the steel components are modeled as isotropic with an elastic modulus (E_s) of 29,000 ksi and a Poisson's ratio (ν_s) of 0.3.

For grade 40 steel, the minimum yield stress is ~40 ksi. Chen (1982, §2.5.1) indicates that hardening typically begins at a hardening strain (ε_h) that is approximately 12 times the yield strain (ε_y) with a strain hardening modulus (E_h) equal to 700 ksi. Ferguson, Breen & Jirsa (1988, Tab. 2.1) indicate that for grade 40 steel, the ultimate stress is approximately 70 ksi.

For grade 60 steel, the minimum yield stress is ~60 ksi. Itani, Gaspersic & Saiidi (1997) indicate that hardening typically begins at a hardening strain (ε_h) that is approximately 5

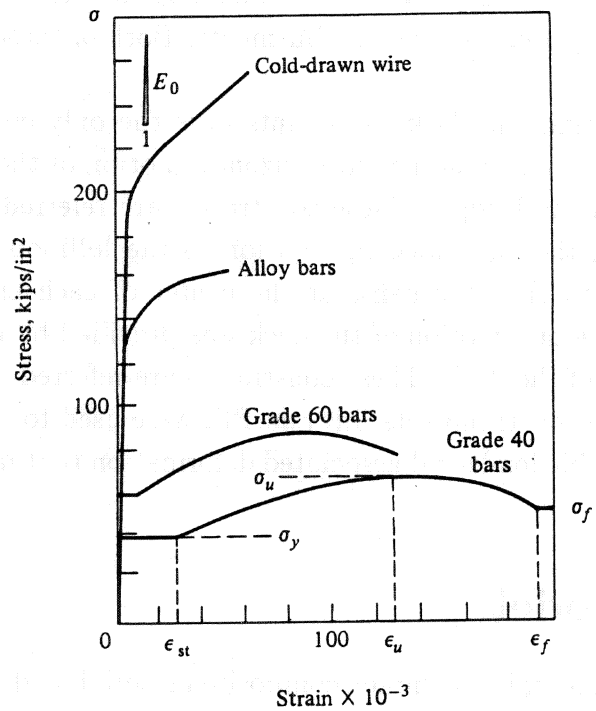

Figure 3.3: Stress-strain models for grade 40 and grade 60 reinforcement steel [After (Chen 1982, Fig. 2.24)].

times the yield strain (ε_y) with a strain hardening modulus (E_h) equal to 700 ksi. Ferguson et al. (1988, Tab. 2.1) indicate that for grade 60 steel, the ultimate stress is ~90 ksi.

For reinforcing bars, the bars are commonly assumed to support very little stress in any direction other than the axial direction of the bar. When such an assumption is reasonable, the uniaxial curves of the type shown in Figure 3.3 serve as reasonable models of the stress-strain behavior[1].

For pipe steel, AISC (1980) indicates that the minimum yield stress is ~36 ksi. For the pipe that encases each pile, the stress-strain conditions of concern are rarely uniaxial in nature. As a consequence, the triaxial stress state must be factored in. For crystalline materials such as steel that deform in a ductile fashion through molecular shear (dislocation motion), it is often reasonable to model inelastic deformation purely in terms of deviatoric stress, or more conveniently in terms of equivalent stress (σ_e) as expressed by

$$\sigma_e = \sqrt{\frac{3}{2}}\left[(\sigma_x - \sigma_y)^2 + (\sigma_y - \sigma_z)^2 + (\sigma_z - \sigma_x)^2 + 6(\tau_{xy}^2 + \tau_{xy}^2 + \tau_{xy}^2)\right]^{1/2} \tag{3.1}$$

[1]The minimum yield stress, for both the grade 40 and grade 60 reinforcing steel, is probably low. Mirza & MacGregor (1979) recorded an average yield stress of ~48.8 kips in^{-2} and ~71 ksi for grade 40 and grade 60 steel, respectively.

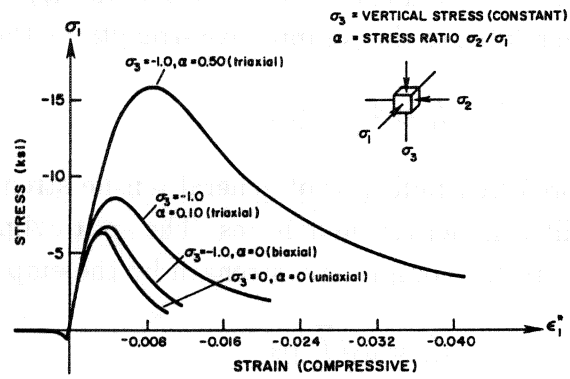

Figure 3.4: Typical stress-strain responses for monotonic loading of concrete, with and without hydrostatic compression. [After (Iding 1986, Fig. 5)].

Notice that for uniaxial stress, this scalar measure of the triaxial state of shear is equal to the uniaxial stress. As a result, the equivalent stress can be compared to the uniaxial stress curve displayed in Figure 3.3 to determine the probability of inelastic yield.

3.3.2 Concrete Behavior

Based on experimental observations, one of the most useful indicators of the structural character of concrete is its ultimate compressive strength under a uniaxial load (f'_c). Many of the parameters associated with the permanent deformation of concrete are strongly correlated with the ultimate compressive strength and are therefore defined in terms of the ultimate compressive strength (f'_c).

When normal concretes are loaded in uniaxial compression without confinement, the stress-strain response is relatively linear up to ~30% of the ultimate compressive strength. In the present model, this behavior was represented by an isotropic material model with an elastic modulus (E_c) of 3600 ksi and a Poisson's ratio (ν_c) of 0.17. Between $0.30f'_c$ and $0.80f'_c$, the stress-strain response shows a gradual decrease in slope, which is typically associated with microcrack development. Beyond $\sim 0.80f'_c$, the response rapidly levels off as the ultimate compressive strength (f'_c) is approached and microcracks presumably begin to coalesce. An example of a uniaxial stress-strain response is presented in Figure 3.4.

Because the behavior of concrete is dependent on the growth and development of microcracks, hydrostatic compressive-stress states can restrain the growth and coalescence of microcracks and as a consequence serve to delay large inelastic contributions to deformation due to non-hydrostatic components. As indicated in Figure 3.4, higher levels of hydrostatic compression result in higher compressive strengths for axially loaded (σ_1) concrete.

On the other hand, when concrete is loaded in tension, pre-existing microcracks are *much* more likely to grow and coalesce than when loaded in compression; therefore, it is not uncommon to assume that concrete has a tensile strength of zero. However, to obtain a more

reasonable value, Chen (1982, Eq. 2.4) indicates that the strength (f'_t) of concrete loaded in direct (uniaxial) tension can be related to the compressive strength by the empirical relation:

$$f'_t \approx 4\sqrt{f'_c} \text{ psi.} \tag{3.2}$$

A secondary and sometimes preferred indicator of general tensile strength is based on the empirical measurements of split-cylinder tensile failures. The split-cylinder tensile strength (f'_{st}) of concrete can be related to the compressive strength by the empirical relation:

$$f'_{st} = a\sqrt{f'_c} \text{ psi,} \tag{3.3}$$

where a can vary between 7.5 and 13 (Park & Paulay 1975, Eq. 2.2). Concrete that has a compressive strength of 4000 psi is, for example, likely to have a tensile strength between 475 and 825 psi. An example stress-strain response for the tensile mode is also shown in Figure 3.4.

3.3.3 Confined Concrete Behavior

When concrete is confined by either reinforcing cages or jackets, the confined concrete will support a much higher compressive stress and behave in a much more ductile fashion than will unconfined concrete. In particular, when confined concrete, such as in a steel jacketed pile, is compressed in a uniaxial fashion, the Poissonic lateral-expansion of the concrete is restricted by the confining reinforcement. This restriction on lateral expansion results in a hydrostatic compressive-stress state that, as discussed in the previous section (§3.3.2), constrains the growth and coalescence of microcracks. As a result, the confined concrete is able to support significantly higher axial loads.

If concrete is confined by a cage of reinforcing bars, then, based on a model developed by (Mander, Priestley & Park 1984), the ratio of confined concrete strength (f'_{cc}) to unconfined concrete strength (f'_{co}) can be approximated by

$$\frac{f'_{cc}}{f'_{co}} = 2.254\sqrt{1 + 7.94\frac{f'_l}{f'_{co}}} - 2.0\frac{f'_l}{f'_{co}} - 1.254, \tag{3.4}$$

where f'_l is a measure of the effective lateral stress exerted on the confined concrete by the reinforcing cage and can be defined by

$$f'_l = \frac{1}{2}\rho_s f_{sy}, \tag{3.5}$$

where ρ_s is the volumetric confining ratio, and f_{sy} is the yield strength of the confining steel. Definitions for the volumetric confining ratio of circular and rectangular reinforcing cages are presented in (Mander, Priestley & Park 1988*a*), along with a discussion of the model and other applications. Comparisons between the model and experimental data are presented in (Mander, Priestley & Park 1988*b*). According to Priestly & Park (1987), typical reinforcing cages can enhance the strength of the confined concrete by as much as a factor of 2.

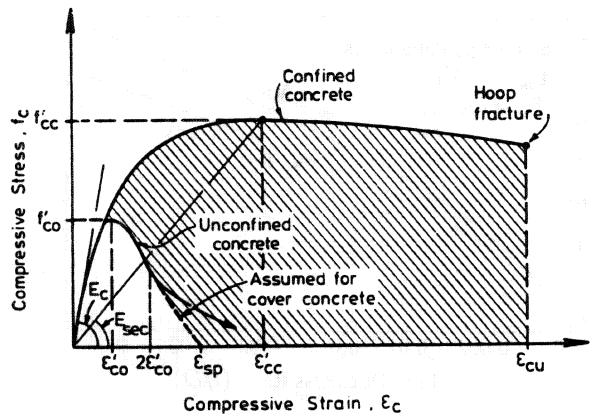

Figure 3.5: Stress-strain responses for confined and unconfined concrete, under monotonic loading [After (Mander et al. 1988*a*, Fig. 1)]. Confinement is provided by steel re-bar cages.

An example of the strength enhancement for concrete confined by a reinforcing cage is displayed in Figure 3.5. Based on this model, concrete that is confined by reinforcing cages maintains its integrity even after reaching its ultimate strength (f'_{cc}) until the hoops in the reinforcing cage begin to fail. These possible strength enhancements should be taken into consideration when reviewing stress-strain data for the pile-cap. Notice, as shown in Figure 3.5, that concrete that is not confined by the reinforcing cage is likely to spall and break free in a manner consistent with the behavior of unconfined concrete. Notice also that the tensile response of concrete is relatively unaffected by confinement.

For concrete encased in steel pipes, the same models can be applied. In this case, the definition for the volumetric confining ratio (ρ_s) reduces to

$$\rho_s = \frac{4}{D/t - 2} \tag{3.6}$$

where t and D are respectively the thickness and diameter of the pipe (Chai 1996, Eq. 2).

As with concrete confined by a reinforcing cage, it is reasonable to assume that the concrete confined by a pipe maintains its integrity until the steel jacket fails. With this assumption, Chai, Priestley & Seible (1994, Eq. 21) show that the ultimate strain for the confined concrete (ε_{cu}) can be defined relative to the failure strain of the steel pipe (ε_{su}) by

$$\varepsilon_{cu} = \varepsilon_{sp} + 1.4\varepsilon_{su}\rho_s\frac{f'_{sy}}{f'_{cc}}, \tag{3.7}$$

where ε_{sp} is the spalling strain for unconfined concrete.

For piles in the FE model, the steel pipe has a diameter to thickness ratio (D/t) equal to 32. Assuming the steel pipe has a yield strength (f_{sy}) of 36 ksi and the interior concrete has an unconfined strength (f'_{co}) between 3 and 4 ksi, then based on the steel-pipe confinement models (3.4-3.6), the concrete confined by the steel pipe has an ultimate compressive strength (f'_{cc}) that is approximately 3 times greater than its unconfined strength (f'_{co}).

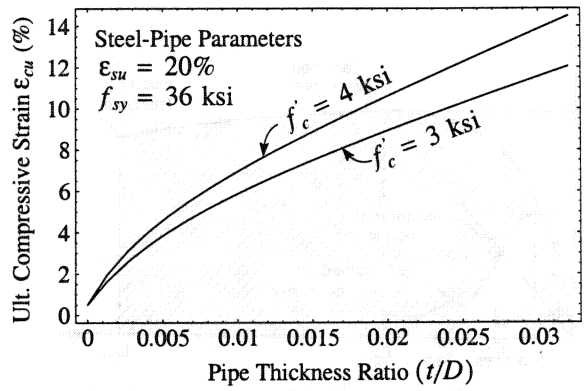

Figure 3.6: Increased ultimate compressive strain of steel-jacketed concrete, due to the confinement provided by the steel jacket [After (Chai 1996, Fig. 2)].

If in addition, the concrete on the pile-interior has a spalling strain of 0.5% and the steel pipe has an ultimate strain capability (ε_{su}) of 20%, then, as shown in Figure 3.6, the ultimate compressive strain (ε_{cu}) for the confined concrete can be plotted as a function of the thickness to diameter ratio (t/D). Notice that for a thickness to diameter ratio of 0.031 (representing a pile in the FE model), if the interior concrete has an unconfined strength (f'_{co}) between 3 and 4 ksi, the confinement model (3.7) indicates that ultimate compressive strain (ε_{cu}) is likely to range between 12 and 14%. The model used to define the ultimate compressive strain (3.7) is based on an energy balance that was derived for monotonic loading. For severe earthquakes, Chai et al. (1994) point out that cyclic loading is likely to lead to fatigue failures at significantly lower strains.

3.3.4 Composite Action

In the initial stages of deformation, while both the concrete and steel are in the elastic range, reinforced concrete can be modeled as a standard composite material, with each constituent (steel and concrete) carrying a fraction of the load based on their relative stiffnesses. However, once inelastic deformation begins, the nature of the interaction between the two materials can play a significant role in the deformation that follows. Factors that should be considered are: tension stiffening, shear retention, doweling, etc.

3.3.5 Discussion

Most of the nonlinear material behaviors discussed in the previous sections are beyond the scope of this investigation; simple linear elastic material models were used in this study. With such linear elastic material representations, the FE model cannot be expected to accurately portray the inelastic behavior of the structure. One of the more significant inaccuracies results from the inability of these simple models to represent tension cracking, i.e., the

capabilities are the same in tension and in compression. None-the-less, it is reasonable to expect an FE analysis with linear elastic material models to reveal areas of high localized stresses where permanent deformation is likely to take place. In Phase II of this study, non-linear analyses will be performed. Material models will be extended to include constitutive relations capable of modeling some of the non-linear behaviors discussed above. ANSYS (1997) provides material models that are capable of modeling many aspects of permanent damage in reinforced concrete.

3.4 Dynamic Behavior

One feature of interest in the analysis of a dynamically loaded structure is the harmonic frequencies of free vibration for the structure, as excitations at or near these frequencies can generate large structural displacements. These natural frequencies are dependent on the fundamental characteristics of the structure, such as: geometry, density, and stiffness. Because these same characteristics can be included in an FE model of a structure, the FE model can be used to determine the natural modes of vibration and corresponding frequencies.

Once the geometry, density, and elastic material models have been defined for the FE model, in the absence of damping which can be factored in later, the dynamic character of the model can be expressed in matrix form as

$$[K]\{u_i\} = \omega_i^2 [M]\{u_i\}, \tag{3.8}$$

where $[K]$ is the stiffness matrix, $[M]$ is the mass matrix, ω_i is the circular frequency of vibration (eigenvalue) for a given mode and $\{u_i\}$ is the mode (eigen) vector that expresses the corresponding mode shape. The finite element program simply uses iterative techniques to determine a set of frequencies and shapes that satisfy the FE matrix equation.

For example, if the unembeded pile length is 200 inches, the FE model yields the harmonic modes and corresponding frequencies shown in Figure 3.7. The deformed geometries in Figure 3.7 illustrate the shape of the structure at a point of maximum deflection, as it pauses before moving toward a state of maximum deflection in the opposite direction. The magnitude of deformation in Figure 3.7 is scaled to make the mode shapes readily identifiable and is otherwise meaningless.

3.5 Loads

In the present study, only two distinct load cases were considered, seismic and ice loads. Both of these load cases were applied as static loads. Seismic loads were applied as body forces that represent a 1g acceleration of the support points of the structure. Ice loads were applied as a distributed pressure that represents forces generated as ice is crushed against the leading surfaces of the pile bent.

Though this study investigates the behavior of the pile/pile-cap connection under only two classes of naturally occurring loads (ice and seismic forces), the conditions that generate

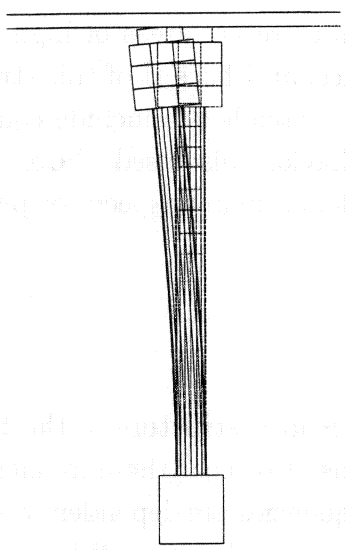

(a) 1st mode (longitudinal, side view)

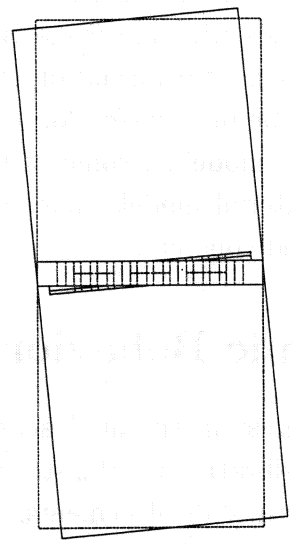

(b) 2nd mode (torsional, bottom view)

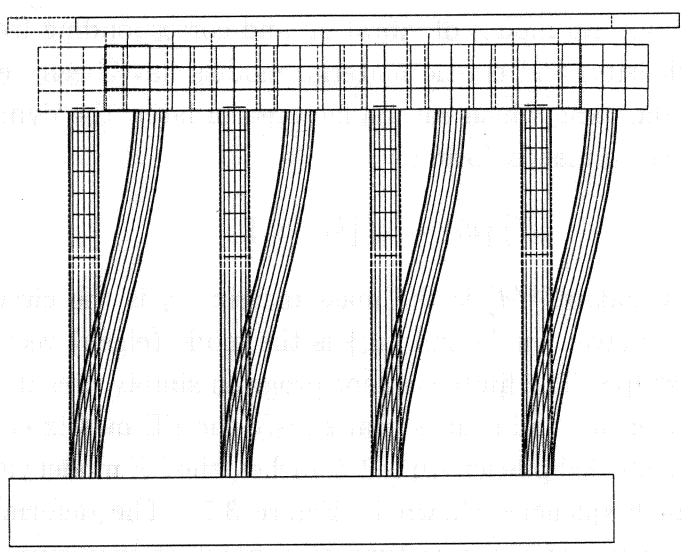

(c) 3rd mode (transverse, longitudinal view)

Mode Shape	Freq. (f) (Hertz)	Period (T) (sec.)	Amplitude (inches)
1st mode, longitudinal (a)	0.85	1.17	13.2
2nd mode, torsional (b)	0.92	1.09	-
3rd mode, transverse (c)	2.12	0.47	2.20
Deck and Pile-Cap Mass	330,000 lb		

(d) Frequency Summary

Figure 3.7: Harmonic responses for the modeled bent with lollipop constraints. The deformed geometry is exaggerated. The amplitude expresses the maximum displacement for any part of the structure for a given vibration cycle under a 1g spectral acceleration.

these loads vary widely. This section discusses the selection of reasonable, meaningful load cases to represent seismic events and ice contact forces.

3.5.1 Seismic Loads

Seismic loads are generated during an earthquake as the ground moves while the inertia (mass) of the structure retards its movement. Any retardation of movement between the structure and the ground requires structural deformation. The loads that generate such structural deformation are often referred to as *inertial loads*. Consequently, inertial loads that are incurred as a result of a seismic event are referred to as *seismic loads*.

As presented in Tonias (1995), seismic loads can be modeled as a function of the following four variables:

1) dead weight of structure,

2) period of vibration,

3) ground motion (acceleration),

4) soil type present.

The dead weight results in a vertical load that places the piles in a pile-bent in a general state of compression. The period of vibration is a function of the structural character and varies as a function of stiffness, mass distribution and damping. Ground motion imposes structural motions or structural excitations. The manner in which these structural excitations are imposed is dependent on the type of soil that serves as a foundation for the structure.

Vertical excitations during seismic events can temporarily alter the vertical load imposed by the dead weight such that the corresponding compressive stresses can temporarily increase or decrease. In the present study, vertical excitations were neglected.

Horizontal excitations during a seismic event can put the piles into a bending mode that varies predominantly as a function of the type of ground motion, the soil type present, and the resulting interaction with the vibration modes of the structure. These load interactions can lead to structural deformation that may result in failure.

Models for the harmonic behavior of the structure have been discussed previously (§3.4). Before equivalent static loads can be applied, probable ground accelerations must be determined for the region of interest. These ground accelerations can be used to define a spectrum of response accelerations based on typical vibration modes of earthquakes and the period of vibration of the structure. This spectrum must include effects of soil interactions. This section presents an overview of the UBC (1994) spectral acceleration models that can be used to estimate structural responses to seismic excitations.

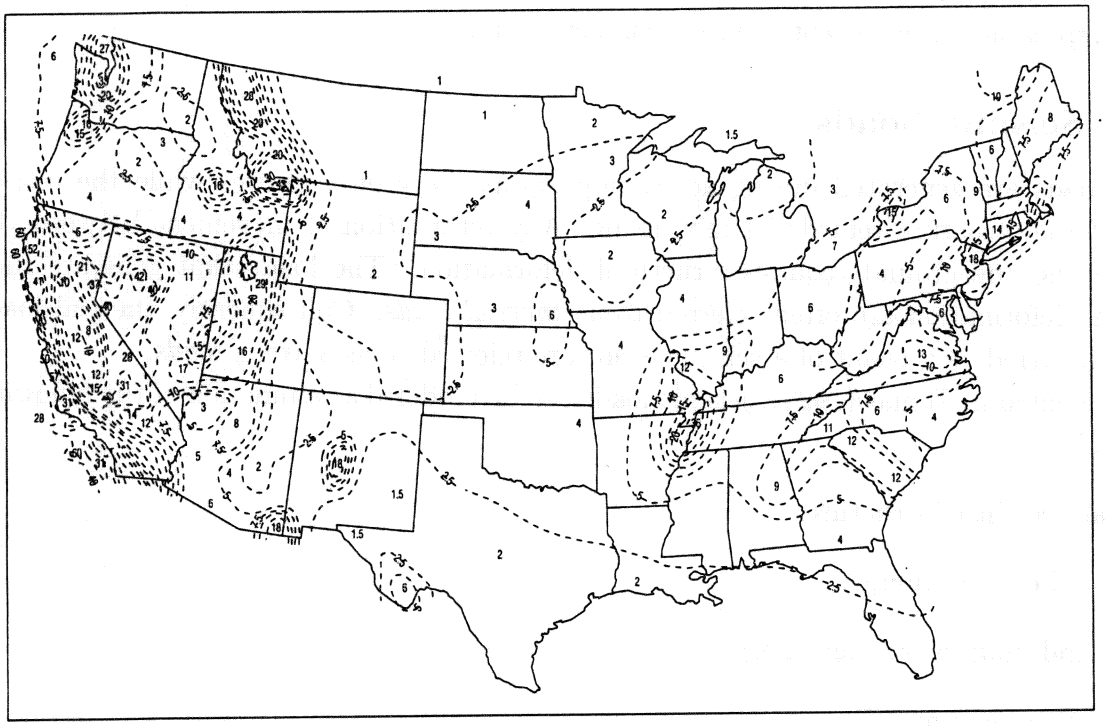

Figure 3.8: Seismic accelerations coefficients for the United States [After (Tonias 1995, Fig. 3.15)]. Coefficients can be obtained by dividing contour values by 100.

Ground Motion

The amplitude of regional ground accelerations is often used to define loads because it is readily measurable and it provides a measure of the energy that is likely to be transferred to a free standing structure. In particular, the ground acceleration can be used to define inertial loads for a structural model. The amplitude of earthquakes that are likely to occur in a given region have been classified in terms of historic records of past "free-field" ground accelerations.

Acceleration coefficients (A) are defined relative to the amplitude of free field ground acceleration (a) for a given region by

$$A = \frac{a}{g}, \tag{3.9}$$

where g is the acceleration due to gravity. According to Tonias (1995), regional acceleration coefficients (A) have been defined by AASHTO (1994) in the manner displayed in Figure 3.8.

As indicated in Figure 3.8, acceleration coefficients in Montana can have values that range from 0.01 to 0.43. The analyses presented in this report are based on an acceleration coefficient A with a value of 0.4.

Before the acceleration coefficient can be applied, a system must be defined to include variations in soil types and how these soil types might influence the acceleration of the structural supports.

Soil Type

Accelerations at a specific site are influenced by local subsurface materials. The definition of the acceleration coefficient (A) is based on the assumption that the subsurface material is primarily rock. To account for variations in the acceleration due to subsurface materials other than rock, a site coefficient is defined for different classes of subsurface material. Site specific acceleration coefficients are then defined by multiplying the standard acceleration coefficient (A) by the site coefficient (S).

According to Tonias (1995), AASHTO (1994) divides soil types into the following three classes:

I: rocky or stiff soils,

II: stiff clay or deep cohesionless soil,

III: soft to medium-stiff clays and sands.

These classifications are then used to specify coefficients that serve to place appropriate bounds on the manner in which the ground and structure interact during a seismic event. For each of these three soil types, AASHTO defines a site coefficient (S) where

$$S = \begin{cases} 1.0; & \text{for soil type I} \\ 1.2; & \text{for soil type II} \\ 1.5; & \text{for soil type III} \end{cases} \tag{3.10}$$

Now the remaining question is, how is the structure expected to respond if the ground acceleration is known and the structural supports are grounded in a known soil type.

Response Spectrum

To model structural responses to an earthquake, it is common to determine a statically equivalent load from a response spectrum. Such a response spectrum models how a structure is likely to resonate with respect to seismic motions and is defined relative to a structure's period of vibration or natural frequency and the soil type in which the piles are embedded.

In particular, a seismic response spectrum can be defined as a function of the period of vibration (T) of the structure, the regional acceleration coefficient (A), and the site coefficient (S). AASHTO defines an acceleration response spectrum using a seismic response coefficient (C_s) as follows

$$C_s = \begin{cases} C_2; & \text{if} C_2 < C_3 \\ C_3; & \text{otherwise} \end{cases} \tag{3.11}$$

where

$$\begin{aligned} C_2 &= \begin{cases} 2.0A; & \text{for soil-type III, if } A > 0.3 \\ 2.5A; & \text{otherwise} \end{cases} \\ C_3 &= \frac{1.2AS}{T^{2/3}}. \end{aligned}$$

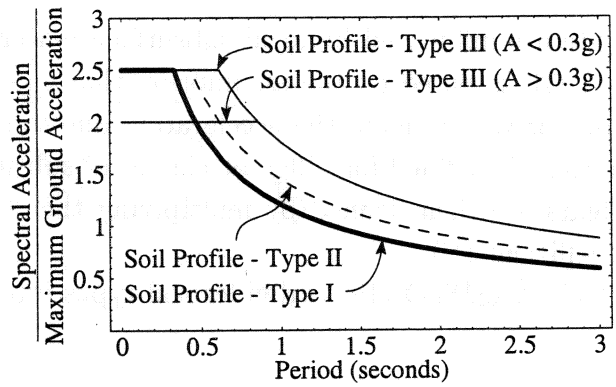

Figure 3.9: Seismic response spectrum normalized with respect to the maximum expected ground acceleration (a) [After (UBC 1994, Fig. 16-3)].

The spectral response coefficient (C_s) can then be used to define the amplitude of the structural accelerations that are likely to develop in response to ground accelerations of a given amplitude. If the response acceleration is presented as a function of the natural period of vibration, the result is referred to as a response spectrum. A spectrum that has been normalized with respect to the regional acceleration coefficient (A) is shown in Figure 3.9.

To model the first harmonic mode in a given direction, the seismic load can be modeled by applying a known spectral acceleration of $C_s g$ to the supports of the structure. To model other harmonic modes, ANSYS (1997) allows a response spectrum to be defined. After a vibrational mode and its frequency have been determined in the manner discussed previously (§3.4), the mode shape is maintained while a spectral acceleration is applied. The stress response is then based on the inertial load resulting from the spectral acceleration. Both techniques were used for the analyses presented in this report.

Applied Seismic Load

For lollipop constraints, as displayed in Figure 3.7d, the first harmonic frequency in the transverse direction has a period of 0.5 seconds. As a consequence, for a 0.4g ground acceleration, corresponding to peak acceleration coefficients in Southwest Montana, the response spectrum (Figure 3.9) indicates that for soil types I and II, a bridge bent is likely to experience maximum structural accelerations on the order of 1g (2.5*0.4g). As different regions of the state are considered or as boundary conditions and geometric parameters are varied, there will be cases where the spectral response will be less than 1g, but very few cases where the spectral acceleration will exceed 1g in Montana. As a consequence, for the purposes of this report 1g serves as a reasonable upper bound on spectral accelerations for bridges in Montana.

With the intent of establishing a convenient reference value, all seismic load cases evaluated in this study are based on a 1g acceleration of the ground supports. In addition,

each analysis includes a 1g vertical acceleration to include the forces resulting from the dead weight of the structure. Because the responses are based on linear models, in those cases where the 1g horizontal acceleration drives the stress-strain response, the responses may simply be scaled or multiplied by the expected spectral acceleration. In those cases where the dead weight drives the stress-strain response in the pile/pile-cap connection, the responses cannot be scaled directly; but these cases appear to be less critical than those dominated by horizontal inertial loads.

3.5.2 Channel (Ice) Loads

Channel forces are classified as those forces that are related to stream flow. These forces typically result from dynamic fluid pressure, that can either be transmitted to the structure directly or through a solid entity that acts to dam a portion of the flow and transmits the damming pressures to the structure through contact forces. Of primary interest in Montana is the formation of ice floes[2] and the forces they generate as they come into contact with structures, such as pile bents. The force that these ice floes can transmit to a structure are dependent on the size, the grain structure and impurity content, the temperature, the thickness, and the mean velocity of the ice floe (Michel 1978, Ashton 1986).

Ice floes commonly create the biggest problems during spring thaw or "spring breakup", as the surface ice cover breaks up and floats down stream. In such a case, the temperature of the ice will be near its melting point and the floes can be relatively large and thick; coincidentally, the stream flow-rate can increase significantly due to melt water runoff. The following discussion presents two extreme load cases that can occur during spring break-up.

3.5.3 Quasi-static Ice Loads

If dynamic effects are neglected, then the pressure that an ice floe can transmit to a structure is bounded by the crushing strength of the ice floe, or possibly the buckling strength depending on the thickness and geometry of the ice floe.

According to Tonias (1995, §3.5.3, Part 4), AASHTO specifies the following guidelines for the pressure (P) that can be transmitted as ice crushes or buckles:

$P = 100$ psi, when ice breaks up at the melting temperature and the pieces move as cakes of partially crushed ice.

$P = 200$ psi, when ice breaks up at the melting temperature and large pieces move down stream undamaged.

$P = 300$ psi, when ice breaks up at the melting temperature and pieces move down stream as large undamaged sheets.

[2]The term *ice floe* refers to large flat mass of ice that forms and is floating "freely" on the surface of a body of water.

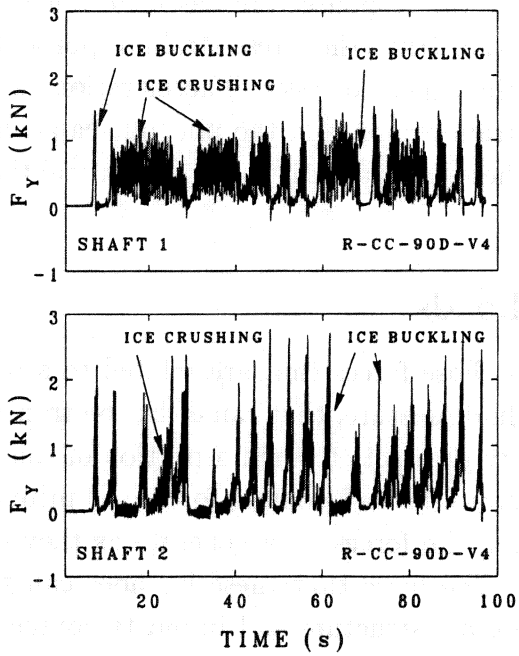

Figure 3.10: Example of load variations as a moving ice sheet buckles and/or crushes against a pile-type structural element [After (Timco et al. 1995, Fig. 4)].

$P = 400$ psi, when ice breaks up well below the melting temperature and pieces move down stream relatively undamaged.

Applying these guidelines to the winding rivers in Montana, it is reasonable to assume that ice pieces are not likely to move down stream as large sheets. In addition, if ice breaks up at relatively low temperatures, then the flow rate and level will also be low. As a result, the applied pressures will be low on the pile bent and are not likely to do any damage to the pile/pile-cap connection. As a consequence, the most extreme load case for the pile/pile-cap connection that is likely to occur will be when the ice-cover breaks up near its melting temperature as the flow rate and level increase due to melt water run-off. With this case in mind, the transmitted pressure was modeled with a magnitude of 200 psi.

3.5.4 Dynamic effects

As discussed in the previous section, ice loads on structures are typically modeled as static pressures based on the crushing strength of ice. However, Timco, Nwogu & Christensen (1995) indicate that ice loads due to interaction forces between moving ice sheets and stationary structures can vary significantly as the ice either buckles or crushes against the structural supports (see Figure 3.10).

Based on their experiments, the velocity of the ice does not significantly affect the magnitude of the peak interaction forces, but increased velocity does tend to increase the mean

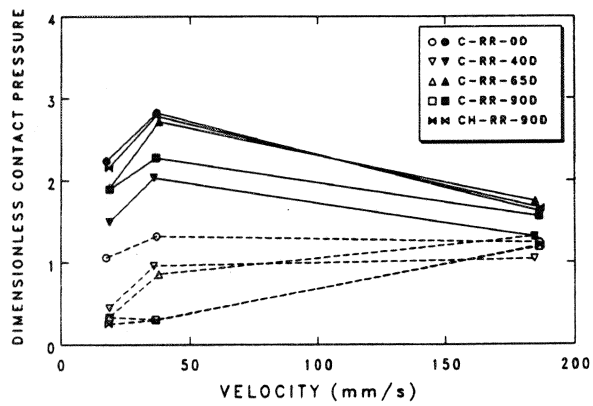

Figure 3.11: Example of a response spectrum as a moving ice sheet buckles and/or crushes against a pile-type structural element [After (Christensen et al. 1995, Fig. 4)].

interaction force as the slack time before an unbuckled section of ice comes in contact with the pile is shortened. This effect, however, is less important than the dynamic effect of the ice floes striking the piles in a rhythmic fashion.

Like seismic events, if the ice buckles and unloads at a frequency that coincides with the natural frequency of the structure, then the amplitude of the force transmitted by the buckling ice can be magnified significantly. The response spectrum for an experimental structure, as recorded by Christensen, Timco & Nwogu (1995, Fig. 4), is illustrated in Figure 3.11. The first case listed in the legend represents a pair of rigidly attached circular piers with ice approaching directly in line with the piers. This situation is similar to the situation in this study for ice loading on a pile, except that there are four piles in this study rather than two. Regarding Figure 3.11, the non-dimensional contact pressure spectrum is analogous to the normalized acceleration spectrum for seismic excitations (Figure 3.9). More specifically, the non-dimensional contact pressure is defined as the effective pressure, as felt by the structure, divided by the uniaxial strength of the ice. At the same time, the velocity of the ice serves as a measure of frequency; the faster the ice moves, the faster it takes up the slack space after buckling. The frequency resulting from a buckling ice sheet is highly dependent on the scale of the pile and ice interaction area and is not readily determined with confidence. However, though the uniaxial strength of ice is slightly less than the crushing strength of ice, Figure 3.11 indicates that the effective pressure can be magnified by more than a factor of 2.

Given the smaller pieces of ice that are likely to come in contact with Montana bridges, such occurrences seem unlikely, particularly for any length of time. As a result, this load case was not further pursued.

4

Frame Model

The primary study tool in this investigation is a finite element (FE) model of a bridge bent. However, to validate the FE model and understand the responses, it is useful to consider the same structure in terms of simple frame models that can be broken into easily understood components of the type shown in Figure 4.1. Therefore, before proceeding with a presentation and discussion of the results obtained from the FE model described in the previous section, a simple frame model–that correlates with the FE model–will be investigated. The results of this investigation can be used to validate the gross behavior predicted by the FE model (e.g., frequencies and overall deformations) and hence give added confidence that the structural forces that are delivered to the local regions of the FE model are accurate.

With simple frame models, principles from mechanics-of-materials are used to express the response of the structure in terms of the properties of its members, rather than developing a solid model of the structure that uses the 3-D distribution of the material in determining the structural response (as was done with the FE Model used in this study). For frame models, the response is instead calculated for the simplified systems of the type shown in Figure 4.1, where k, m, and c are determined from the gross properties of the structure so that this simple model reasonably mimics the behavior of the real structure.

In this model, k is the structural stiffness, which is related to the rigidity (EI) and length of the structural members that deform; m is the lumped mass of the system and is related

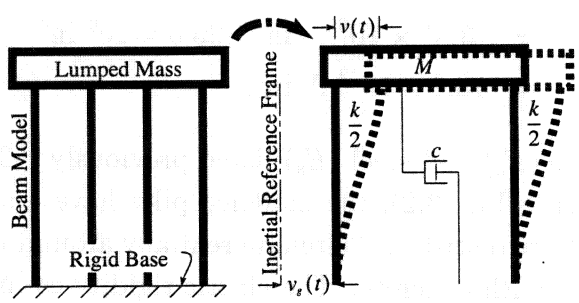

Figure 4.1: Frame model for a bent.

to the weight of the members that move as the frame deforms; and c is related to the energy dissipation characteristics of the structure (damping) as it deforms.

4.1 Geometry

In this case, the 2-D frame model was developed specifically for the purpose of checking the performance of the FE model; its properties are based on the structure as represented in the FE model (see Figures 3.1 and 3.2). The primary difference in the frame model is that different parts of the structure were lumped into a single quantity or were otherwise represented with a beam-type model.

4.2 Structural Mass

As discussed previously (§3.1.1), the deck was modeled as a slab with dimensions $720 \times 320 \times 7.5$ in and the density of the concrete was doubled to include the added weight of supporting girders without modeling them in detail. Given a concrete unit weight of 0.087 lb in^{-3} (150 lb ft^{-3}), the superstructure model had a total weight of 302,000 lb. It was useful for some of the hand calculations, to express this weight as a weight per unit deck length (w) equal to 0.419 kips in^{-1} ($\sim$5 kips ft^{-1}).

Though the deck provided the dominant portion of the mass, the mass of the pile cap was not insignificant. The pile cap, with dimensions $288 \times 34 \times 34$ in, weighed $\sim$28,000 lb.

4.3 Elastic Rigidity

The deck was modeled with smeared reinforcement oriented in the longitudinal direction. Given the dimensions of the modeled deck (§3.1.1), the cross sectional inertia (I_D) that serves to resist transverse bending is 20.5×10^6 in^4 (988 ft^4). With 1% smeared reinforcement, then, based on the rule of mixtures (Jones 1975, Eq. 3.69), the bending rigidity of the deck (EI_D) can be expressed as

$$\begin{aligned} EI_D &= (0.01E_s + 0.99E_c)I_D && (4.1)\\ &= (3.85 \times 10^6 \text{ lb in}^{-2})20.5 \times 10^6 \text{ in}^4 && (4.2)\\ &= 78.9 \times 10^{12} \text{ lb in}^2, && (4.3) \end{aligned}$$

using the moduli for concrete (E_c) and steel (E_s) listed previously (§3.3).

As presented earlier (§3.1.3, Fig. 3.2), the modeled piles have a steel pipe for an outer shell and 8 vertical bars that are distributed circumferentially around the interior of the pile. The remaining space is filled with concrete. The elastic rigidity estimates for each portion of the cross-section of a pile are listed in Table 4.1.

Comp.	Standard Inertia (in^4)	Transf. Inertia (in^4)	Elastic Rigidity (10^9 lb in^2)
Pipe	732	5896	21.23
Bars	113	911	3.28
Concrete	2485	2485	10.24
Total (1 pile)	-	9330	33.6
Bent (4 piles)	-	37320	134.4

Table 4.1: Rigidity parameters for a pipe pile.

Regarding the components listed in Table 4.1, the terms pipe, bar and concrete refer to the outer pipe, interior vertical reinforcement[1], and interior concrete, respectively, for a single pipe pile. The "Total" components represent values for a single pile, while the "Bent" component represents values for a four pile bent as shown in Figures 3.2 and 4.1. For example, the rigidity for a single pile (EI_P) is 33.6×10^9 lb in^2, while the rigidity for the modeled bent (EI_B) is 134.4×10^9 lb in^2.

For the structural parameters presented in Table 4.1, the standard inertia is based solely on geometric dimensions, the transformed inertia refers to inertia that has been transformed by multiplying by the modular ratio ($n = E_s/E_c$), as discussed in (Gere & Timoshenko 1997, §6.3), and the elastic rigidity (EI) serves as a measure of deformation (bending) resistance.

4.4 Static Behavior

The first step in using a 2-D frame model to analyze the response of the bent was to consider the behavior of a frame model under static loads. As discussed previously, to represent a bridge structure with a frame model, the dominant parts of the structure are lumped into components. For the present frame model, the piles and superstructure were considered the dominant components and each of these components was modeled with beam equations.

[1]In the finite element model, the internal reinforcement is modeled using ANSYS link8 elements. These elements overlap with the ANSYS solid65 elements that are used to model the concrete. As a result, the inertial values listed in Table 4.1 reflect this overlap such that the bending rigidity for a single pile is overestimated by 0.406×10^9 lb in^2, this is an increase of ~1% over what standard models would indicate for elastic rigidity.

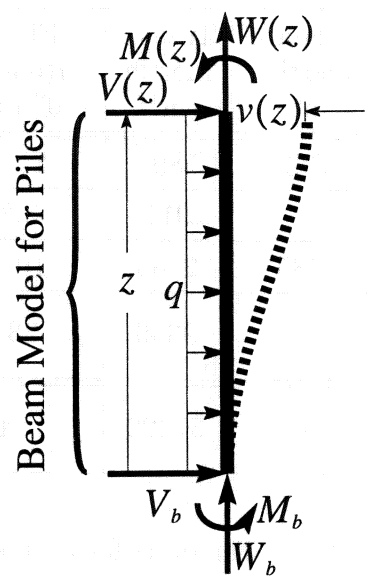

Figure 4.2: Free body diagram for an unbraced pile length (elevation).

4.4.1 Pile Model

To model a pile with beam equations, it is appropriate to consider only the unbraced length of the pile, where reactions at the ends of the pile are represented by forces and moments. The free body diagram for an unbraced section of a pile is displayed in Figure 4.2. If the structure is loaded inertially, through a 1g acceleration to the right, then the distributed load q_P will represent inertial loads from the mass in the piles, themselves, and will essentially be the weight per unit height. Using the dimensions given in Figure 3.2c with the density of steel equal 0.284 lb in^{-3} (490 lb ft^{-3}), the density of concrete equal 0.0868 lb ft^{-3} (150 lb ft^{-3}), and a 1g horizontal acceleration,

$$q_P \approx -22.3 \text{ lb in}^{-1} = -267 \text{ lb ft}^{-1}, \tag{4.4}$$

for a single pile. The vertical force $W(z)$ represents the weight that is supported by the piles at the vertical position z. $V(z)$ is the corresponding lateral force and represents the inertial force that is transmitted from the pile cap to the piles. The moment $M(z)$ is the corresponding moment. V_b and M_b are then respectively the reaction force and reaction moment at the base of the unbraced piles.

Using z as the vertical coordinate with a value of zero at the base and expressing the deformation of the unbraced pile length in terms of simple beam equations, one arrives at

the following forms:

$$\begin{aligned} EI_P v'''' &= q_P, \\ EI_P v''' &= q_P z + V_b = -V(x), \\ EI_P v'' &= q_P \frac{z^2}{2} + V_b z + M_b = -M(x), \\ EI_P v' &= q_P \frac{z^3}{3!} + V_b \frac{z^2}{2} + M_b z, \\ EI_P v &= q_P \frac{z^4}{4!} + V_b \frac{z^3}{3!} + M_b \frac{z^2}{2!}, \end{aligned} \tag{4.5}$$

where EI_P is the bending rigidity (§4.3) and v is the lateral displacement.

Notice that the last of these expressions (4.5) can be used to determine the flexural stiffness (k) of a beam model. In particular, if the distributed load is neglected and the moment at h is zero, so that the beam is statically determinate, then $V_b = -V(h) = -V$ and $M_b = Vh$. Substituting into the lateral displacement equation (4.5), $EI_P v = Vh^3/3! + Vh^3/2!$. As a result, the flexural stiffness can be expressed as

$$k = \frac{V}{v} = \frac{3EI_P}{h^3}. \tag{4.6}$$

If the distributed load is neglected and the moment at h reflects the moment at the base, then $V_b = -V(h) = -V$ and $M_b = Vh/2$. Then the flexural stiffness can be expressed as

$$k = \frac{V}{v} = \frac{12EI_P}{h^3}. \tag{4.7}$$

These expressions are also given in (Paz 1994, Eq. 4.1) along with other flexural stiffness models.

In both of these approximations for the flexural stiffness (k), it is often appropriate to substitute a characteristic height (H) for the unbraced pile height (h) to model the effective distance between representative end points in the flexural model. For example, to model bending in the longitudinal direction, it would be more accurate to use the first stiffness model (4.6) with a characteristic height (H) equal to the distance from base of the piles to the deck bearing at the top of the cap, where the deck bearing is the point at which there is no moment transfer.

Analogous to the description for the bending load, the axial load ($W(z)$) can be expressed as

$$W(z) = -\left(q_P z + W_b\right). \tag{4.8}$$

The base parameters V_b and W_b can be related to the forces $V_h = V(h)$ and $W_h = W(h)$ imposed at the cap by

$$V_b = -(q_P h + V_h), \tag{4.9}$$

$$W_b = -(q_P h + W_h). \tag{4.10}$$

If the moment at the cap $M(h)$ is zero, then the base moment can be defined through static equilibrium. Otherwise, the base moment is statically indeterminant. If the moment is

applied such that the pile is prevented from rotating at the cap, then the base moment can be defined by[2]

$$M_b = \frac{q_P h^2}{3} + \frac{V_h h}{2}. \tag{4.11}$$

Because the distributed load q_P is already defined in equation (4.4), if the pile-cap fully restricts rotation, the entire beam model for a given pile can be defined with a knowledge of the shear force $V(h)$ and weight $W(h)$ applied by the pile cap.

The stress component due to bending (σ_b) can then be represented by

$$\sigma_{sb} = \frac{yE_s M(z)}{EI_P}, \tag{4.12}$$

where y is the distance from the neutral axis in the direction of bending (Gere & Timoshenko 1997, §6.2). Similarly, the axial stress component due to the weight (σ_w) of the structure can be represented by

$$\sigma_{sw} = \frac{W(z)E_s}{(E_s A_s + E_c A_c)}, \tag{4.13}$$

where $A_s = 24.4$ in^2 and is the cross-sectional area of steel and $A_c = 177$ in^2 and is the cross-sectional area of concrete in a single pile (Gere & Timoshenko 1997, §2.4).

The axial stress (σ_{sz}) in the steel components can then be modeled as a sum of the two axial stress components,

$$\sigma_{sz} = \sigma_{sb} + \sigma_{sw}. \tag{4.14}$$

These models (4.5-4.14) will be used to explain and validate the range of behaviors displayed in the following subsections. At the same time, these models are intended to provide the reader with a set of tools that can be used to explore details beyond what is discussed.

For lollipop constraints, all of the lateral inertial loads from the deck or otherwise are transferred directly to the bent and the superstructure does not play an active role in limiting the lateral deformation. In this case, the shear force at the top of each pile can be determined quite readily.

For pinned end constraints, the superstructure can play a very significant role in limiting the structural displacements. To estimate the significance of the decks role, the deck can also be modeled with beam equations, as discussed in the following section.

Notice that the beam equations presented in this section can also be expressed in terms of "Bent" parameters. In this case, the rigidity for the bent ($EI_B = 4EI_P$) would be substituted for the rigidity of a single pile (EI_P) and the distributed load for the bent ($q_B = 4q_P$) will be substituted for the distributed load for a single pile (q_P). As a consequence, the reaction force (V_b) and the reaction moment (M_b) will also increase by a factor of four.

[2]For large deformation, the moment at the base (M_b) is also affected by the classic $P - \delta$ effect, i.e.,

$$M_b = \frac{q_P h^2}{3} + \frac{V_h h}{2} - W_h v_h.$$

For linear models (e.g. Equation 4.11), corresponding to small deformation ($v_h \approx 0$), the $P - \delta$ effect is neglected; for large deformation (non-linear) models, the $P - \delta$ effect must be accounted for.

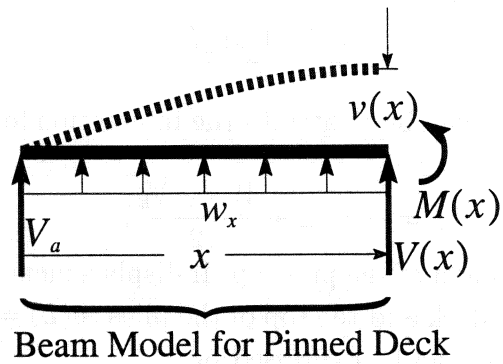

Figure 4.3: Free body diagram for one span of the deck (plan view).

4.4.2 Deck Model

If lollipop constraints are applied, then the deck is free to move essentially as a rigid body and can be modeled as a simple lumped mass. If pinned end constraints are applied, then the deck deforms with the bent and must be included in the frame model as a deforming component with distributed mass and can no longer be modeled as a simple lumped mass.

To model the deck with pinned end constraints using beam equations, it is appropriate to consider only one span or half the length of the deck by imposing symmetry boundary conditions at the center of the deck length, above the bent. The free body diagram for half of the deck with pinned end constraints is displayed in Figure 4.3. If the structure is loaded inertially, through a 1g acceleration to the right, then the distributed load w_x will represent inertial loads from the mass in the piles themselves and will essentially be the weight per unit length. As discussed previously (§4.2), the distributed weight (w_x) for the modeled deck is

$$w_x \approx -5 \text{ kips ft}^{-1} = -417 \text{ lb in}^{-1}. \tag{4.15}$$

$V(x)$ is the corresponding lateral force and represents the inertial force that is transmitted from the pile cap to the piles. The moment $M(x)$ is the corresponding moment. V_a is the reaction force at the abutment.

Using x as the horizontal coordinate with a value of zero at the abutment and expressing the deformation of the deck in terms of simple beam equations, one arrives at the following forms:

$$\begin{aligned}
EI_D v'''' &= w_x, \\
EI_D v''' &= w_x x + V_a = -V(x), \\
EI_D v'' &= w_x \frac{x^2}{2} + V_a x = -M(x), \\
EI_D v' &= w_x \frac{x^3}{3!} + V_a \frac{x^2}{2} - \phi, \\
EI_D v &= w_x \frac{x^4}{4!} + V_a \frac{x^3}{3!} - \phi x,
\end{aligned} \tag{4.16}$$

where EI_D is the bending rigidity (§4.3), v is the lateral displacement, and

$$\phi = \frac{w_x L^3 + 3V_a L^2}{6}. \tag{4.17}$$

The abutment parameter V_a can be related to the interaction force imposed by the bent, $V_h = V(h)$, by

$$V_a = -(w_x L + \frac{W_C - V_h}{2}), \tag{4.18}$$

where $W_C \approx -28$ kips is the weight of the pile-cap. If displacement compatibility is enforced between the mid-section of the deck and the top of the piles ($v(L) = v(h)$), then the reaction force at the top of the piles (V_h) can be expressed by

$$V_h = \frac{(5w_x L^4 + 4W_c L^3)EI_B/EI_D - q_B h^4}{4L^3 EI_B/EI_D + 2h^3}, \tag{4.19}$$

where EI_B is the rigidity of the bent (§4.3). Notice that, as with the piles (§4.4.1), the last of beam equations for the deck (4.16) can be used to approximate the flexural stiffness (k) of the deck. In this case, if the distributed load is neglected, $k = 3EI_D/L^3$.

This set of equations (4.16 - 4.19) can then be used in combination with the beam model for the piles, equations (4.5-4.14), to approximate the gross behavior of the modeled bridge with pinned end constraints.

4.5 Dynamic Behavior

The dynamic behavior of structures becomes important when the motions of the structure induce internal stress and strains that are likely to lead to failure. As discussed previously, dynamic loads can be approximated with statically equivalent loads. This section presents a set of tools that can be used to determine statically equivalent loads for the frame model.

4.5.1 Model Formulation

As a first approximation, consider the behavior of a bent and the associated superstructure as a single degree of freedom (SDOF) system. As illustrated in Figure 4.4, a bridge structure can be modeled in a very simplified form. In this case, the mass of the supporting components (piles) is neglected and the mass of the super-structure and pile cap are lumped into a single effective mass (M). When the ground moves in the horizontal plane (v_g), the inertia of the effective mass (M) leads the structure to deform with a displacement (v) relative to its structural supports in the horizontal plane. This deformation results in the structural deformation of components that will generate a restoring force (kv) that will pull the structure back toward its undeformed configuration. The inertial resistance to this restoring force can be expressed as the effective mass (M) times the acceleration ($\ddot{v}$) relative to the structure's supports. In the process, internal friction will also provide resistance to deformation. In one of the simplest forms[3], this resistance to motion can be modeled as proportional to the rate

[3]This simple model for frictional resistance is not typically very accurate, but serves as a reasonable and useful first approximation

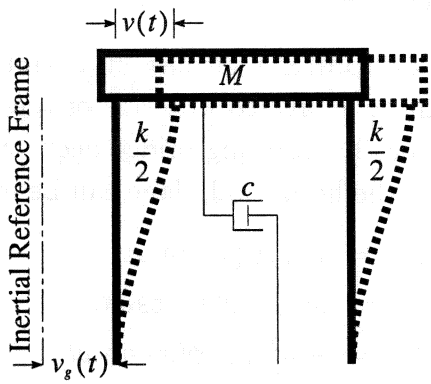

Figure 4.4: Seismic model for SDOF system [After (Clough & Penzien 1993, Fig. 2-3)].

of deformation ($\dot{v}$). The dynamic equilibrium equation for such a model can then be written as

$$M\ddot{v}(t) + c\dot{v}(t) + kv(t) = -Ma_g(t), \tag{4.20}$$

where c is the damping coefficient, k is the effective stiffness of the system, and $a_g = \ddot{v}$ is the acceleration of the ground relative to an inertial reference frame (Clough & Penzien 1993, Eq. 2.17). Each dot above a symbol represents a derivative with respect to time.

In particular, if this SDOF system is allowed to vibrate freely ($a_g = 0$) and damping is neglected, then

$$\ddot{v}(t) + \frac{k}{M}v(t) = 0. \tag{4.21}$$

Then the motion of the effective mass relative to its supports can be modeled by

$$v(t) = v_{max} \sin \omega t, \tag{4.22}$$

where $\omega = \sqrt{k/M}$ is referred to as the circular frequency and v_{max} is the maximum amplitude of the displacement (v). Vibrations that can be modeled in this form are referred to as *harmonic vibrations*.

Given the amplitude of a seismic excitation ($a_{max} = \max a_g(t)$) and the circular frequency of the structure, it is possible to place an approximate bound on the structural acceleration ($\ddot{v}_{max}$) and hence on the structural deformation (v_{max}). The techniques and tools for determining this bound are discussed in the following subsections. Using this bound, in combination with the FE model, it is then possible to discuss the possibility of structural failure under a given seismic excitation.

In some cases, the mass and stiffness of the system cannot be considered to be independent of one another as they are in the SDOF model. Fortunately, the SDOF model can be expanded to a more useful form to encompass some of these situations. In the following section, a simple expansion of the SDOF model is considered for determining the harmonic frequency of the modeled structure for both lollipop and pinned end constraints, and is used to validate the responses from the FE model.

4.6 Harmonic Frequencies

If the deck is considered the primary provider of mass in a vibrating bridge, then the vibrational energy for the bridge can be expressed in terms of the movements of the deck in the horizontal plane. For a harmonically vibrating bridge deck, transverse displacement(v), velocity ($\dot{v}$), and acceleration ($\ddot{v}$) in the horizontal plane can be expressed as

$$v(x,t) = v_{max}\psi(x)\sin\omega t, \tag{4.23}$$

$$\dot{v}(x,t) = \omega v_{max}\psi(x)\cos\omega t, \tag{4.24}$$

$$\ddot{v}(x,t) = -\omega^2 v_{max}\psi(x)\sin\omega t, \tag{4.25}$$

where x is a coordinate parallel to the length or span of the bridge, ω is the circular frequency, and t is the time. ψ is a shape function that can have values ranging between -1 and 1 and is used to describe the relative displacements in the horizontal plane along the length (x) of the deck. v_{max} is the maximum horizontal displacement of any point along the length of the deck, i.e., v_{max} is the amplitude of the shape function (Clough & Penzien 1993, Eq. 8.25).

Notice that as time varies, the displacement (v) is a maximum when the displacement rate ($\dot{v}$) goes to zero and similarly the displacement rate is a maximum when the displacement goes to zero. In a corresponding fashion, the potential energy (U) in the system is maximized when the kinetic energy goes to zero, as the kinetic energy (T) is maximized when the potential energy goes to zero. If energy dissipation due to damping is neglected, then an energy balance between the two states indicates that the maximum potential energy (U_{max}) is equal to the maximum kinetic energy (T_{max}), i.e.,

$$U_{max} = T_{max}. \tag{4.26}$$

For a deck with lollipop constraints (§ 3.2), the shape function (ψ) takes the form of a constant with a value of 1. In this case, the maximum kinetic energy (T) can be expressed as

$$T_{max} = \frac{1}{2}m\dot{v}^2 = \frac{1}{2}m\omega^2 v_{max}^2, \tag{4.27}$$

where m is the mass of the deck. Similarly, the maximum potential energy (U_{max}) can be expressed as

$$U_{max} = \frac{1}{2}kv_{max}^2, \tag{4.28}$$

where k is the effective spring constant for horizontal deflection of the bent. As a consequence, substitution into the energy balance (4.26) indicates that

$$\omega = \sqrt{\frac{k}{m}}. \tag{4.29}$$

For a continuous deck modeled with pinned end constraints (§ 3.2), the shape function describing horizontal displacements is not constant. In this case, the maximum kinetic energy (T_{max}) can be expressed as

$$T_{max} = \frac{\omega^2 v_{max}^2}{2}\int_0^{2L}\frac{w(x)}{g}\psi^2(x)dx, \tag{4.30}$$

where $w(x)$ is the weight per unit length of the deck and g is the acceleration due to gravity. Unfortunately, for a deck with pinned ends, the expression for the potential energy is not quite so simple. In this case, elastic energy is stored in both the bent and the deck. As a result, it is simpler to assume that the maximum potential energy is imparted to the system through the work (W_i) of body (inertial) forces resulting from a 1g acceleration in the horizontal plane. With such an assumption, the maximum elastic (potential) energy (U) can be expressed as

$$U_{max} = W_i = \frac{v_{max}}{2} \int_0^{2L} w(x)\psi(x)dx. \tag{4.31}$$

Substituting these expressions (4.30 & 4.31) into the energy balance (4.26) yields

$$\omega = \sqrt{\frac{g\beta}{\gamma}}, \tag{4.32}$$

where

$$\beta = v_{max} \int_0^{2L} \psi(x)w(x)dx, \tag{4.33}$$

$$\gamma = v_{max}^2 \int_0^{2L} \psi^2(x)w(x)dx, \tag{4.34}$$

and v_{max} is the maximum horizontal displacement due to a distributed inertial force resulting from a horizontal acceleration of 1g. The distribution parameters β and γ are analogous to seismic analysis parameters defined by AASHTO (1994, §4).

As a result, the harmonic vibration period (T) can be written as

$$T = \frac{2\pi}{\omega} = 2\pi\sqrt{\frac{\gamma}{g\beta}}, \tag{4.35}$$

for a modeled bridge. [4]

To clarify the relationships, notice that given the lollipop constraint ($\psi = 1$) with a uniform weight distribution ($w =$ constant), then

$$\beta = v_{max} w 2L \qquad \text{and} \qquad \gamma = v_{max}^2 w 2L. \tag{4.36}$$

[4]This model for the vibration period (4.35) is similar the form used by Tonias (1995, Eq. 3.4) where the period of harmonic vibration (T) is approximated by

$$T = 2\pi\sqrt{\frac{\gamma}{g\alpha p_o}},$$

where p_o is a force per unit length and α is defined by

$$\alpha = v_{max} \int_0^{2L} \psi(x)dx.$$

In the case discussed here, αp_o is represented by β.

As a consequence, the period of vibration reduces to

$$T = 2\pi\sqrt{\frac{v_{max}}{w2L}\frac{w2L}{g}} = 2\pi\sqrt{\frac{v_{max}}{g}} \tag{4.37}$$

$$= 2\pi\sqrt{\frac{m}{k}}, \tag{4.38}$$

where

$$m = \frac{w2L}{g} \quad \text{and} \quad k = \frac{v_{max}}{w2L}. \tag{4.39}$$

4.6.1 Lollipop Constraints

For the lollipop model, the deck and pile cap can be grouped to represent the mass of interest. The elastic restoring force is then generated by the bending response of the piles. For the first span-wise (longitudinal) mode, the bent can be modeled with a fixed end condition at the base and a pin connection at the deck-bearing interface. In this case, the elastic restoring force for such a SDOF system can be modeled by $k = 3EI_P/H^3$, Equation (4.6). For the first transverse mode, each pile can be modeled with fixed end conditions at both the base and at the pile/pile-cap connection. For each of these cases, the elastic restoring force for such a SDOF system can be modeled by $k = 12EI_P/H^3$, Equation (4.7).

For the structure that was modeled for this investigation, recall (§4.3) that the bending rigidity (EI_B) for the bent model is $\sim 134 \times 10^9$ lb in^2. The characteristic height (H) for the span-wise mode, from the base of the embedded pile to the top of the cap bearing, is ~246 in and the characteristic height for the transverse mode, from the base of the embedded pile to the top of the embedded pile, is ~216 in. Substituting these parameters into the frame model approximations for lollipop constraints (Equations 4.6, 4.7, and 4.38), the period of vibration for first span-wise mode is ~1.1 seconds, corresponding to a natural frequency of ~0.9 Hz. Similarly, the period of vibration for the first transverse mode is 0.46 seconds, corresponding to a natural frequency of ~2.2 Hz. Comparing each of these estimates with the FE estimates (Figure 3.7), the SDOF estimates come within 10% of the FE model values. These comparisons, indicate that the response of the FE model (Figure 3.7d) is consistent with the given approximations for the structure.

4.6.2 Pinned End Constraints

For pinned end constraints, the distribution parameters, β and γ, need to be evaluated before the period of vibration (T) can be determined for the structure, Equation 4.35. The displacement function for the deck (4.16) can be substituted for the product of v_{max} and the shape function ψ, i.e.,

$$v_{max}\psi(x) = \left(w_x\frac{x^4}{4!} + V_a\frac{x^3}{3!} - \phi x\right)/EI_D, \tag{4.40}$$

so that β and γ can be determined using equations 4.33 and 4.34 by integrating over one span ($0 < x < L$) and doubling the result.

A second though less accurate option is to model the shape function (ψ) by

$$\psi(x) = \sin\left(\pi \frac{l}{2L}\right), \tag{4.41}$$

where $2L$ is the length or distance between abutments (NHI 1993, §4.1).Then the integration parameters reduce to

$$\beta = v_{max} w \frac{2L}{\pi} \quad \text{and} \quad \gamma = v_{max}^2 w \frac{L}{2}. \tag{4.42}$$

In this case, the period of vibration is modeled by

$$T = 2\pi \sqrt{\frac{\pi}{4} \frac{v_{max}}{wL} \frac{wL}{g}} = \sqrt{\frac{\pi^3 v_{max}}{g}}, \tag{4.43}$$

where the maximum displacement (v_{max}) can be determined from the displacement function for the deck (4.16).

For the structure that was modeled for this investigation, recall (§4.3) that for the deck model, the bending rigidity (EI_D) is $\sim 78.9 \times 10^{12}$ lb in^2 and the weight density (w_x) is $\sim$419 lb in^{-1}. Similarly, for all four piles combined, the bending rigidity (EI_B) is $\sim 134 \times 10^9$ lb in^2 and the weight density (q_B) is $\sim$89 lb in^{-1}. Then for a deck span of $L = 30$ ft and an unbraced pile height $h = 16$ ft, the maximum displacement ($v_{max} \approx v(L)$) is $\sim$0.024 in. Substituting into the second approximation (4.43) for pinned end constraints indicates that the first transverse mode has a period on the order of 0.044 seconds with a corresponding natural frequency of $\sim$23 Hz. For the same boundary conditions, the FE model indicates that the structure has a period of vibration of 0.059 seconds and a corresponding natural frequency of $\sim$17 Hz.

The difference between the estimates from the two models appears to be primarily due to differences in deformation constraints at the ends of the deck. The frame model requires that plane sections remain plane and that shear stresses be distributed evenly over the cross-section; the FE model does not impose either of these constraints. As a result, when loads are localized (as with pinned end constraints), deformation in the FE model can also be very localized in a manner that can increase gross deformation. Such a case is illustrated in Figure 4.5a. Figure 4.5b, shows the displacement curves for the center of the deck based on both models (FE & Frame) due to inertial loads resulting from a 1g transverse acceleration of the ground supports. Displacement is displayed as a function of the normalized longitudinal coordinate (x/L), where L is the span length and the deck is pinned at $x = 0$. Notice that in the frame model the deck displaces in a continuous fashion, while in the FE model the deck displaces in a rather discontinuous fashion immediately adjacent to the pinned end. As displayed in Figure 4.5, the local deformation and the pinned end leads to a significant increase in gross deformation of the deck and hence the top of the bent.

If constraints are imposed on nodal displacements in the FE model—to partially simulate the constraints imposed by the frame model—then the displacement pattern for the deck in the FE model (labeled in Figure 4.5b as FE Model with Constraints) is much closer to the deformation pattern for the deck in the frame model. With these constraints, the FE

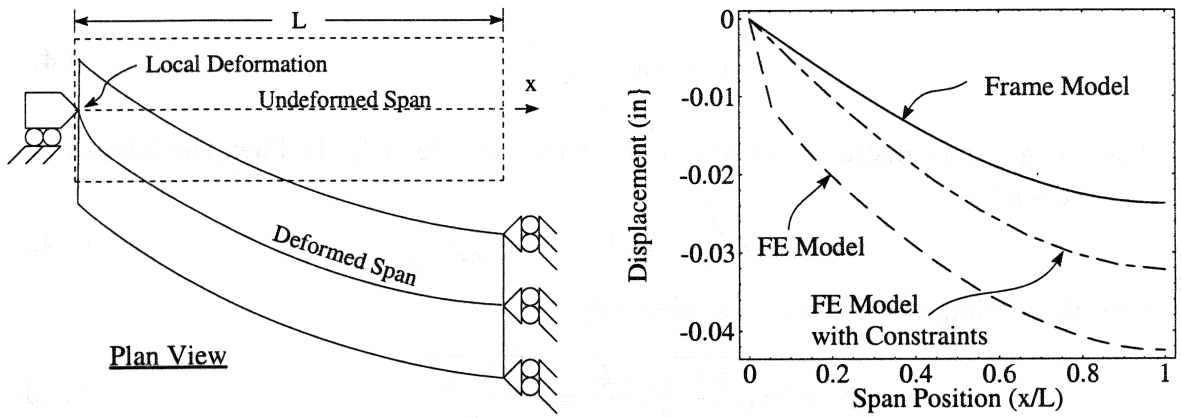

(a) Sketch of local deformation (FE model) (b) Comparison of centerline displacements

Figure 4.5: Comparison of displacements, Frame vs. FE model, for the deck center line.

model indicates that the period of vibration for the structure would be approximately 0.05 seconds, with a corresponding natural frequency of ~20 Hz. These estimates also compare reasonably well with those from the frame model. Based on these model comparisons for pinned end conditions, local deformation at the span ends plays a significant role in the harmonic behavior of the structure. Keeping this point in mind, the results from the FE model can be used with reasonable confidence.

4.7 Structural Damping

In the previous discussion of harmonic vibrations, structural damping was for the most part neglected. When damping is considered, it is often presented in terms of a damping ratio,

$$\xi = \frac{c}{c_{cr}}, \tag{4.44}$$

where the damping coefficient (c) is divided by the critical damping coefficient (c_{cr}) as defined by the dynamic equilibrium equation (4.20), see Paz (1985, Ch. 2). Using the damping ratio, the damped circular frequency (ω_D) can be defined in terms of the undamped circular frequency (ω) by

$$\omega_D = \omega\sqrt{1-\xi^2}. \tag{4.45}$$

Then with damping, the deformation of the structure (v) can be modeled with an expression of the form:

$$v(x,t) = v_{max}\psi(x)\sin(\omega_D t)\exp(\xi\omega t). \tag{4.46}$$

Typically, bridge-type structures are considered to have damping ratios of approximately 5% as long as they remain elastic. In this case,

$$\omega_D \approx 0.999\omega, \tag{4.47}$$

so that

$$v(x,t) \approx v_{max}\psi(x)\sin(\omega t)\exp(\xi\omega t). \tag{4.48}$$

When the structure deforms inelastically, the dissipation of energy increases significantly and the previously developed harmonic models become increasingly inaccurate.

Additionally, the significant increase in damping due to inelastic deformation leads to significant reductions in the spectral response of the structure. These variations will not be considered in the present study. For further discussion on the altered responses due to inelastic deformation (ductility), consider (Park 1987, Fig. 1.3) or (Berrill, Priestley & Chapman 1980, Berrill, Priestley & Peek 1981).

4.8 Loads

With simplified 2-D frame models, the manner in which the loads are applied must also be simplified. This section presents frame loads, corresponding to seismic loads specified for the FE model (§3.5). Because behavioral comparisons–between the frame and FE model–were in agreement for seismic loads, validation of ice loads was not extended beyond simple hand checks.

For a frame model, as with the FE model, once the period of vibration is determined for a particular deformation mode, a response spectrum can be used to define a spectral acceleration coefficient (C_s). In the present study, spectral accelerations were determined from Equation 3.11. The coefficient (C_s) can then be used to define the amplitude of the structural acceleration ($\ddot{v}_{max}$) by

$$\ddot{v}_{max} = C_s g, \tag{4.49}$$

This can also be expressed in a normalized form relative to the amplitude of the ground acceleration (a_{max}) by

$$\frac{\ddot{v}_{max}}{a_{max}} = \frac{C_s}{A}. \tag{4.50}$$

This normalized definition is plotted as a function of the period (T) in Figure 3.9 and is referred to as the *normalized response spectrum*. Recall that this result implies that the structural motions relative to the supports are then more generally modeled by

$$\begin{aligned} v(x,t) &= v_{max}\psi(x)\sin\omega t, && (4.51)\\ \dot{v}(x,t) &= \omega v_{max}\psi(x)\cos\omega t, && (4.52)\\ \ddot{v}(x,t) &= -\omega^2 v_{max}\psi(x)\sin\omega t, && (4.53) \end{aligned}$$

as presented previously (§4.6), where

$$\ddot{v}_{max} = \omega^2 v_{max}. \tag{4.54}$$

If this form is used to apply the inertial load (F_i) that represents dynamic equilibrium in a state of maximum structural deformation, then[5]

$$F_i(x) = m(x)\ddot{v}(x) = m(x)\ddot{v}_{max}\psi(x). \tag{4.55}$$

For a regular deck modeled with lollipop constraints, this equation reduces to

$$F_i = mC_s g. \tag{4.56}$$

In this case, the seismic response can be modeled by simply applying an acceleration of $C_s g$ to the supports of the structure. The other cases are more complex, but are handled quite easily with the FE model (ANSYS 1997).

[5]This expression for structural acceleration (4.55) is analogous to the expression for equivalent force,

$$p_e(x) = \frac{\beta C_s}{\gamma} w(x) v(x),$$

as presented by Tonias (1995, Eq. 3.6) and (AASHTO 1994, §4).

5

Experimental Effort

In addition to the 2-D frame model, a modest experimental program was conducted to a) validate the performance of the finite element model and b) obtain an indication of the types of distress these connections may experience under extreme loads. The accuracy of a finite element analysis can be difficult to assess when the structures under study are made with several materials and have complicated geometries. In such situations, existing "hand-calculations" do not offer the level of sophistication necessary to adequately verify the local response of the finite element model. Therefore, a simple, physical model of a section of a typical interior pile-to-pile cap connection was constructed and tested. The pile was subjected to quasi-static lateral loads applied in one direction (reversed loads were not considered). Strain and displacement data were collected during the test and compared with the response from an FE analysis of the model. Qualitative observations were also made on the over-all behavior of the pile-to-pile cap connection.

5.1 Description of the Model

The physical model consisted of an interior section of the pile cap (from centerline-to-centerline between piles) and the associated pile (cut off at one-half of its length), as shown in Figure 5.1. Detailed plans for the model are presented in Appendix A. The primary factors considered in selecting this model geometry were the size and complexity of the structure to be tested and analyzed. Based on the time and resources available for this effort, the decision was made to use the simplest possible model that would exhibit the basic behaviors of interest. A 2-D frame analysis of a typical bent under lateral loads revealed that a) the interior pile-to-pile cap connections experienced higher moments and shears than the exterior pile-to-pile cap connections, b) points of inflection occurred in the pile cap approximately at the midpoint between the piles, and c) points of inflection occurred approximately at the mid-height of each pile. Therefore, to reduce the physical size and complexity of the model, the decision was made to model an interior section of the bent, as bounded by the points of inflection described above. Thus, the ends of the model were supported with pinned connections, consistent with the zero moment condition at points of inflection.

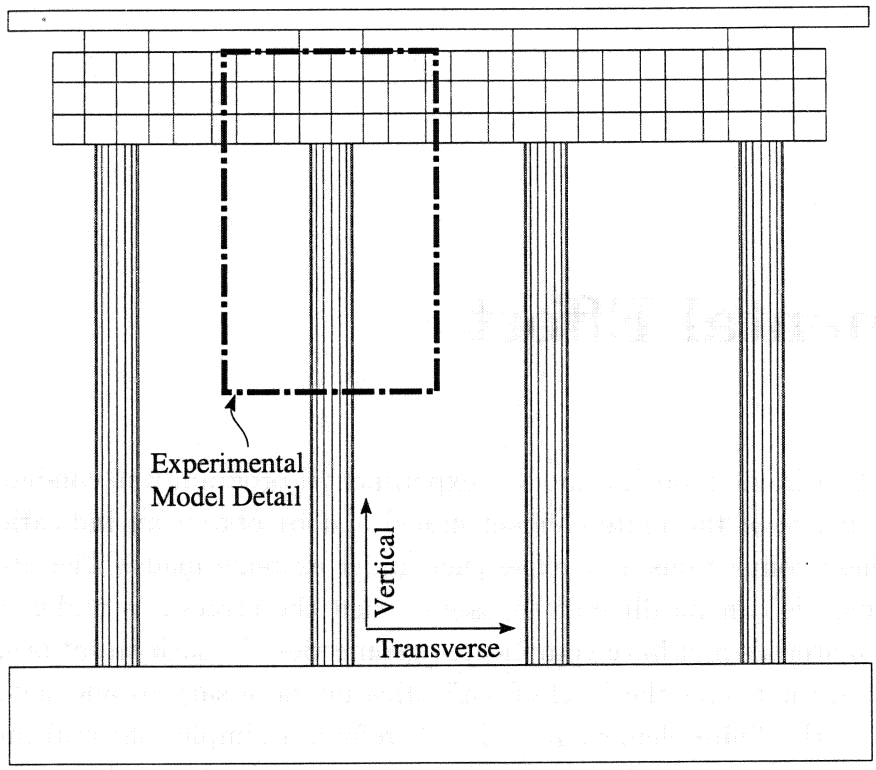

Figure 5.1: Overview of detail regions studied with the experimental model.

To minimize scaling issues, the decision was made to use the largest size model that could be reasonably handled and tested in the laboratory. This model was found to be approximately one-half the size of the actual system. While an effort was made to reasonably construct the model so that it would behave similar to the actual structure, the laws of similitude were not rigorously applied. The model geometry was accurately scaled from the full size system, as were the strength, general locations, and approximate amount (as a percent of the concrete volume) of reinforcing steel. Thus, the model was expected to demonstrate similar types of behavior as would be observed in the actual structure (which is sufficient to validate the ability of the finite element analysis to represent these behaviors), but it was not expected to precisely represent the behavior of the actual structure.

The model was specifically configured to resemble the Timber Creek Bridge (MDT Reference), which is similar to the Beaverhead River bridge used in developing the analytical models discussed earlier in this report. In the Beaverhead River bridge, longitudinal reinforcing steel extends out of the steel pipe pile and into the pile cap, while the Timber Creek Bridge has no longitudinal steel in the pile. The Timber Creek Bridge was constructed with 16-inch outside-diameter piles embedded a distance of 2'-0" into a 3'-0" square continuous cap. Thus, the experimental unit was constructed with an 8-inch outside-diameter pile embedded a distance of 1'-0" into a 1'-6" square cap. The inflection point in the 2D frame analysis occurred approximately 4 feet from the centerline of the piles, so a distance of 2'-0"

was used on either side of the model pile for an overall cap length of 4'-0". Grade 60 reinforcing steel was used throughout the model. The longitudinal reinforcement pattern used in the model was selected so that the reinforcing ratios (ratio of the area of steel to the area of concrete in a cross-section) in the model matched those of the Timber Creek pile cap. The strength of the concrete used in the model was approximately 6,600 psi at the time of the test.

An 8-inch diameter, 10-gage, Grade A steel pipe (minimum yield strength of 30,000 psi) was used to model the steel pipe for the pile. This section was selected based on price and availability of sections to satisfy this need. The area of steel provided by this section was less than that necessary to provide the same steel ratio (area of steel pipe divided by area of concrete) in the model as exists in the actual bridge structure. Therefore, the area of the steel pipe was augmented by adding twenty-five # 3 reinforcing bars spaced evenly around the inside circumference of the steel pipe. These bars were "tack-welded" to the inside of the steel shell and extended the entire length of the pile. Due to their deformed surfaces, among other things, these bars were expected to act more integrally with the concrete than the actual steel shell material that they were intended to represent.

5.2 Test Setup

The model was tested by applying a gradually increasing lateral point load to the tip of the pipe pile using a hydraulic ram. Although true seismic loads are expected to be both dynamic and cyclic in nature, a quasi-static single cycle test to failure was expected to reasonably reveal areas of high localized stress in the connection zone and to provide a general indication of the ductility of the connection response. The model was oriented with the longitudinal axis of the steel pipe pile in the horizontal rather than in the vertical plane. In this orientation, only nominal fixturing was required to hold the model and the loading device in position, as these items rested directly on the floor. No effort was made to produce the axial forces that are generated in the real structure from its self weight. The FE calculations indicated that in critical seismic response situations such stresses were low in magnitude compared to the stresses generated by seismic lateral loads. (Vertical loads may be considered in future tests, if analyses indicate that P-Δ effects are significant.)

5.3 Instrumentation

Load, displacement, and strain measurements were made during the pile tests. The load applied by the hydraulic ram was measured using a load cell which was included in the load apparatus. The displacement of the tip of the pile was measured using a linear potentiometer. The displacement measurements were confirmed by dial gage. Strain measurements were made at 5 locations in the immediate vicinity of the pipe-to-pile cap connection, as shown in Figure 5.2. Two of the gages were placed on a short length of reinforcing bar that was located just inside the surface of the pile cap (Gages 1 and 4). The bar, parallel to the surface of the

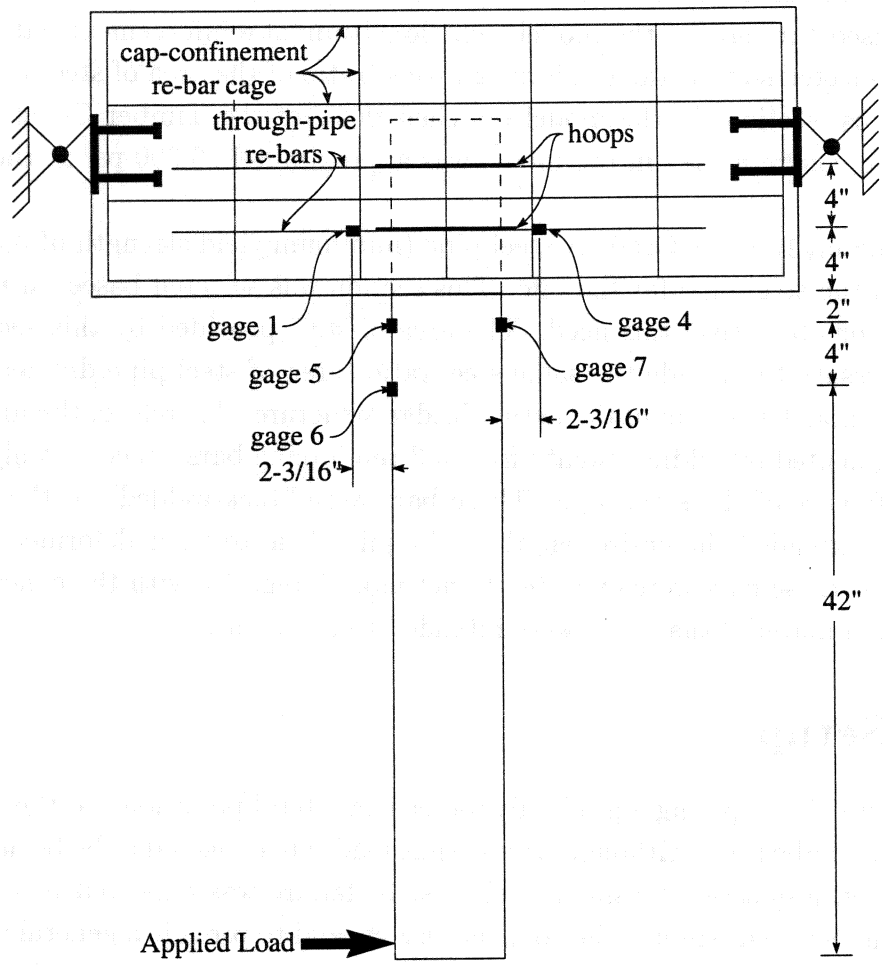

Figure 5.2: Overview of geometry and strain gage locations for experimental model.

cap, extended through the pipe pile (in the plane of the applied load). One gage was placed on each end of the bar as it exited the pile. Three strain gages were attached to the exterior of the steel pipe pile close to the point at which it entered the pile cap. These gages were all oriented parallel to the longitudinal axis of the pile. Two of the gages were positioned on opposite sides of the pile (in the plane of the applied load), 2 inches from the surface of the pile cap (Gages 5 and 7). The remaining gage was placed on the tension side of the pile, in line with one of the above gages, 6 inches from the surface of the pile cap (Gage 6).

5.4 Test Chronology

While the intention was to load the model to failure in a single event, problems with the test fixturing resulted in the loading being interrupted three times. The first attempt at loading the model was terminated at an applied force of 6,000 pounds when the model began to lift vertically off the floor. The load was removed, and a simple restraint system was installed

to prevent uplift of the model. The model was only stressed elastically during this load event, based on the linear nature of the load versus strain curves generated from the test data. The model was subsequently loaded to 12,000 pounds of applied force when one of the pinned supports on the end of the pile cap failed. The load was released and the support was repaired. Hairline cracks were observed in the pile cap at the time the load was released, and the strain data indicated that some plastic behavior occurred during the test event. The model was subsequently loaded to 22,000 pounds, at which point the repaired pinned connection again failed. Plastic strains were recorded during this test by the gages on the steel pipe pile. The pinned support was repaired, and the model was reloaded to 25,000 pounds of applied force. The same pinned connection failed at this load, and testing was terminated.

5.5 Test Results

Visual Distress - The first distress observed in the loaded model consisted of hairline cracks in the concrete in the pile cap. These cracks first appeared at a load of approximately 10,000 pounds and ran transverse to the longitudinal axis of the cap. While the cracks lengthened as the load increased, they remained relatively small in width throughout the tests. The primary distress observed in the model occurred during the fourth and final load event, in which the steel pipe bulged out on the compression side of the pile immediately adjacent to the surface of the pile cap. The permanent bulge created in the wall of the pipe, located $1\frac{1}{8}$ inches above the surface of the cap, measured approximately 1 inch in width, was $\sim\frac{1}{32}$ of an inch high, and extended over a 60 degree arc. The tip of the pile was also permanently displaced in the direction of the applied load ($\sim\frac{1}{8}$ inch of displacement over a cantilever length of 48 inches).

Measured Response - The strains measured during each test event were plotted as a function of applied load to establish the nature of the model response at various load levels. In interpreting these plots, the fraction of applied load carried by the various components of the model were assumed to be relatively constant. This assumption was judged to be valid after initial cracking of the concrete occurred, which was expected at relatively low load levels, up to the load at which the structure would begin to break up. Load sharing between the various elements of the structure should have been constant in this range of responses. Under these conditions, the occurrence of plastic deformations in the elements of the model should correlate with the occurrence of non-linearities in the strain versus applied load histories.

The strain histories for the first load event (Figure 5.3a) were linear in shape, which indicated that the model behaved elastically during this event. The model was only loaded to an applied force of 6,000 pounds in this event. The maximum measured strain was 0.06 percent, which was significantly below the expected yield strain for both the pipe steel (calculated to be 0.11 percent using a yield stress of 30,000 psi) and the reinforcing steel

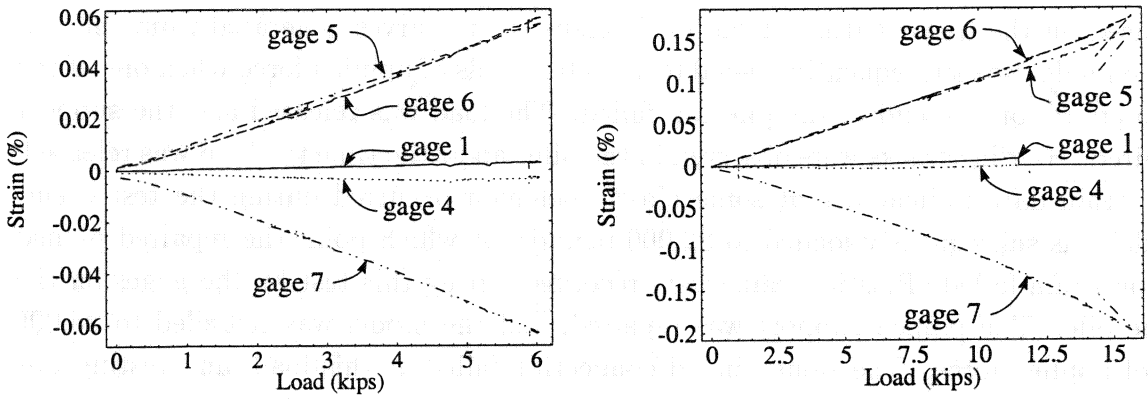

(a) Run 1 (b) Run 2

Figure 5.3: Recorded strain gage responses for Runs 1 and 2.

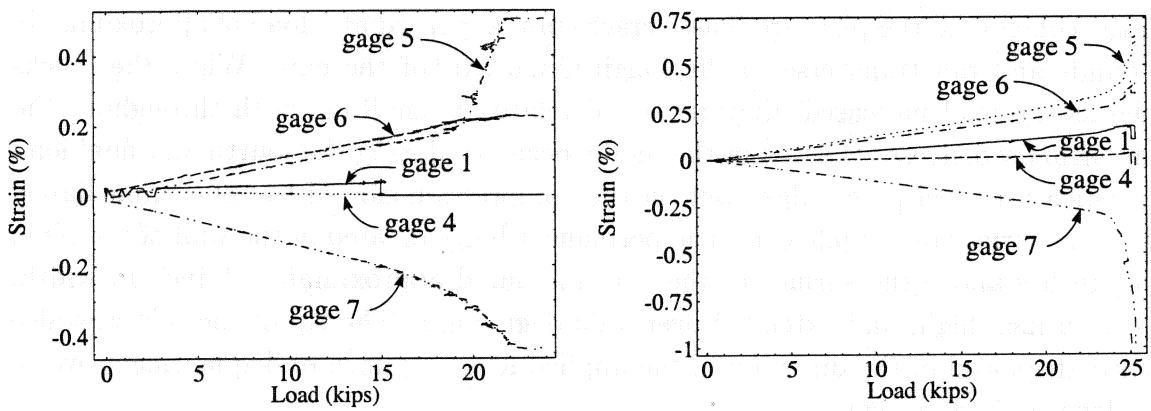

(a) Run 3 (b) Run 4

Figure 5.4: Recorded strain gage responses for Runs 3 and 4.

(calculated to be 0.24 percent using a yield stress of 71,000 psi for grade 60 steel).

Plastic deformations were observed during the second load event at the exterior surface of the pipe pile near the face of the pile cap. The strain histories for this event are presented in Figure 5.3b. Non-linearities are evident (though not pronounced) in the strain histories plotted for the pipe pile (Gages 5,6, and 7) at loads at and above 10,000 pounds. These non-linearities begin at strains on the order of magnitude of 0.10 percent, which closely correlate with the calculated yield strain of 0.11 percent for the pipe material. The largest plastic strains (up to 0.19 percent) were recorded on the compression side of the pile (Gage 7) at a load of 15,000 pounds. The strains measured on the reinforcing steel (Gages 1 and 4) were relatively low in magnitude, reaching a maximum value of only 0.04 percent.

The strain histories from the third test event are presented in Figure 5.4a. Referring to Figure 5.4a, the model behaved linearly at load levels less than 16,500 pounds. Starting at

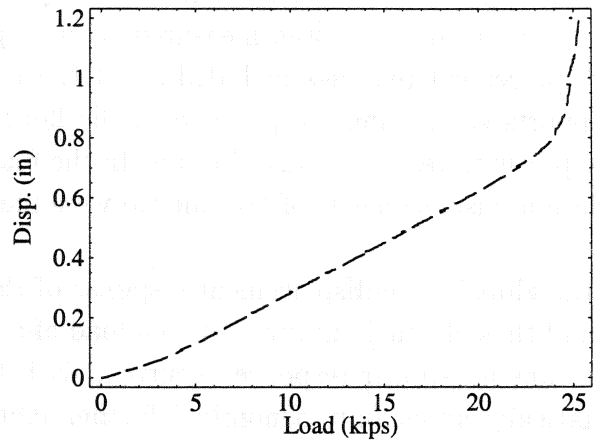

Figure 5.5: Tip displacement as a function of tip load (Run 4).

a load of 16,500 pounds, the strain history for Gage 7 became nonlinear, indicating plastic deformation occurred at this location (which is on the compression side of the steel pipe). Plastic behavior began at approximately 0.20 percent strain. Plastic behavior was also observed during this load event at the location of Gage 5 (which is on the tension side of the steel pipe). This plastic behavior began at a load of approximately 18,500 pounds at a strain of 0.18 percent.

The strains measured on the reinforcing steel in the pile cap during this same test event were significantly lower (80 percent lower) than the strains measured on the surface of the pipe pile (gage 1 & 2, Figure 5.2). Note, however, that only one of the gages on the reinforcing functioned during the test and that this gage only functioned up to an applied load of 15,000 pounds.

The strain histories from the fourth test event are presented in Figure 5.4b. The model appeared to respond elastically up to an applied load of 22,500 pounds. The strain-load histories become non-linear at this load for two of the gages mounted on opposite sides of the exterior surface of the pile (Gages 6 and 7) and for one of the gages mounted on the reinforcing steel in the pile cap (Gage 4). Non-linear behavior began in the wall of the pipe pile at strains of approximately 0.30 percent. Once again, this strain significantly exceeds the expected yield strain of the pipe material, although some strain hardening of the pipe material may have occurred as a result of the plastic deformations experienced during the previous test event. A distinct and permanent bulge appeared in the wall of the pile adjacent to the surface of the pile cap on the compression side of the pile at this load. This permanent deformation is consistent with the plastic strains measured on the pile. Plastic behavior in the reinforcing steel (Gage 6) began at a strain of approximately 0.25 percent, which is consistent with the calculated yield strain of 0.24 percent.

The load displacement history from the fourth test event is presented in Figure 5.5. These histories are not presented for the first three test events, due to problems with the manner

in which the displacement of the pile tip was measured in these events. In the early tests, the displacement of the tip of the loaded pile was measured with respect to the floor of the laboratory. Thus, the displacement readings included all of the movement associated with deformations in the supports connecting the pile cap to the floor, in addition to the displacement of the tip of the pile with respect to the pile cap. In the fourth test, the system was modified such that the lateral displacements of the pile tip were measured with respect to the pile cap.

Referring to Figure 5.5, the global force-displacement response of the model during the fourth test event was linear and thus elastic in nature out to a load of approximately 22,500 pounds. At this load, significant non-linear response occurred, with the displacement of the pile tip increasing dramatically under only a nominal further increase in the applied load. This behavior is very consistent with that observed in the strain versus load histories discussed above, notably with respect to the occurrence of significant deformations at loads in excess of 22,500 pounds. Thus, there is a high likelihood that the strain gages were appropriately positioned to capture the local behavior that was primarily influencing the gross behavior of the structure.

5.6 FE vs. Experimental Model

The experimental pile/pile-cap connection was intended primarily as a means of determining the accuracy that could be expected from the FE model. This section presents a comparison between the responses of the FE model and of the test results for the experimental connection.

5.6.1 FE Model Specifications

The geometry for the FE model of the experimental pile/pile-cap connection is presented in Figure 5.6. Only the steel components in the model are illustrated in Figure 5.6; concrete is modeled interior to the geometry outlined by the steel components.

As with the full bent model, the cross-sectional dimensions of the cap were reduced so that cap-confining steel reinforcement could be placed on the outer faces without changing the rigidity of the cap significantly. In this case, the modeled cap had dimensions of 16 × 16 × 48". The steel pile-jacket was embedded 11" into the cap and extended 49" exterior to the cap. The jacket was modeled with an outer diameter of 8" and a thickness of 3/8". Steel reinforcement bars that lined the pile-jacket were smeared with the concrete immediately adjacent to the steel-jacket. Pile restraining reinforcement in the cap (through-pipe and hoops) was modeled with link elements.

To simulate the fixed end conditions on the pile-cap, the center of each end (a region approximately 6 × 6" square), was fixed and held rigid. The material models for each component were those specified for the full bent model (§3.3).

To obtain an accurate comparison, because the strain gages in the experiment indicated linear behavior for loads up to 10 kips, a force (F) of 10 kips was applied to the

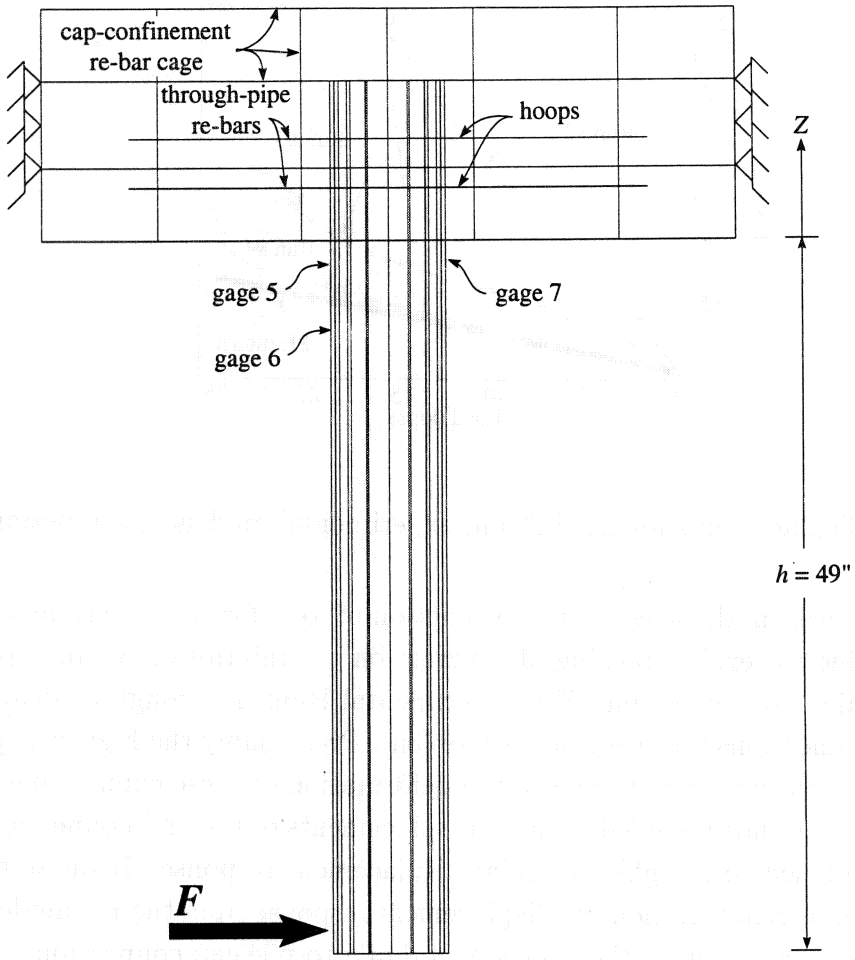

Figure 5.6: Overview of experimental geometry, as modeled

cantilevered end of FE model of the experimental pile. Because the finite element model yields stress-strain responses for the entire structure, comparisons with strain gages were made by comparing strain gage values with strain responses at corresponding points in the FE model, under equivalent end loads. Strain gage locations are illustrated on the FE model in Figure 5.6 for comparison with the experimental model.

5.6.2 Elastic Response

For the first comparison between the two models (experimental and FE), consider the tip displacement of the cantilevered pile as a function of load. In the FE model, a force of 20 kips at the tip resulted in a tip displacement of 0.523". Because the FE model was linear, this response indicated that the tip displacement was a linear function of load with a slope of 0.523/20 in kip^{-1}. This linear function from the FE model is plotted with displacement records from the experimental model, in Figure 5.7. The tip-displacement comparison between the FE model and Run 4 of experimental model appear to be quite reasonable. In this

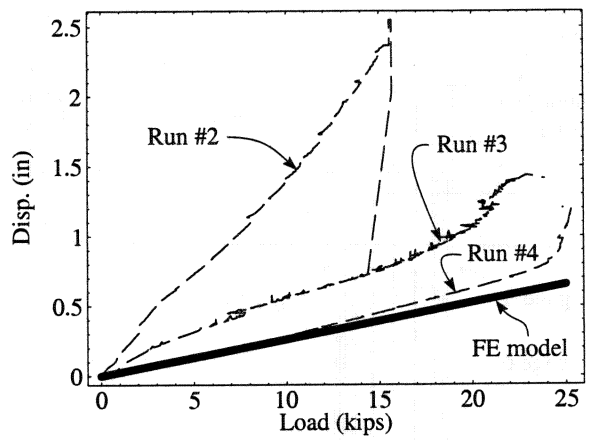

Figure 5.7: Tip displacements for the FE and experimental models as a function of load.

case, the slight increase in displacement as a function of load for the experimental model is more than likely due to tensile cracking of concrete on the interior of the pile, particularly near the pile-to-pile cap connection. For experimental Runs 1 through 3, deformation of the pile cap end connections was a prevalent problem. Presumably the higher displacements recorded for Runs 1 through 3 were due to the deformation of these connections. Displacements from Run 1 were not included because displacements of the end connections, as they lifted from the floor, led to a highly irregular displacement response. If the data recorded from Run 4 is taken as reliable, then the displacement response from the FE model compares quite well with the response from the experimental pile-to-pile cap connection.

As a second comparison, consider the strain responses in the pile-jacket. Figure 5.8 provides a comparison between the pile-jacket strain response of the FE model and the recorded experimental strains from Run 2 at a tip load (F) of 10 kips. This comparison indicates that the linear-elastic FE model is underestimating the strain response and consequentially the load carried by the pile-jacket. At first glance the difference is rather disconcerting, but if the difference is considered relative to the inability of concrete to support tensile loads, then it seems quite likely that in the experimental model, the tensile portion of the bending load was supported predominantly by the steel components; such a load increase in the steel jacket would then result in higher strains. If this load transfer did occur, then the difference between the experimental and FE modeled responses is reasonable. Explained or not, the resulting difference indicates that the FE model with linear elastic material parameters is not conservative.

In the experimental test series, data from Run 2 recorded strains before any significant permanent deformation had taken place. Loads in Run 3 resulted in permanent deformation of the pipe near adjacent to the cap (see Figure 5.4a). After Run 3, new strain gages were attached to the pile jacket and strain measurements recorded data for a pile jacket that had been strain hardened. In this case, strain data remained relatively linear to loads in

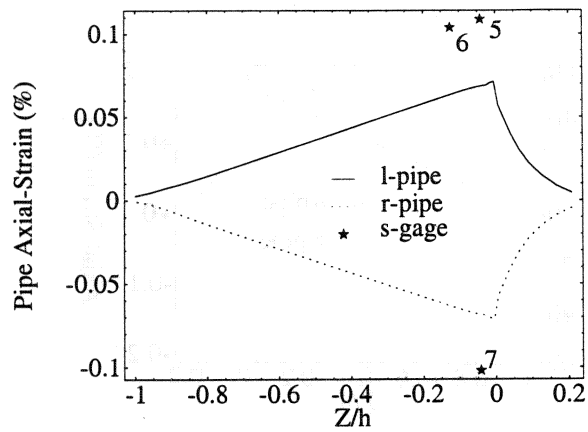

Figure 5.8: Strain comparison between the FE and experimental model (Run 2) for a 10 kip tip load. Numbers 5, 6, and 7 represent strain gage numbers (see Figure 5.6).

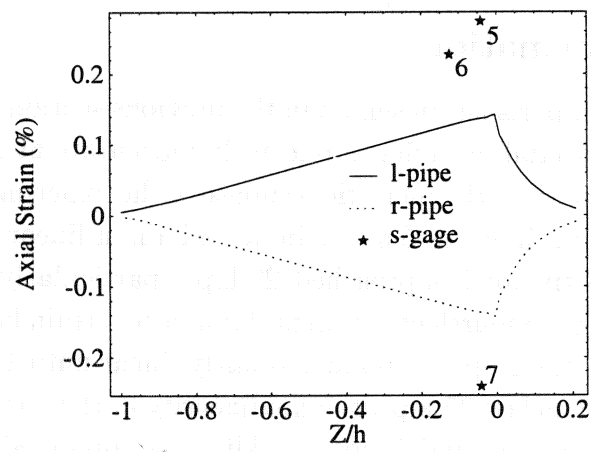

Figure 5.9: Strain comparison between the FE and experimental model (Run 4) for a 20 kip tip load. Numbers 5, 6, and 7 represent strain gage numbers (see Figure 5.6).

excess of 20 kips. Figure 5.9 provides a comparison between the pile-jacket strain response of the FE model and the recorded experimental strains from Run 4 at a tip load of 20 kips. As with the previous comparison (Figure 5.8), Figure 5.9 indicates that the linear-elastic FE model is underestimating the strain response and consequentially the load carried by the pile-jacket. In this case, the difference is even more exaggerated, presumably due to an increase in tensile cracking of the pile-interior concrete. As a result, these comparisons indicate that the FE model will not provide accurate stress-strain responses for relatively high loads until nonlinear behaviors, such as tensile cracking, are included in the model.

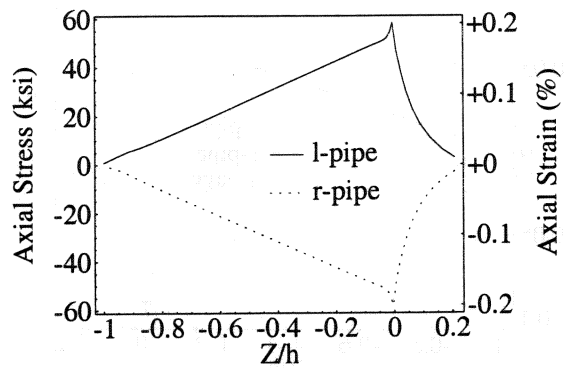

Figure 5.10: Stress-strain response in the pile jacket of the FE model corresponding to permanent and observable flexure of the experimental model[2].

5.6.3 Inelastic Deformation

Though FE-experimental comparisons presented in the previous section indicate that the FE model with linear elastic material behavior is relatively inaccurate at high loads, it is still quite useful. In particular, consider the inelastic response of the experimental model. During the third experimental run, strain gages 5 and 7 indicated a non-linear response (indicating plastic deformation) as the tip load approached 20 kips, particularly on the tensile side (Figure 5.4a, gage 5). During the fourth experimental run, after strain hardening to a certain extent during the third run, the response remained fairly linear until the tip load exceeded 22 kips. As the tip load approached 25 kips, the nonlinearity in the strain responses became significant (Figure 5.4b, gages 4, 6, and 7) and buckling was observed on the compression side (near gage 7). Unfortunately, a failure of the connections prevented further testing.

Though the linear elastic FE model may not be conservative, consider the stress-strain response of the FE model at loads that induced permanent deformation in the experimental model. Because permanent deformation became significant as the tip load approached 25 kips, consider Figure 5.10. Figure 5.10 represents the stress-strain response in the FE model for a tip load of 25 kips. Notice that the peaked stress-strain response from the FE model indicates that permanent deformation is likely to initiate immediately adjacent to the pile/pile-cap interface. Observed responses from the experimental model (i.e., the non-linear response of strain gages 5 and 7 in Figure 5.4b along with observed buckling adjacent to the

[2]In this model, the stress-strain response is dominated by the axial bending stresses. As a result, if the Z-axis corresponds to the axis of the pile, then for the linear elastic model

$$\varepsilon_Z = \frac{1}{E_s}\left[\sigma_Z - \nu(\sigma_X + \sigma_Y)\right] \approx \frac{\sigma_Z}{E_s}$$

The strain values on the right side of the plot frame are based on this approximation.

interface) are in agreement with indications from the FE model.

Though the FE model underestimates the strain response and most likely overestimates the stress response, as a first approximation, it is reasonable to assume that responses that are similar to or exceed this stress-strain profile are likely to result in permanent damage that will, at the least, require repair.

6

Parametric Studies with Seismic Loads

Having introduced the FE model and having validated its behavior to some extent using the 2-D frame model and the results of a simple experiment, the next step was to use the FE model to investigate the response of pile/pile-cap connections under seismic loads with a variety of conditions. Responses were studied for different deck-end support conditions (lollipop vs. pinned end constraints), different pile lengths, different pile embedments, and for different percentages of pile-interior reinforcement. To minimize variables, in all cases analyzed, a spectral acceleration of 1g was applied laterally in combination with a vertical acceleration of 1g, which was used to include stresses imposed by the dead weight of the structure. In the FE model, as shown in Figure 6.1, particular attention was given to the left exterior and interior pile/pile-cap connections. Responses from the right exterior and interior connections were similar in magnitude.

6.1 Horizontal Fixity

This section addresses the variations in stress-strain responses in the pile/pile-cap connection that result under seismic loads as end conditions on the deck are varied. The end conditions that were applied to the deck (lollipop vs. pinned ends) are considered extreme. In one case (lollipop constraints), the lateral deck motion is restrained only by the bent; in the second case (pinned-end constraints), the deck is pinned to the abutments at the center of each end. These two extreme cases are used to place bounds on the range of possible loads that can be transmitted to the pile/pile-cap connection by inertial loads resulting from seismic excitations. In both cases, the deck was assumed to be continuous between the abutments. This assumption should be reviewed for any future calculations, taking into consideration MDT's standard practices regarding deck construction and the use of expansion joints.

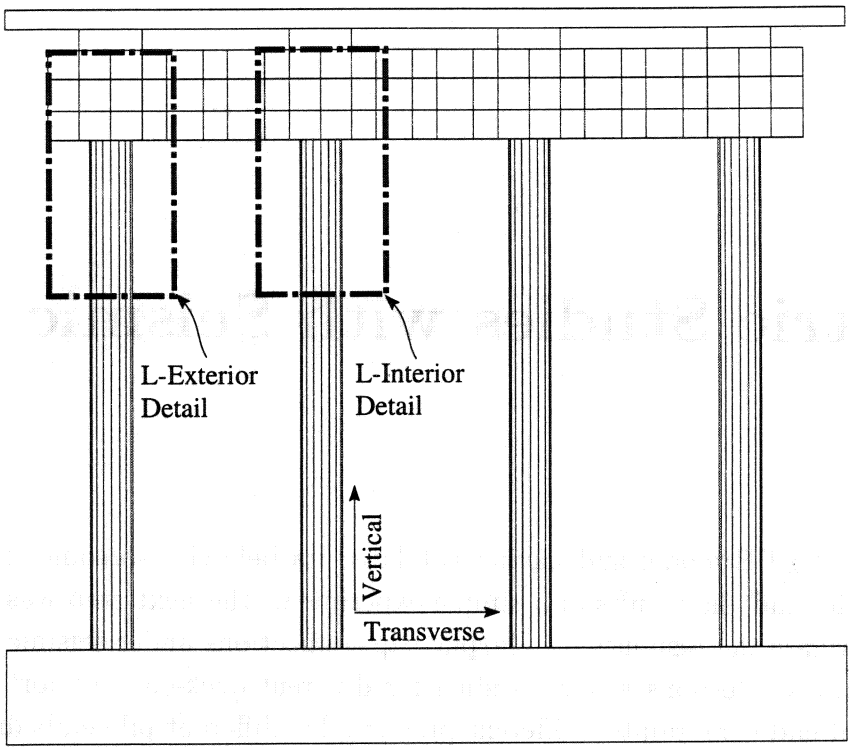

Figure 6.1: Overview of detail regions analyzed. Left (L-) exterior and interior pile/pile-cap connections are considered in this section.

6.1.1 Transverse Loading

For the transverse load case, the pile-cap acts as a fixed end for the piles. As a consequence, a moment that serves to restrict rotation ($v'(z)$) develops at the pile/pile-cap connection ($z = h$, Figure 3.2a). If the bent supports the horizontal inertial loads of the superstructure in addition to its own inertial loads (lollipop constraints), then large bending stresses develop at the pile/pile-cap connection. If the deck is pinned to the abutment, the deck and hence the abutments carry a significant portion of the inertial loads generated by the deck's mass. As a result, the loads passed to the pile/pile-cap connection are reduced dramatically.

Lollipop Constraints (L = 30 ft) With lollipop constraints, the deck is free to move in the horizontal plane and is restricted only by its connection with the bent through the soft-elastic bearings. As a result, the bent is required to carry the entire horizontal load of the deck in addition to its own inertial loads. In this case, as shown in Figures 6.2 and 6.3, the modeled stress-strain response in the pile/pile-cap connection was dominated entirely by the bending stresses that are generated as the bent resists flexural deformation in the transverse direction.

In this case, the stresses generated in the interior concrete (σ_{ct}~7300 psi > 750 psi) are likely to result first in significant tensile cracking. Then, even if the concrete were to support

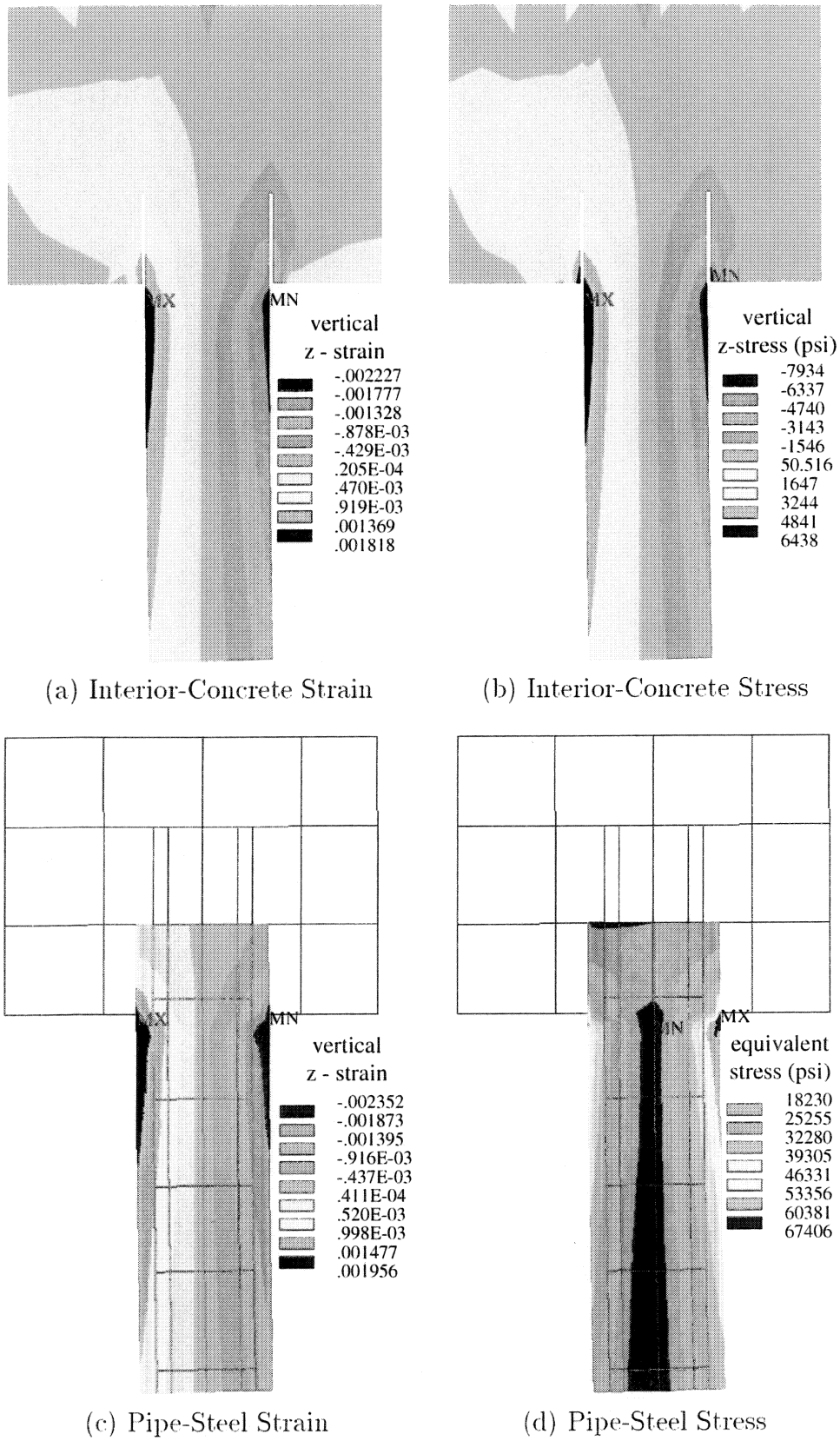

(a) Interior-Concrete Strain (b) Interior-Concrete Stress

(c) Pipe-Steel Strain (d) Pipe-Steel Stress

Figure 6.2: Stress-strain contours for the left-exterior pile/pile-cap connection under a 1g transverse acceleration. (a) and (b) are transverse cross-sections through the mid plane of the pile/pile-cap connection. (c) and (d) are interior views of the steel tube and the steel reinforcement in the corresponding half.

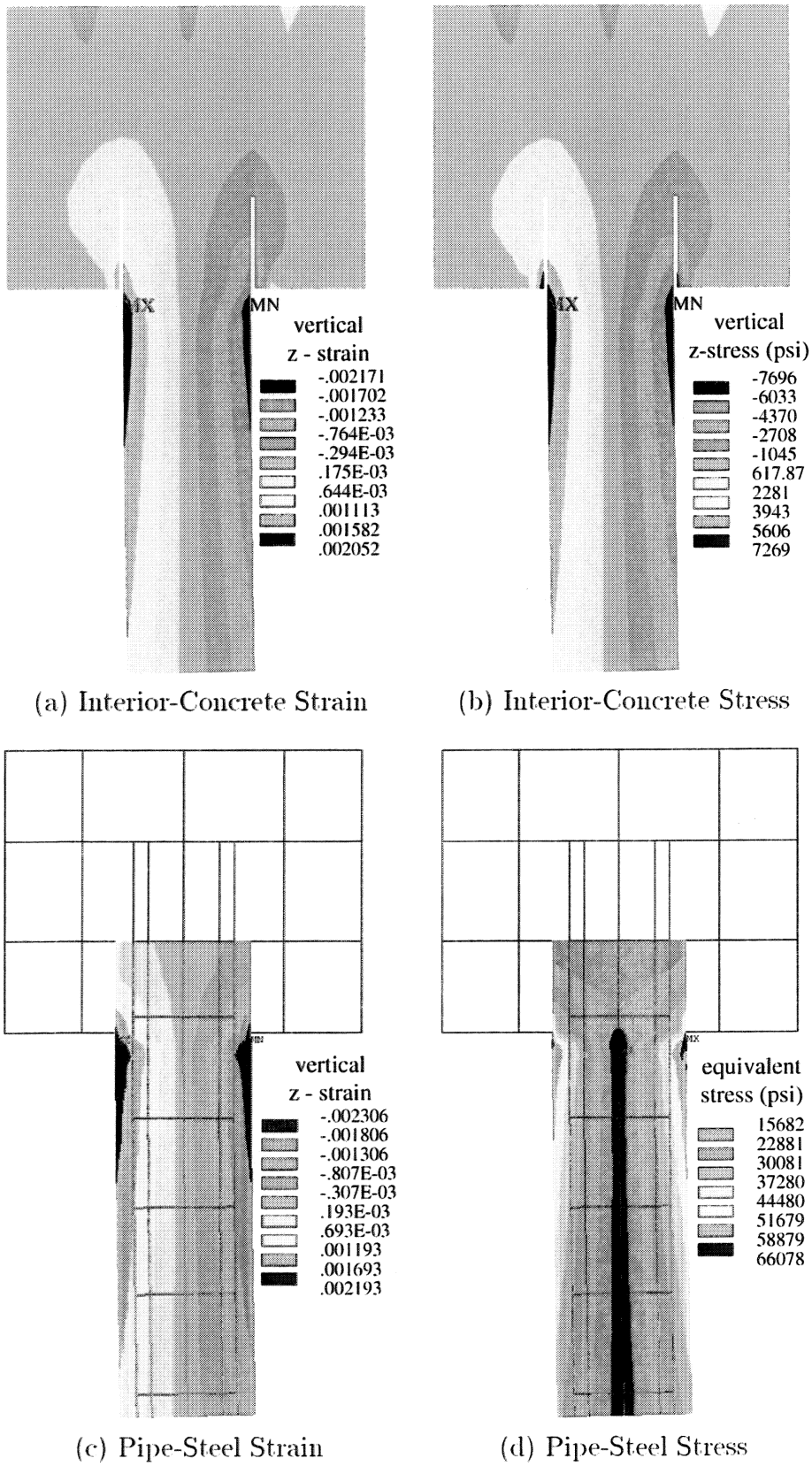

(a) Interior-Concrete Strain (b) Interior-Concrete Stress

(c) Pipe-Steel Strain (d) Pipe-Steel Stress

Figure 6.3: Stress-strain contours for the left-interior pile/pile-cap connection under a 1g transverse acceleration with a 1 ft embedment. (a) and (b) are transverse cross-sections through the mid plane of the pile/pile-cap connection. (c) and (d) are interior views of the steel tube and the steel reinforcement in the corresponding half.

Pile		
Reaction	Left-Exterior	Left-Interior
V_h^* (kips)	-82.5	-82.5
V_h (kips)	-83.0	-85.7
W_h^* (kips)	-51.6	-51.6
W_h (kips)	-251	-72.8
M_h (in kips)	-8230	-8590
V_b (kips)	86.8	86.8
W_b (kips)	55.9	55.9
M_b (in kips)	-8240	-8240

Table 6.1: Pile reactions with lollipop constraints ($L = 30$ ft, $h = 16$ ft). Reactions at the top of the pile (subscript h) are based on hand calculations (V_h^* & W_h^*) and the FE model (V_h & W_h). Reactions at the base of the pile (subscript b) are calculated, Equations (4.9-4.11), from estimated values (V_h^* & W_h^*).

a tensile load as it does in this model, the equivalent stresses (σ_{se}~67 ksi > 36 ksi) in the steel jacket indicate that a significant plastic hinge will develop adjacent to the cap. With the linear model, it is not possible to tell whether or not the connection would continue to support load; but, the model does indicate that damage would be significant.

To get a feel for how reasonable these results are, it is relatively straight forward to estimate the reactions at the top of the pile. In particular, because the four piles provide the only resistance to the lateral motion of the deck, the shear force carried by each pile (V_h^*)) can be approximated as one fourth of the inertial load generated by the deck and pile-cap (330 kips). Then based on the frame model for the deck (see also (Popov 1990, Fig. 10-11)), the bent should vertically support approximately five-eights of the weight of the deck. Adding to this the weight of the pile cap and dividing by four to determine the approximate load supported by each pile (W_h^*) results in a value of 51.6 kips. The corresponding base reactions, for an unbraced height (h) of 16 ft, are listed in Table 6.1.

In this case, the bending stress in the steel jacket, which exceeds 60 ksi near the pile-cap, dominates the axial stress due to the vertical dead load (< 2 ksi). The resulting stress response is presented in Figure 6.4b. This figure includes the response as modeled by the frame model, denoted l-beam, and the responses from the FE model for a 1g horizontal acceleration. The corresponding strain response is illustrated in Figure 6.4a. In Figure 6.4, the vertical coordinate Z is measured from the bottom of the pile cap, so that $Z = h - z$.

Notice that in Table 6.1 the vertical reactions from the FE model (W_h) vary significantly from the dead load estimate (W_h^*). This difference is due to the vertical position of the deck above the pile-cap. The transverse acceleration results in a moment that imposes a higher

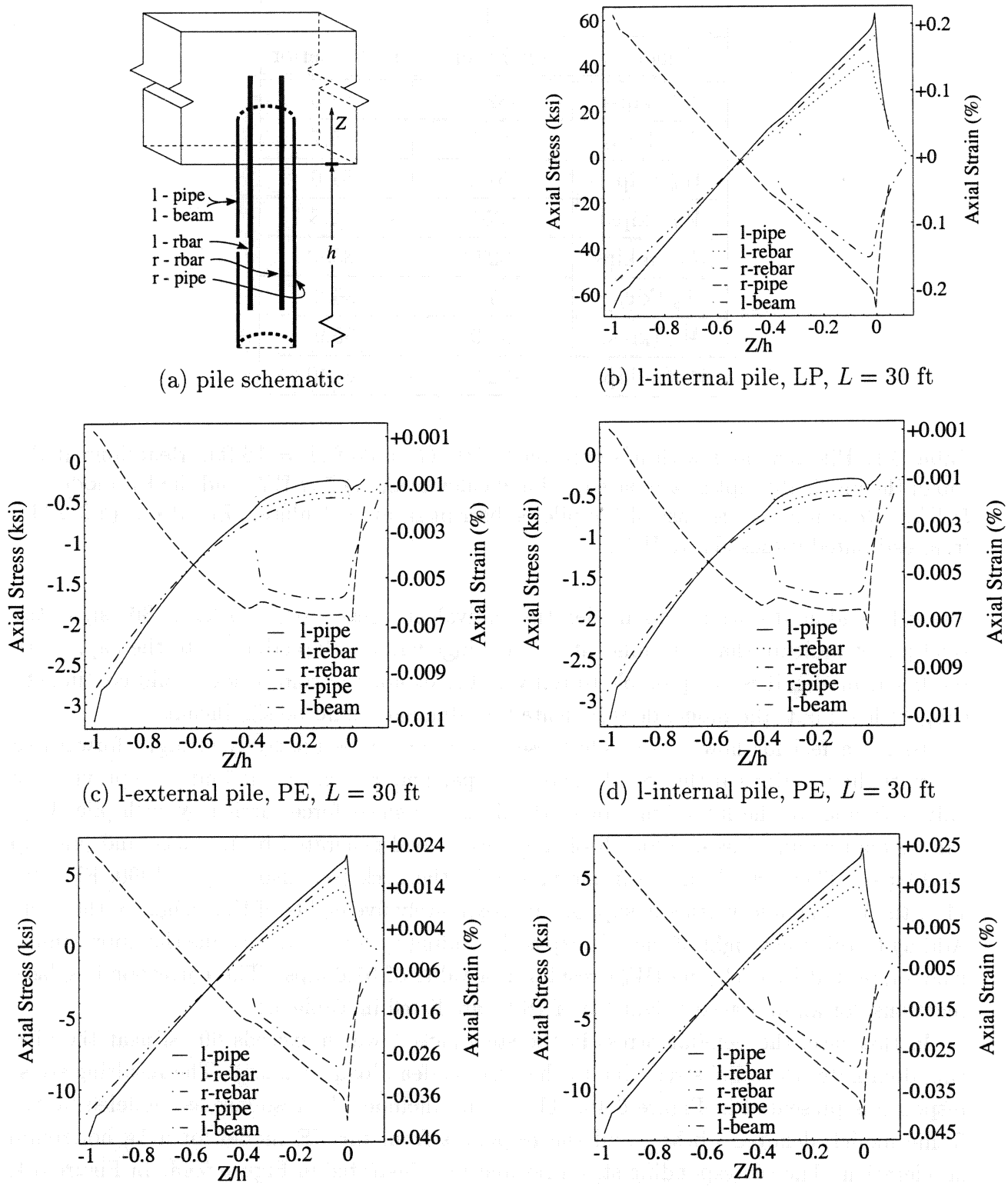

(a) pile schematic

(b) l-internal pile, LP, $L = 30$ ft

(c) l-external pile, PE, $L = 30$ ft

(d) l-internal pile, PE, $L = 30$ ft

(e) l-external pile, PE, $L = 60$ ft

(f) l-internal pile, PE, $L = 60$ ft

Figure 6.4: Stress-strain responses along pipe and re-bar in the center plane for a 1g transverse acceleration with an unbraced pile height (h) of 16 feet. l - denotes left and r - denotes right. The vertical coordinate Z is measured from the bottom of the pile cap.

compressive load on the left exterior pile than on the left interior pile (Table 6.1). The effect of the moment is so significant that the vertical reaction force at the top of the right exterior pile is tensile (~138 kips) rather than compressive. As a result, the estimate of the vertical force (W_h^*) based on dead weight alone is inaccurate. However, because with lollipop constraints the bending stresses dominate the axial (vertical) stresses imposed by the vertical load, the inaccuracy in the vertical load (W_h^*) is relatively insignificant (Figure 6.4b).

In Figure 6.4b, except for the stress concentration at the pile/pile-cap interface, the response from the beam model (l-beam) closely resembles the FE model's response. For the region near the pile-cap ($Z/h < -0.4$), where the pile contains interior steel reinforcement corresponding to the estimate of the structural rigidity ($EI_P = 33.6 \times 10^9$ lb in^2) for the frame model, the slope of the two responses is quite similar, Figure 6.4. When the interior reinforcement, denoted by l-rebar and r-rebar in Figure 6.4, comes to an end ($Z/h < -0.4$) the slope of the response from the FE model increases, due to the decrease in bending rigidity, while the frame model, which does not include the reduction in stiffness, maintains a relatively constant slope. Additionally, note that the results of the FE model (Figure 6.4) consistently include a slight perturbation, at $Z/h = 0.4$, in response to the change in internal reinforcement. Similarly, the stresses in the steel components reduce dramatically in magnitude inside the pile-cap itself, due to the massive nature of the cross section of the cap relative to that of the pile. Because the FE model is in relative agreement with the simple frame model and at the same time varies according to expectations, we can have confidence that the more detailed results from the FE model are reasonable.

In Figure 6.4b, notice that, for a 1g transverse acceleration, pipe stresses are on the order of 60 ksi near pile cap connection ($Z/h = 0$) and the FE model yields corresponding strains on the order of 0.2% (Figure 6.4b). Because the stresses peak at the pile/pile-cap connection, the steel piles are likely to yield at the interface. Assuming the steel jacket has a yield strength on the order of 36 ksi, yield induced deformation will be substantial.

Because strains (Figure 6.4b) in the concrete adjacent to the pipe (l-pipe) and steel reinforcement (l-rebar) will be of the same order as strains in the steel, this model indicates that tensile side cracking of the interior concrete will be substantial.

With lollipop constraints, the transverse mode of deformation has a harmonic period of on the order of 0.5 seconds (Figure 3.7). As a consequence, for seismic ground accelerations on the order of 0.4g's, spectral accelerations of 1g are possible (§3.5.1). However, because lollipop constraints represent an extreme case, these stress-strain responses from the FE model provide an upper bound on an actual pile/pile-cap stress-strain response.

Pinned-End Constraints ($L = 30$ ft) For pinned-end deck constraints, the response of the system is dramatically different from that of the lollipop model. The deformation of the bent is no longer dominated by the lateral inertial load of the deck. For a continuous deck with pinned ends (central shear keys), the deck carries most or all of its lateral inertial load. As an example, consider the same model discussed in the previous section ($L = 30$ ft) except with the deck pinned at the center of each end.

Pile		
Reaction	Left-Exterior	Left-Interior
V_h (kips)	0.364	0.398
W_h (kips)	-54.0	-55.8
M_h (in kips)	-118	-114
V_b (kips)	3.93	3.90
W_b (kips)	58.3	60.1
M_b (in kips)	-241	-238

Table 6.2: Pile reactions with pinned end constraints ($L = 30$ ft). Reactions at the top of the pile (subscript h) are taken from the FE model. Reactions at the base of the pile (subscript b) are calculated, Equations (4.9-4.11).

In this case, as listed in Table 6.2, the FE model indicates that the shear force (V_h) at the top of the piles is now positive and such that the deck is restraining rather than promoting pile deformation. As a result, the deformation of the pile is driven by the inertial force of its own mass rather than being dominated by the inertial force of the superstructure. As a result, bending stresses remain small and the axial load due to the dead weight of the structure is sufficient to keep the entire pile in compression at a level that is not likely to induce permanent deformation. The stresses for the steel pipe and interior reinforcement are shown in Figures 6.4c and 6.4d. The stress response from the beam model (l-beam, using values from Table 6.2) is included for the sake of comparison.

Pinned-End Constraints ($L = 60$ ft) Lollipop models have been used in the past to represent the deformation of the middle half of the supported spans of a deck with pinned end constraints. The results obtained by this approach can be compared with those obtained using the FE model developed herein. In this case, a pinned end calculation was done for a structure with two 60 foot spans. Thus, based on the commonly applied approximation, the response of the center part of the model should be similar to that obtained for the lollipop model with two spans of length (L) equal to 30 feet, discussed at the beginning of the section.

For a span length of 60 feet, as with the previously pinned-end case ($L = 30$ ft), the deformation of the bent was not driven by the inertial load of the deck. Now, however, the deck did indeed load the bent, as in the lollipop case. As listed in Table 6.3, the FE model indicates that the shear force (V_h) at top of piles is negative, such that the shear force is promoting rather than restraining pile deformation. However, the reaction force is still quite small, indicating that in this case the deck carries most, but not all of its own inertial load. Because the deck carries most of its own inertial load, bending stresses remain small and the axial load due to the dead weight of the structure is sufficient to keep the pile-to-pile cap

	Pile	
Reaction	Left-Exterior	Left-Interior
V_h (kips)	-11.0	-11.4
W_h (kips)	-122	-111
M_h (in kips)	-1228	-1279
V_b (kips)	15.3	15.7
W_b (kips)	126	115
M_b (in kips)	-1340	-1380

Table 6.3: Pile reactions with pinned end constraints ($L = 60$ ft). Reactions at the top of the pile (subscript h) are taken from the FE model. Reactions at the base of the pile (subscript b) are calculated, Equations (4.9-4.11).

joint in a state of stress that is not likely to induce permanent deformation. The stresses for the steel pipe and interior reinforcement are shown in Figures 6.4e and 6.4f. The stress response from the beam model (l-beam, using values from Table 6.3) is included for the sake of comparison.

If the case with lollipop constraints ($L = 30$ ft) is compared with this case (pinned-end constraints, $L = 60$ ft), it is clear that for the geometry modeled, the lollipop case serves as an overly conservative and hence poor representation of the mid-span of a bridge that has pinned ends.

6.1.2 Longitudinal Loading

For the longitudinal load case, the bent is oriented so that it is relatively free to bend. In this case, the primary restriction on deformation is likely to come from the interaction between the deck and the abutments. In particular, if the bridge is subjected to a 1g acceleration in the longitudinal direction, the FE model with lollipop constraints indicates that the deck and top of the bent will move 14 inches in the longitudinal direction. The restriction that the abutments place on longitudinal deformation is difficult to define, but it is not likely that the deck will be allowed to move 14 inches and yet remain seated on the abutment.

However, because the present study is focused on the pile/pile-cap connection, it is worth mentioning that even when the deck is allowed to move 14 inches, the concrete stresses in the pile/pile-cap connection reach a maximum on the order of 4000 psi. Because the deck bearings allow almost no transmission of moments to the bent while the bent is fixed at the footing, the bending moment is small near the pile/pile-cap connection and increases as the footing is approached. As a consequence, the longitudinal mode is more likely to induce permanent deformation in the pile near the footing than near the pile-cap.

6.1.3 Discussion

In essence, a continuous deck that is pinned at each end with shear keys is likely to "carry its own weight". In such a case, the loads incurred on the bent will be sufficiently small as to prevent permanent deformation. For those cases where the shear keys fail or the deck is other wise free to move in the transverse direction, inertial loads from the superstructure are likely to induce significant damage. The exact level of damage cannot be defined with any accuracy from the linear model. However, the model does indicate that inelastic deformation is likely to take place predominantly in the piles immediately adjacent to the pile cap.

6.2 Unbraced Pile Length Variations

All of the previous analyses were based on a bent model with an unbraced pile height of 16 ft. Such a restriction leads one to question what variations are likely if this unbraced pile height is varied. As discussed in a previous section (§4.6), for the bent model with lollipop constraints the natural period of vibration can be modeled as a first approximation by

$$T = \frac{1}{f} = 2\pi\sqrt{\frac{m}{k}} = 2\pi\sqrt{\frac{mH^3}{g_c a E I_B}}, \tag{6.1}$$

where H is the effective height, a varies as a function of end fixity[1], and g_c is the gravitational constant. As a result, it is reasonable to expect the period of vibration (T) to vary roughly as $H^{3/2}$ and the natural frequency (f) as $H^{-3/2}$. It should then be possible to express the effective length (H) as a function of the unbraced length (h) plus a constant (h_c) that depends on the type of connection and hence on the direction of vibration. If so, then the period of vibration (T) can be expressed as

$$T = \frac{1}{f} = 2\pi\sqrt{\frac{m(h+h_c)^3}{g_c a E I_B}}. \tag{6.2}$$

For the frame model (§4), $m = 330,000$ lb and the rigidity of the bent, $EI_B = 134.4 \times 10^9$ lb in^2. Using these values, it is possible to obtain least square estimates for the parameters a and h_c as shown in Figure 6.5d. Because the curve fits are non-linear, the least squares fit for frequency (f) was weighted different than the least square fit for the period of vibration (T). In light of these differences, curve fits were applied to both the period of vibration and to the natural frequency. The period and frequency data, from the FE model, and least square curve fits are shown in Figure 6.5.

In particular, notice that the parameter estimates (a & h_c) for the longitudinal and transverse modes are in relatively close agreement for both frequency and period data. The estimates for the torsional mode do not agree quite as closely. In general, if these results are compared with the frame model approximations, the longitudinal mode should have a

[1]Recall that, based on frame models discussed in a previous section (§4.6), for longitudinal (first mode) vibrations, $a = 3$; for transverse (first mode) vibrations, $a = 12$.

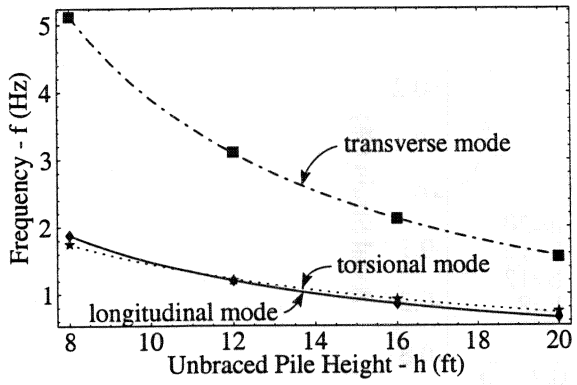

(a) Natural Frequency

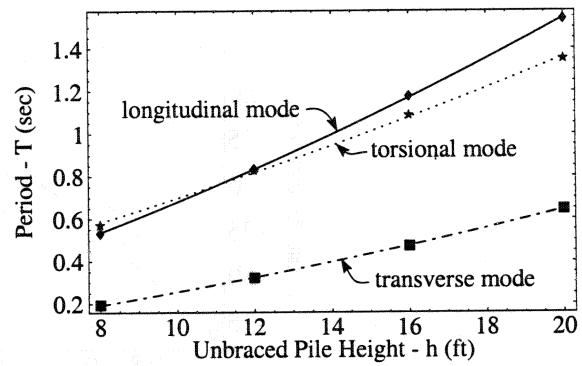

(b) Natural Vibration Period

Unbraced Pile Height	Frequency (Hz)		
	Long. Mode	Tors. Mode	Trans. Mode
8 ft	1.88	1.75	5.12
12 ft	1.20	1.21	3.11
16 ft	0.854	0.920	2.12
20 ft	0.647	0.738	1.55

(c) Frequency Data

Model		a	h_c (ft)
Longitudinal Mode	f	2.35	3.54
	T	2.43	3.71
Torsional Mode	f	4.54	7.10
	T	5.02	7.78
Transverse Mode	f	11.3	1.98
	T	10.8	1.74

(d) Curve-Fit Parameters (a & h_c)

Figure 6.5: Variations in vibrational parameters due to variations in unbraced pile height.

coefficient a with a value of approximately 3, which it does. Then because the longitudinal mode has a pinned end condition where it is allowed to rotate at the deck bearing, the expected effective height would be equal to the unbraced height (h) plus a constant (h_c) of approximately 3 ft to reach the deck bearing. Again, this is in approximate agreement with the least squares estimates in Figure 6.5d. Similarly, for the transverse mode, the constant a should be approximately equal to 12 and the expected constant addition to the unbraced height should be on the order of 2 ft or less, ~1 ft for each end of the pile. Based on these comparisons the parameters for the transverse mode appear to be quite reasonable. In essence, the frame type model appears to work quite well for the longitudinal mode and the transverse mode, and reasonably well for the torsional mode.

The influence of the unbraced pile height on the stress response is shown in Figure 6.6. These responses are for a transverse acceleration of 1g with lollipop deck constraints. Notice that the stress levels increase almost linearly with each increase in the unbraced pile height.

For the lollipop constraints, as shown previously (§6.1.1), the stress response is dominated by the bending stresses imposed by the shear force (V_h) due to inertial loads from the deck

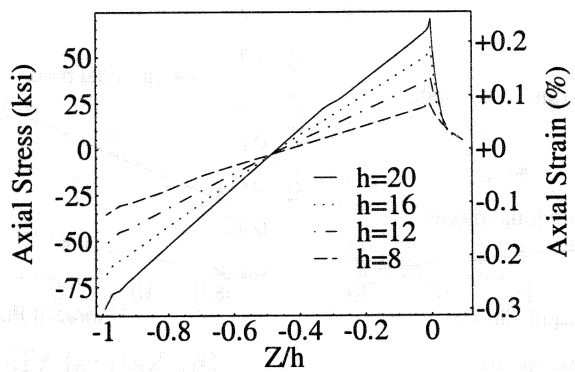

Figure 6.6: Axial stress-strain variations as a function of vertical position (z) for the left side of the pile pipe due to variations in unbraced height (h). The vertical positions are normalized relative to the unbraced height.

and pile-cap. In this case, the stress in the steel jacket (σ_s) can be approximated by

$$\sigma_s = \frac{DE_s M_h^{\cdot}}{2EI_P} = \frac{DE_s V_h}{4EI_P} h, \tag{6.3}$$

where D is the diameter of the pile jacket. If the shear force due to inertial loading (V_h) is distributed evenly over the four piles, then

$$V_h = \frac{C_s mg}{4g_c}, \tag{6.4}$$

where C_s is the spectral response coefficient (3.11).

Fortunately, as displayed in Figure 6.5b and Equation 6.2, an increase in unbraced pile height (h) also implies an increase in the period of vibration. If the period of vibration exceeds the period for the right edge of the spectral response plateau (Figure 3.9), then an increase in the period of vibration corresponds to a decrease in the spectral coefficient (C_s). If the approximation for the period of vibration (6.2) is substituted into the definition for the spectral coefficient (3.11), then the spectral coefficient to the right of the plateau (C_3) can be approximated by

$$C_3 = \frac{6AS}{5\pi^{2/3}} \left\{ \frac{ag_c EI_P}{m} \right\}^{1/3} \frac{1}{h + h_c}. \tag{6.5}$$

Substituting these relations (6.5 & 6.4) into the approximation for the bending stress (6.3) yields

$$\sigma_s = \frac{3ASDE_s g}{40g_c} \left\{ \frac{ag_c m^2}{(\pi EI_P)^2} \right\}^{1/3} \frac{h}{h + h_c}. \tag{6.6}$$

In essence, the stresses at the pile/pile cap connection increase in a linear fashion only while the period of vibration corresponds to the plateau of the spectral response. Once

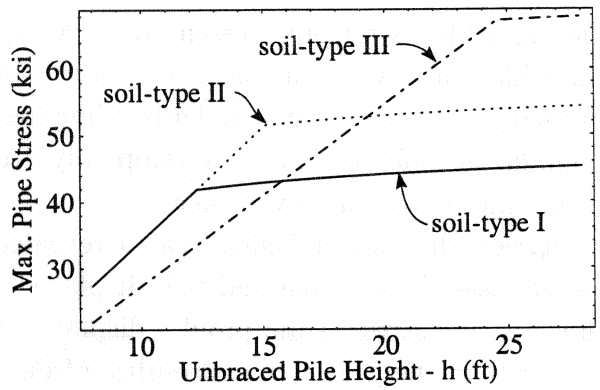

Figure 6.7: Variations in the maximum pipe stress, adjacent to the pile cap, as unbraced height (h) is varied. Stresses are based on a peak ground acceleration of 0.4g's.

the period of vibration lies outside the plateau, the increase in bending moments due to increasing height (h) is balanced in a rough sense by a decrease in the spectral response (C_s) and hence in the seismic load. For a peak ground acceleration of 0.4g's, Figure 6.7 illustrates the variation in maximum stress at the pile/pile-cap connection as the unbraced pile height is varied. These responses, which are based on the frame model with parameters from Figure 6.5, underestimate the stresses from the FE model by 10 to 15 percent, but show the general trends in the maximum stress as the unbraced pile height is varied.

In all cases, when stresses are sufficient to induce inelastic deformation, the FE model indicates that the pile is likely to deform immediately below the pile-cap. Independent of pile length, the stress levels in the steel jacket still attenuate rapidly within the pile-cap, approaching a common level that is significantly lower than the stress level in the piles.

6.3 Pipe Embedment

Other than varying those parameters that are controlled somewhat by the overall geometry of the bridge and its surroundings, it seemed reasonable to investigate those changes in the connection that would result in significant differences in behavior (while using elastic material models). In particular, a question of interest was: What is the best embedment depth for the pile shell, if any.

Results displayed in previous analyses (see Figures 6.2, 6.3, and 6.4) are based on pile embedment depths of approximately 1 foot, implying that the steel jacket extends upward into the pile-cap one foot. Analyses were completed for embedment depths of 23 inches, 11 inches, 0 inches, and -1.5 inches (implying that the pipe stopped 1.5 inches below the pile cap). Stress-strain contours for embedment depths of 0 inches and -1.5 inches are displayed in Figures 6.8 and 6.9, respectively.

The differences between the stress-strain responses for embedment depths of 11 and 23

inches were relatively insignificant. Near the bottom surface of the pile cap (Figure 6.4b), stress-strain responses for the embedded steel pipes essentially overlapped. The primary difference between the two embedded cases was that the pile with the 23 inches embedment continued well into the low stress region of the pile cap under bending loads due to transverse accelerations. As a result, a significant difference would develop only if the concrete did not remain bonded to the steel pipe—and maybe not even then.

Though the comparison between the two embedded cases revealed nothing of major significance, the two unembeded cases, Figures 6.8 and 6.9, displayed very significant differences. Notice that in both cases, the stress-strain profiles display peak concrete stresses that are two or three times higher than the peak stresses resulting from the model with pile embedment of 11 inches or more (Figures 6.2 and 6.3). The peak stress responses illustrated in Figures 6.8 and 6.9 cannot be considered accurate for a number of reasons, the primary reason being that the stress responses indicate that the pile would have suffered extensive damage, both in tension and in compression. At the same time the stresses in the steel jacket have not changed significantly, except that rather than reaching a peak stress immediately below the cap, peak stress occurs slightly below the cap and drops immediately below the cap. In essence, the FE model indicates the pile/pile-cap connections with unembeded piles are likely to fail long before those with embedded connections.

6.4 Interior-Reinforcement Patterns

Analysis presented thus far are based on the reinforcement pattern defined for the Montana bridge (Station 2+42.00, Bent No. 2) over the Beaverhead river. To evaluate variations in the stress-strain responses due to variations in reinforcements patterns, the reinforcement pattern for a Montana bridge (STA. 9 + 34.50) over Timber creek was modeled and evaluated. For the Timber creek pile bent, the pattern is similar to that used in the Beaverhead bridge bent except that the piles contain no interior reinforcement in the pile while additional steel reinforcement is included in the pile cap. For the FE model used in the present study with the Timber creek reinforcement pattern, the stress-strain responses were very similar except that the magnitude of the stress-strain responses showed approximately a 6% increase over those displayed for the Beaverhead bent model. As a consequence, pile bents with the Timber creek reinforcement pattern are likely to suffer permanent damage at slightly lower load levels than pile bents with the Beaverhead reinforcement pattern.

If the Beaverhead pattern was modeled minus internal reinforcement in the pile, the stress-strain responses increased by approximately 1%. This small change indicates that for the Timber creek pattern, which lacks internal pile reinforcement, the higher stresses in the piles were predominantly due to the increased stiffness of the pile-to-pile cap connection, due to added reinforcement in the connection area.

In the present models, though the change in magnitude resulting from modified reinforcement pattern is relatively small (~1 to 6%). This relatively minor difference is not surprising with the linear elastic material model used for concrete, because the interior pile concrete is

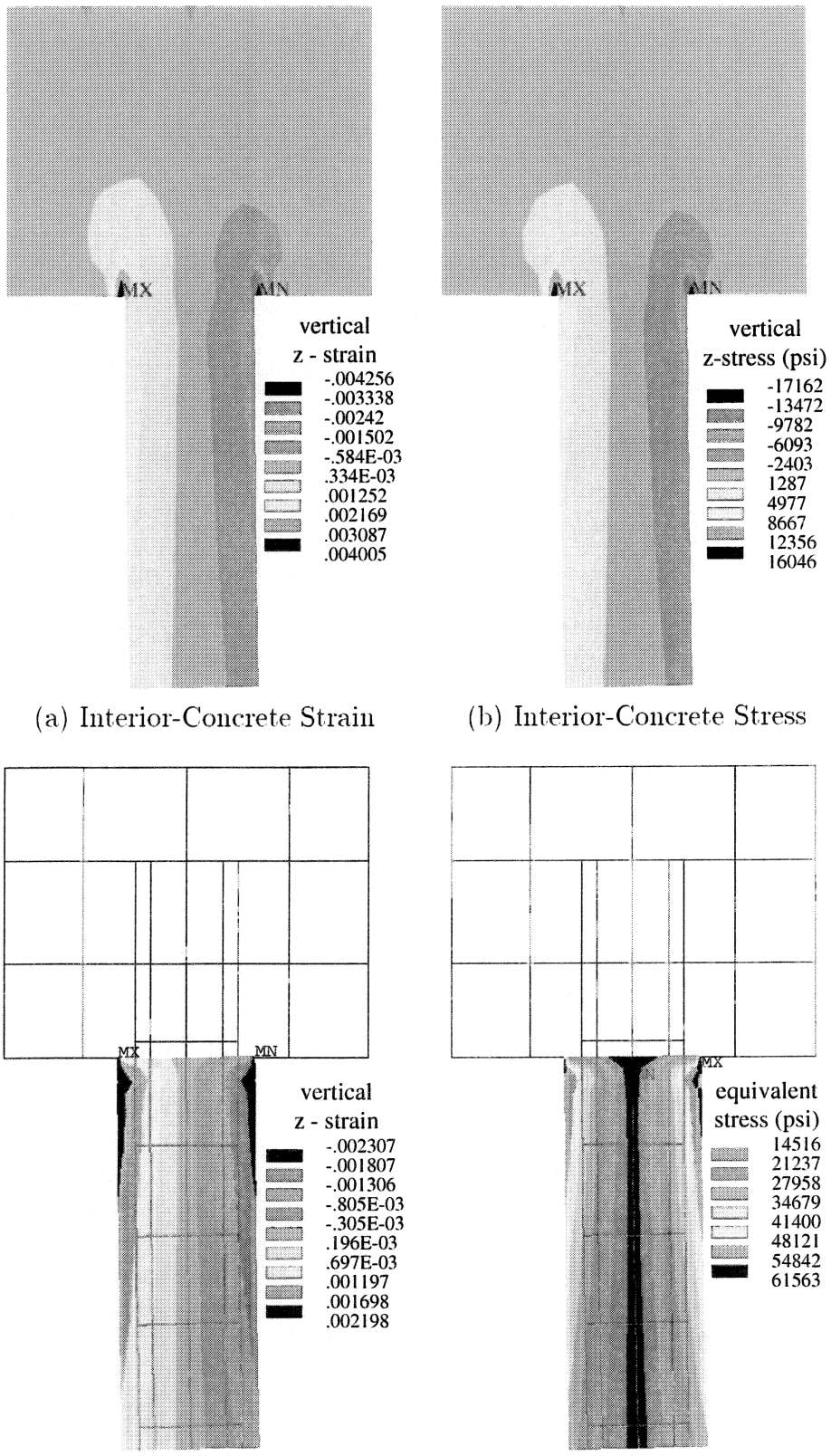

(a) Interior-Concrete Strain (b) Interior-Concrete Stress

(c) Steel-Pipe Strain (d) Steel-Pipe Stress

Figure 6.8: Stress-strain contours for the left-interior pile/pile-cap connection under a 1g transverse acceleration with a pile embedment depth of 0 inches. (a) and (b) are transverse cross-sections through the mid plane of the pile/pile-cap connection. (c) and (d) are interior views of the steel tube and the steel reinforcement in the corresponding half.

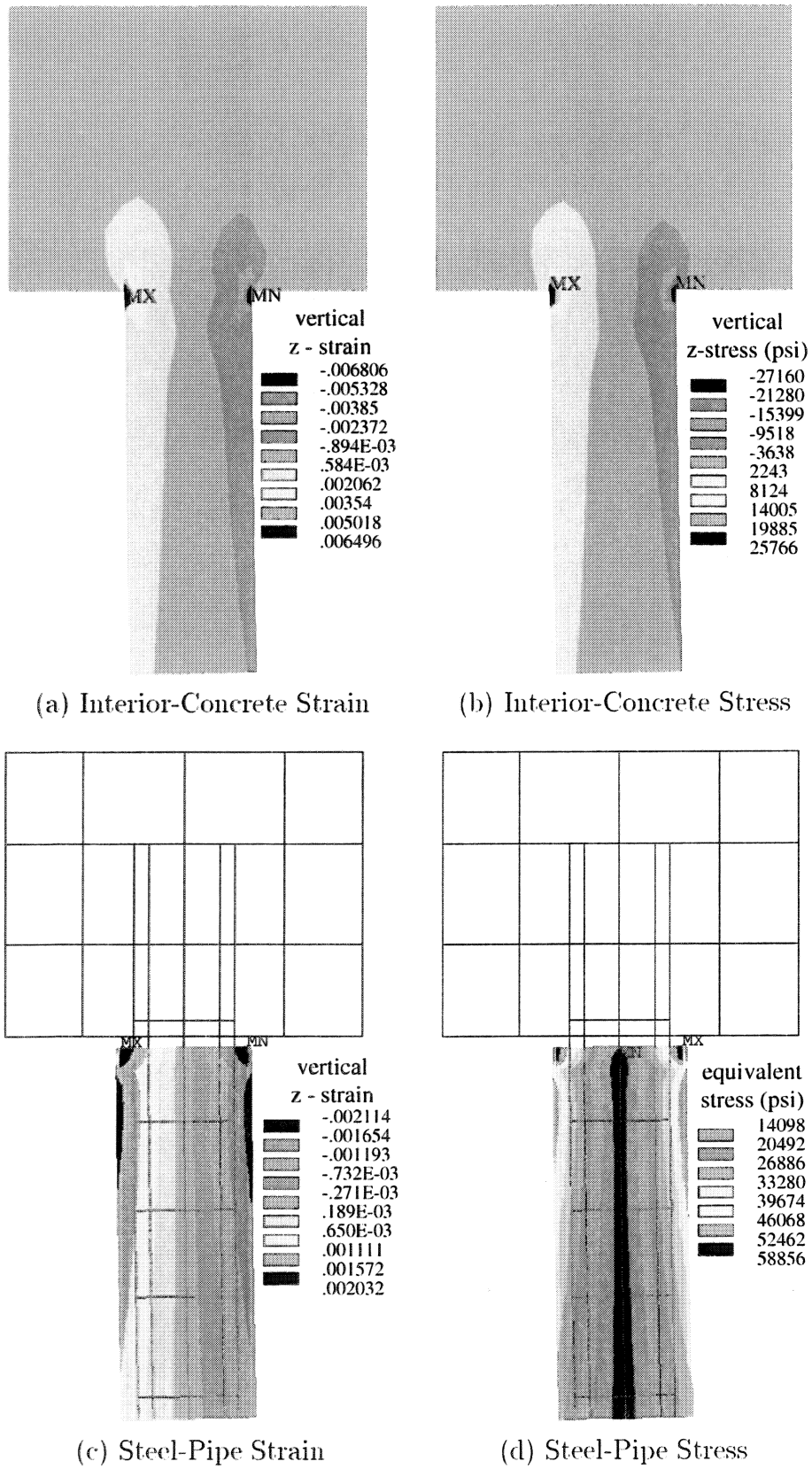

(a) Interior-Concrete Strain (b) Interior-Concrete Stress

(c) Steel-Pipe Strain (d) Steel-Pipe Stress

Figure 6.9: Stress-strain contours for the left-interior pile/pile-cap connection under a 1g transverse acceleration with a pile embedment depth of -1.5 inches. (a) and (b) are transverse cross-sections through the mid plane of the pile/pile-cap connection. (c) and (d) are interior views of the steel tube and the steel reinforcement in the corresponding half.

considered capable of supporting unbounded loads in tension as well as in compression. As a consequence, the addition or subtraction of reinforcement bars in the FE model will not show a significant difference until nonlinear material responses such as cracking and crushing are included in the model, where the steel members become the dominant load carriers of tensile stresses.

7

Responses to Ice Loads

In Montana, forces generated by ice floes can generate significant loads on bridges. To evaluate the effect that these loads might have on the pile/pile-cap connection, two cases were considered. In one case, the modeled ice pressure (200 psi) was applied to the pile cap. In a second case, the modeled ice pressure was applied to the lead pile. These load cases were chosen to simulate ice contact during high flow levels resulting from spring run-off.

7.1 Ice Load on Cap

To model the resulting ice load on the pile cap, a pyramidal-type pressure distribution was applied to the left end of the pile cap. Dropping below the top of the cap, the pressure was ramped from 0 to 200 psi over a six inch span to represent the pile-up of crushed ice at the interface. Over approximately the next 12 inches the pressure distribution was maintained at a constant 200 psi to represent the contact of a solid piece of ice that was 12 inches thick. Below that, the pressure distribution was again tapered to zero to represent the pile up of crushed ice below the contacting piece of ice. No pressure was applied to represent the flow of water. In addition to the applied pressure model for ice, a vertical acceleration of 1g was applied to include loads due to the dead weight of the structure.

In this case, because the load was distributed between the piles by the pile-cap, there was little difference between the stress profiles in the left-exterior and left-interior pile/pile-cap connections. Compressive stresses and strains in the left-exterior pile were about 10% less than those in the left-interior pile. Tensile stresses and strain were almost identical in both piles. The stress-strain contours for the left-interior pile are shown in Figure 7.1. The localized compressive stress contours at the top of the cap indicate that the ice load is bending the pile-cap slightly upward. This upward bending is being resisted by the deck, through the deck bearings.

If these responses are viewed relative to the material behavior parameters discussed previously (§3.3), then it is clear that the steel pipe with an assumed yield strength of 36 ksi is well below yield with peak equivalent stresses less than 22 ksi. For the interior concrete, tensile stresses on the order of 2.3 ksi indicate that cracking will take place on the interior of

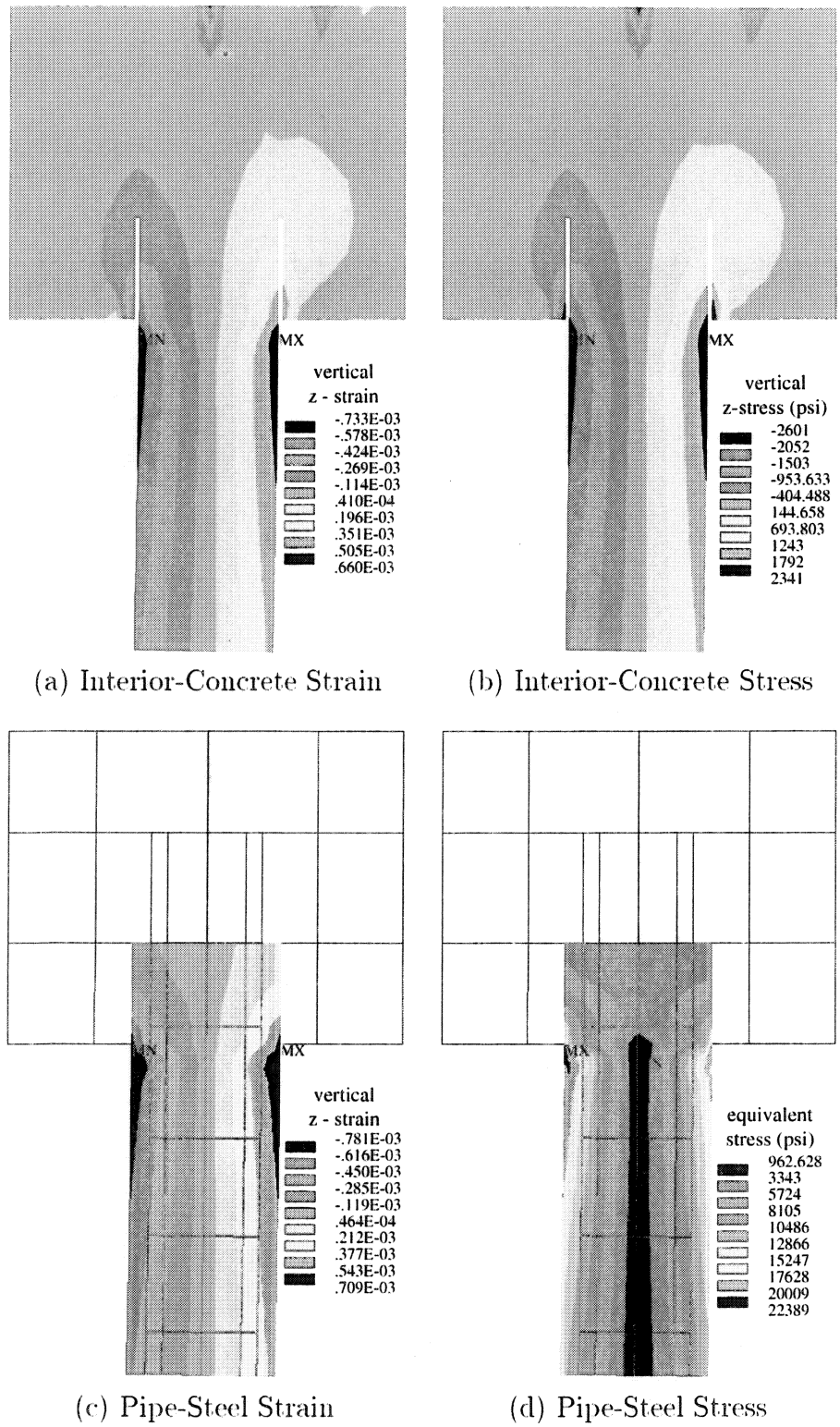

(a) Interior-Concrete Strain (b) Interior-Concrete Stress

(c) Pipe-Steel Strain (d) Pipe-Steel Stress

Figure 7.1: Stress-strain contours for the left-interior pile/pile-cap connection under a 200 psi ice load on the pile-cap. (a) and (b) are transverse cross-sections through the mid plane of the pile/pile-cap connection. (c) and (d) are interior views of the steel tube and the steel reinforcement in the corresponding half.

the pile. However, compressive stresses (~2.7 ksi) on the left side of the pile are not sufficient to induce crushing. Overall the pile/pile-cap connection, with an extreme ice load applied to the cap, is likely to suffer only minimal damage.

7.2 Ice Load on Pile

To model an extreme ice load on the lead pile, a similar pressure distribution was applied to the left exterior pile, as viewed in Figure 3.2. Immediately below the pile cap, over approximately 12 inches, a pressure distribution was maintained at a constant 200 psi over the front face of the pile to again represent the force applied by a solid 12 inch thick piece of ice. Below that, the pressure distribution was tapered over the next 12 inches to zero to represent the force applied by the pile up of crushed ice below the contacting piece of ice. Again, no pressure was applied to represent the flow of water, and, in addition to the pressure model for ice loads, a vertical acceleration of 1g was applied to represent loads due to the dead weight of the structure.

In this case, because the load was not distributed so evenly amongst the piles by the pile-cap, there was a more significant difference between the stress profiles in the left-exterior and left-interior pile/pile-cap connections. As a result, the stress-strain contours for both piles are illustrated in Figures 7.2 and 7.3.

Surprisingly, the compressive stresses and strains are more severe in the left-interior pile than in the left-exterior pile, which is bearing the applied load directly. Also surprising is the significant reduction in the overall stress-strain values relative to the first load case. Again, as with the previous load case, the localized compressive stress contours at the top of the cap indicate that the ice load is bending the pile-cap slightly upward, but that the deformations are being restrained by the deck. Overall, the stresses are low enough, particularly in the left-exterior pile, that, for these loads, very little damage would be expected.

7.3 Discussion

Of the two ice load cases considered, the case where ice loads were applied to the pile-cap proved to generate the most significant stresses. However, even when ice loads (simulated by a pressure of 200 psi) were applied to the pile cap, stress-strain responses indicated that only minimal damage would occur.

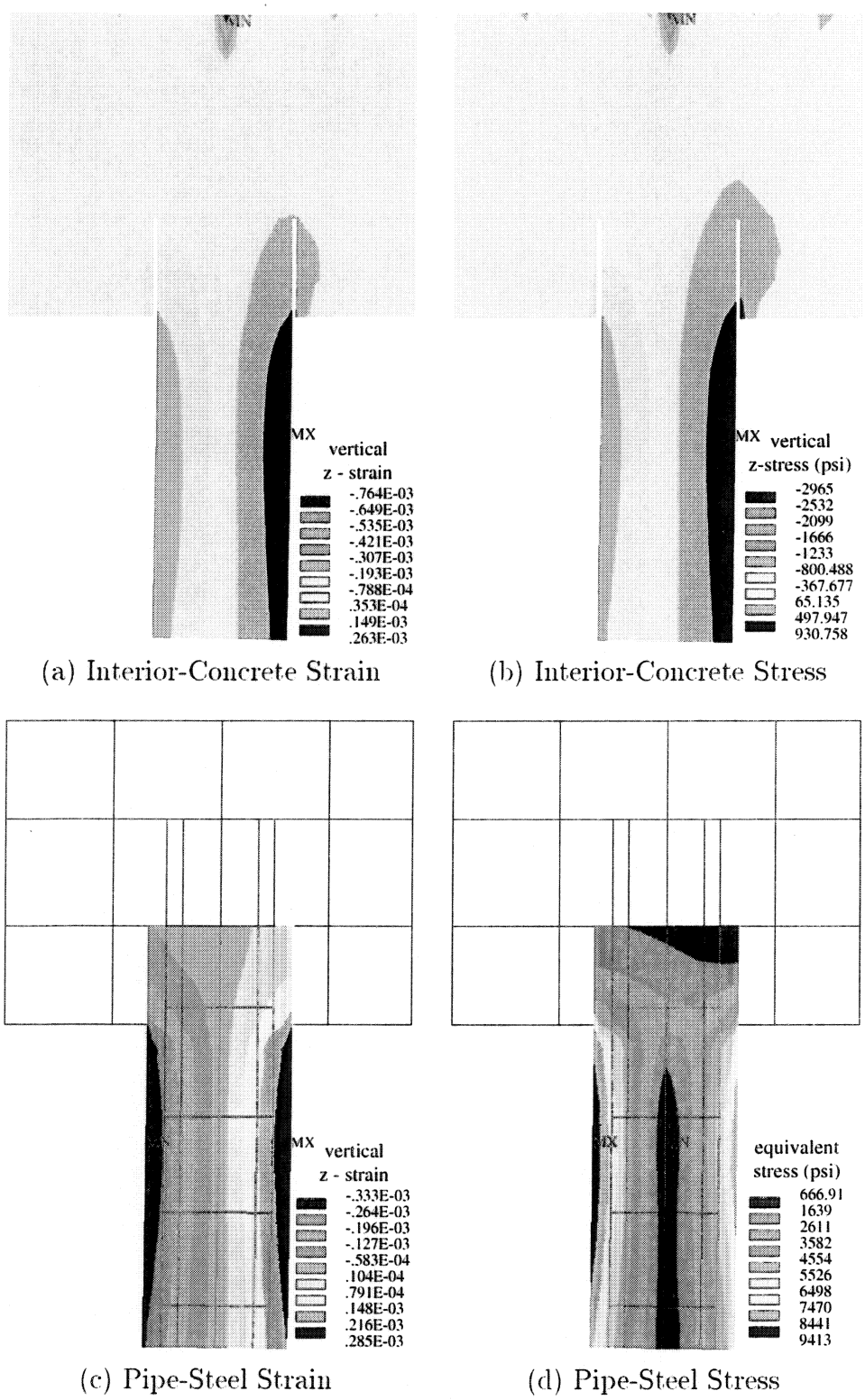

(a) Interior-Concrete Strain (b) Interior-Concrete Stress

(c) Pipe-Steel Strain (d) Pipe-Steel Stress

Figure 7.2: Stress-strain contours for the left-exterior pile/pile-cap connection under a 200 psi ice load on the left exterior pile. (a) and (b) are transverse cross-sections through the mid plane of the pile/pile-cap connection. (c) and (d) are interior views of the steel tube and the steel reinforcement in the corresponding half.

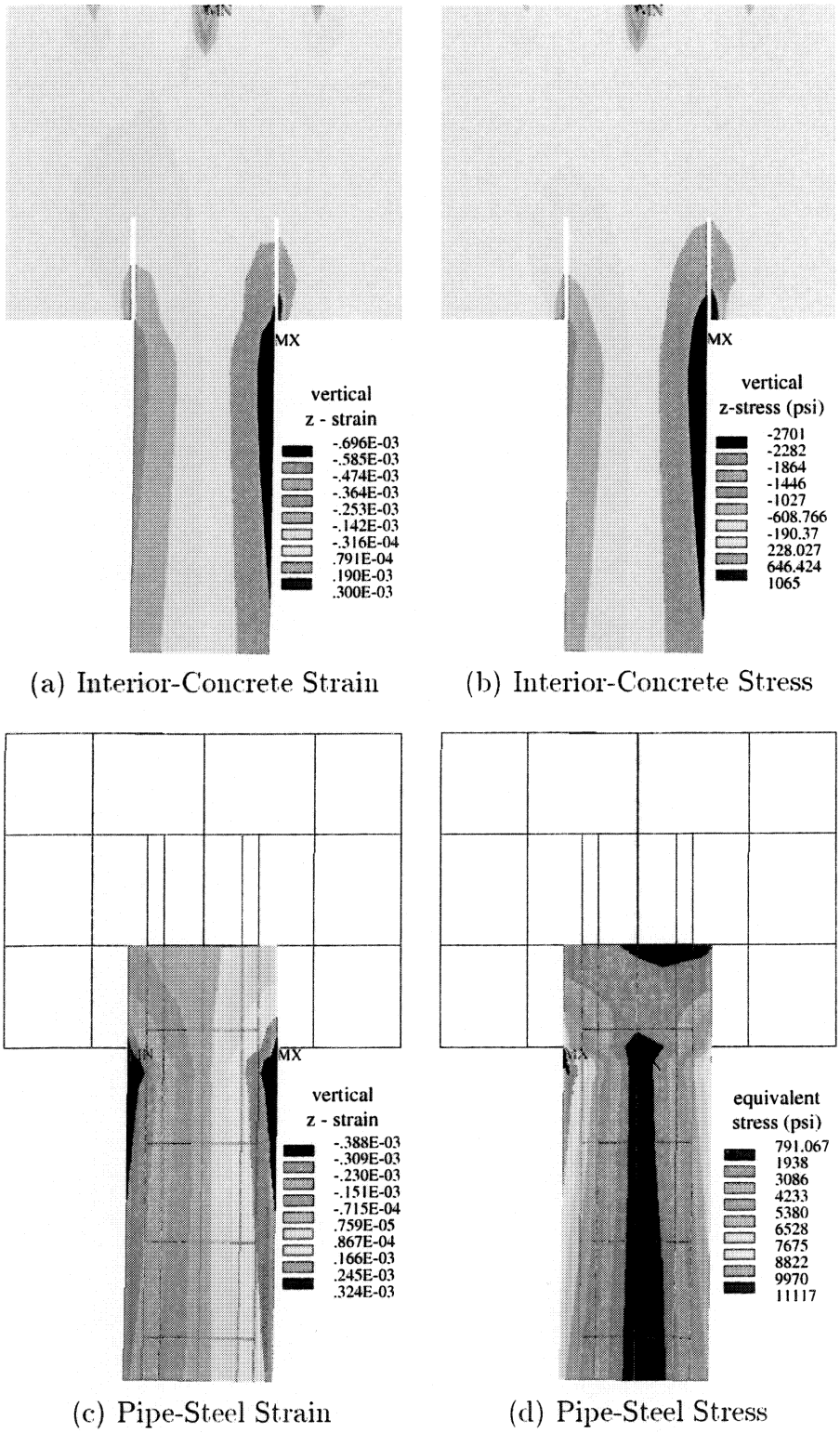

(a) Interior-Concrete Strain (b) Interior-Concrete Stress

(c) Pipe-Steel Strain (d) Pipe-Steel Stress

Figure 7.3: Stress-strain contours for the left-interior pile/pile-cap connection under a 200 psi ice load on the left exterior pile. (a) and (b) are transverse cross-sections through the mid plane of the pile/pile-cap connection. (c) and (d) are interior views of the steel tube and the steel reinforcement in the corresponding half.

8

Summary and Conclusions

Steel jacketed pile/pile-cap connections were studied based on the responses of a three-dimensional finite element (FE) model of a typical Montana bridge bent with an associated superstructure. This investigation considered the behavior of these pile/pile-cap connections under natural load conditions with a focus on their response to seismic and ice loads. Supplementary calculations, using two dimensional frame models, were used to validate and explain responses from the FE model. The model was also compared with a half-scale experimental test case. The comparison with the experimental test case indicates that the FE model is reasonable for determining stress-strain profiles for order of magnitude studies, but that non-linear aspects must be included in the model to generate more accurate outcomes.

The effect that seismic loads have on the pile/pile-cap connection is dependent on a range of factors. Modeled responses indicate that the most significant factor is the horizontal fixity of the superstructure, which effects the loads transmitted to the pile bent by the superstructure. If the superstructure is relatively free to move on the abutments and is tied to the pile bent, then transverse ground accelerations on the order of 0.4 g's are likely to induce significant damage in the piles immediately adjacent to the pile/pile-cap connection. If the superstructure is continuous and is prevented from moving in the transverse direction at the abutments, then the loads on the bent are not likely to induce significant damage. Longitudinal (in the direction of traffic) ground acceleration is more likely to induce damage in the piles near the ground, via plastic hinging, and is less likely to induce damage in the pile/pile-cap connection.

In addition to deck constraints, pile height and soil type serve as significant factors in a structure's spectral response. The interaction between these factors was studied and summarized. In general, the taller the bent, the higher the maximum stress in the pile; however, for taller bents (depending on the soil type), joint loads approach a limiting value as bending moments due to increased height tend to be balanced roughly by decreased spectral accelerations and hence decreased seismic loads.

Analyses of varied pile/pile-cap embedment depths indicate that embedment is strongly preferred, because embedment leads to a significant reduction in the peak stress in the concrete at the pile/pile-cap connection with only a small increase in the stresses imposed on the steel jacket. Embedment depths of 12 inches or more appear to be sufficient as long

as the embedment depth is sufficient for complete development of bond surfaces, between the concrete and steel.

According to the elastic model with seismic loads, the reinforcement pattern used in a Timber creek bridge (STA. 9 + 34.50) leads to stresses in the pile that are approximately 6% higher than those that occur with the reinforcement pattern used in the bridge over the Beaverhead river (Station 2+42.00, Bent No. 2). Internal steel reinforcement in the pile itself did not change stress-strain responses by more than 1%. These results were based on linear elastic models, internal reinforcement plays a more significant role in extending the ductility of the connection, i.e., if the joint region undergoes inelastic deformation.

Analyses indicate that ice loads, generating maximum pressures on the order of 200 psi, are relatively benign and are not likely to induce any significant damage in the pile/pile-cap connection. Some damage is possible if ice sheets with a thickness of 1 foot or more come in contact with the pile-cap at high water. At lower water levels, damage is likely to be minimal.

The FE models used to analyze the behavior of a typical pile/pile-cap connection were based on linear elastic material models. Trends indicated by these responses can be used with relative confidence, particularly for cases indicating minimal load levels. Evaluations of connection behavior at critical loads, that are likely to result in inelastic deformation, cannot be used with confidence. A confident understanding of these responses will require further experimental evaluations in conjunction with FE analyses that include inelastic material behavior.

9

Implementation

With respect to existing pile/pile-cap configurations, the results of this preliminary investigation indicate that under lateral load events the piles should dissipate any dynamic energy through ductile yielding, thereby preventing the cap from failing in a catastrophic fashion under dynamic loads. In particular, seismic excitations on the order of 0.4 g are likely to induce significant yielding in the piles if the deck motion relative to the ground is resisted primarily by the pile bent; if deck motion relative to the ground is resisted primarily by connections at the abutments, then the pile-to-pile cap connections are not likely to suffer any significant damage, i.e., except under the most extreme load cases.

Based on observations by other investigators, cap designs should be reviewed to insure adequate shear strength is provided to resist demands during seismic events, and consideration should be given to possible strength reductions associated with the use of transverse anchorage bars inserted through the pile jacket within the pile cap.

References Cited

AASHTO (1994), *LRFD Bridge Design Specifications*, American Association of State Highway and Transportation Officials, Washington, D.C.

AISC (1980), *Manual of Steel Construction*, 8th edn, American Institute of Steel Construction, New York.

ANSYS (1997), *Engineering Analysis System*, Swanson Analysis Systems, Inc., Houston, Pennsylvania. Revision 5.3.

Ashton, G. D. (1986), *River and Lake Ice Engineering*, Water Resources Publication, Littleton, Colorado.

Berrill, J., Priestley, M. & Chapman, H. (1980), 'Design earthquake loading and ductility demand', *Bulletin of the New Zealand National Society for Earthquake Engineering* **13**(3), 232–241.

Berrill, J., Priestley, M. & Peek, R. (1981), 'Further comments on design loads for bridges', *Bulletin of the New Zealand National Society for Earthquake Engineering* **14**(1), 3–11.

Chai, Y. (1996), 'An analysis of the seismic characteristics of steel-jacketed circular bridge columns', *Earthquake Engineering and Structural Dynamics* **25**(2), 149–.

Chai, Y., Priestley, M. & Seible, F. (1994), 'Analytical model for steel-jacketed rc circular bridge columns', *Journal of Structural Engineering* **120**(8), 2358–2376.

Chen, W. (1982), *Plasticity in Reinforced Concrete*, McGraw Hill, New York.

Christensen, F., Timco, G. & Nwogu, O. (1995), 'Compliant model tests with the Great Belt West Bridge piers in ice. Part II: Analyses of results', *Cold Regions Science and Technology* **23**(2), 165–182.

Clough, R. W. & Penzien, J. (1993), *Dynamics of Structures*, 2nd edn, McGraw-Hill, New York.

Cooper, J. D., Friedland, I. M. & Buckle, I. G. (1994), 'The northridge earthquake: Progress made, lessons learned in seismic-resistant bridge design', *Public roads* **58**(1), 26–36.

Ferguson, P. M., Breen, J. E. & Jirsa, J. O. (1988), *Reinforced Concrete Fundamentals*, 5th edn, Wiley, New York.

Gere, J. M. & Timoshenko, S. P. (1997), *Mechanics of Materials*, 4th edn, PWS, Boston.

Iding, R. H. (1986), Nonlinear finite element analysis of reinforced concrete in engineering practice, *in* C. Meyer & H. Okamura, eds, 'Finite Element Analysis of Reinforced Concrete Structures', Japan Society for the Promotion of Science and U.S. National Science Foundation, American Society of Civil Engineers, Tokyo, Japan, pp. 544–556.

Itani, A., Gaspersic, P. & Saiidi, M. S. (1997), 'Response modification factors for seismic design of circular reinforced concrete bridge columns', *ACI Structural Journal* **94**(1), 23–30.

Joen, P. H. & Park, R. (1990), 'Simulated seismic load tests on prestressed concrete piles and pile-pile cap connections', *PCI journal* **35**(6), 42–.

Jones, R. M. (1975), *Mechanics of Composite Materials*, Taylor and Francis.

Mander, J., Priestley, M. & Park, R. (1984), Seismic design of bridge piers, Research Report 84-2, University of Canterbury, New Zealand.

Mander, J., Priestley, M. & Park, R. (1988*a*), 'Theoretical stress-strain model for confined concrete', *Journal of Structural Engineering* **114**(8), 1804–1826.

Mander, J., Priestley, M. & Park, R. (1988*b*), 'Observed stress-strain behavior of confined concrete', *Journal of Structural Engineering* **114**(8), 1827–1849.

Michel, B. (1978), *Ice Mechanics*, Les Presses De L'Universite Laval, Quebec.

Mirza, S. & MacGregor, J. (1979), 'Variability of mechanical properties of reinforcing bars', *Journal of the Structural Division, ASCE* **105**(ST5), 921–937.

Mori, A., Carr, A. & Moss, P. (1996), 'Compression behaviour of bridge bearings used for seismic isolation', *Engineering Structures* **18**(5), 351–362.

NHI (1993), Seismic design of highway bridges: Participant workbook, Technical Report FHWA HI-93-040, Federal Highway Administration, National Highway Institute.

Park, R. (1987), Seismic performance of steel encased concrete piles, Technical Report 87/5, Civil Engineering Department, University of Canterbury, Christchurch, New Zealand.

Park, R. & Paulay, T. (1975), *Reinforced Concrete Structures*, Wiley, New York.

Park, R., Priestley, M. & Walpole, W. (1983), 'Seismic performance of steel encased reinforced concrete bridge piles', *Bulletin of the New Zealand National Society for Earthquake Engineering* **16**(2), 123–140.

Paz, M. (1985), *Structural Dynamics : Theory and Computation*, 2nd edn, Van Nostrand Reinhold, New York.

Paz, M., ed. (1994), *International Handbook of Earthquake Engineering : Codes, Programs, and Examples*, Chapman and Hall, New York.

Popov, E. P. (1990), *Engineering Mechanics of Solids*, Prentice-Hall, Englewood Cliffs, New Jersey.

Priestly, M. & Park, R. (1987), 'Strength and ductility of concrete bridge columns under seismic loading', *ACI Structural Journal* **84**(1), 61–67.

Sam, C. & Iyer, P. K. (1995*a*), 'Non linear finite element analysis of reinforced concrete two-pile caps', *International Journal of Structures* **15**(1), 18–34.

Sam, C. & Iyer, P. K. (1995*b*), 'Nonlinear finite element analysis of reinforced concrete four-pile caps', *Computers and Structures* **57**(4), 605–622.

Silva, P., Seible, F. & Priestley, N. (1996), Pile to pile cap connections test series - Phase 1, *in* 'Proceedings of the Fourth Caltrans Seismic Research Workshop', Caltrans, California Department of Transportation Engineering Service Center, Sacramento, California, p. ??

Sritharan, S., Priestley, M. N. & Seible, F. (1996), Seismic response of column/cap beam tee connections with cap beam prestressing, Technical Report SSRP - 96/09, University of California.

Timco, G., Nwogu, O. & Christensen, F. (1995), 'Compliant model tests with the Great Belt West Bridge piers in ice. Part I: Test methods and key results', *Cold Regions Science and Technology* **23**(2), 149–164.

Tonias, D. E. (1995), *Bridge Engineering*, McGraw-Hill, New York.

UBC (1994), *Uniform Building Code*, International Conference of Building Officials, Whittier, California.

Appendix A

Experimental Model

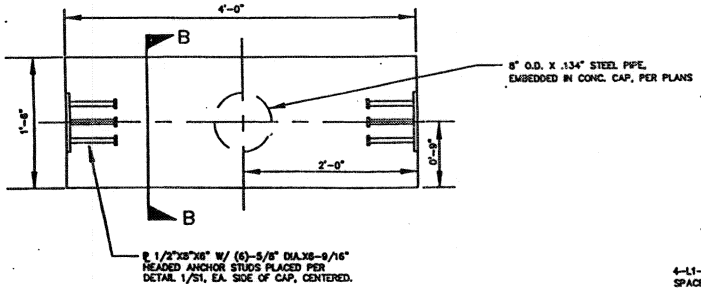

PLAN
SCALE: 1½" = 1'-0"

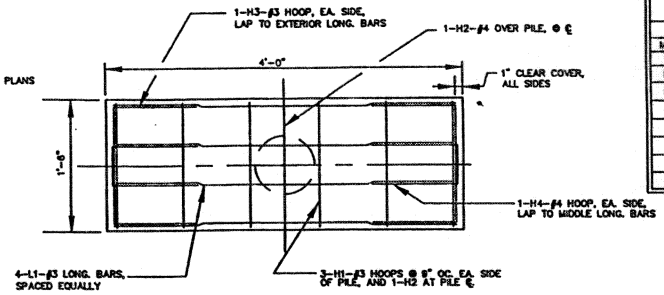

TOP STEEL MAT
SCALE: 1½" = 1'-0"

BILL OF REINFORCING STEEL

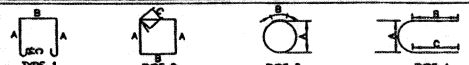

STRAIGHT BARS			
MARK	SIZE	QTY	LENGTH
L1	#3	14	3'-10"
L2	#3	2	1'-8"
L3	#3	2	3'-0"
V1	#3	25	4'-11"

BENT BARS							
MARK	SIZE	QTY	TYPE	LENGTH	A	B	C
H1	#3	6	2	75"	16"	16"	4"
H2	#3	1	1	69	16"	16"	2.5
H3	#3	8	1	40"	12"	16"	0"
H4	#3	2	1	30"	12"	5.25"	0"
H5	#3	4	1	32"	12"	8"	0"
H6	#3	2	3	42"	12"	4"	
H7	#3	8	4	24"	2.5	8"	8"

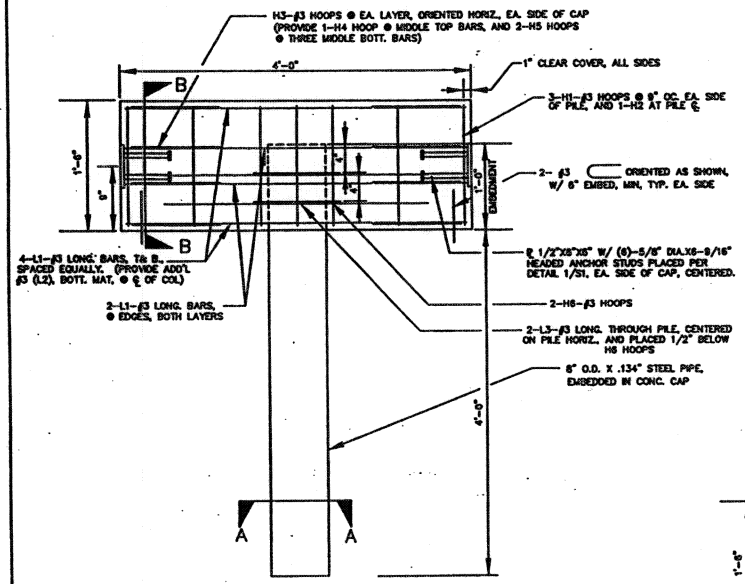

ELEVATION
SCALE: 1½" = 1'-0"

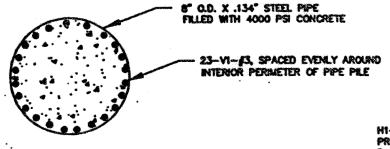

SECTION A-A
SCALE: 3" = 1'-0"

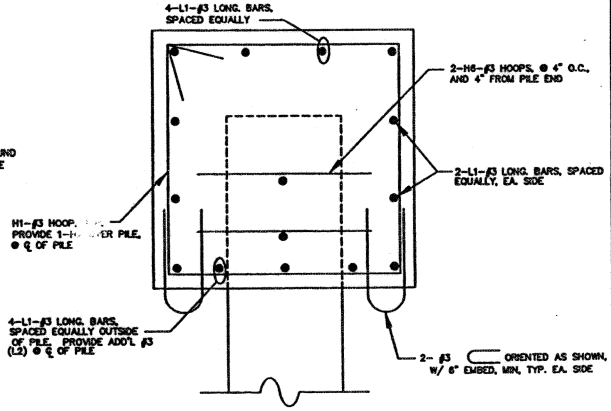

SECTION B-B
SCALE: 3" = 1'-0"

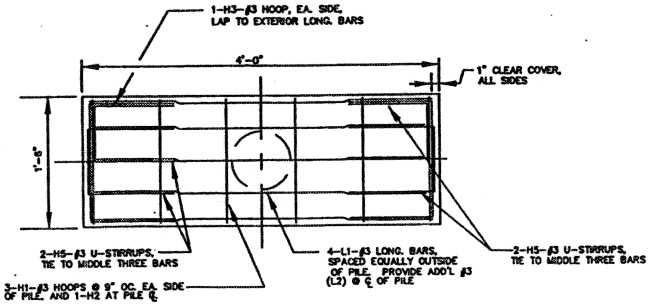

BOTTOM STEEL MAT
SCALE: 1½" = 1'-0"

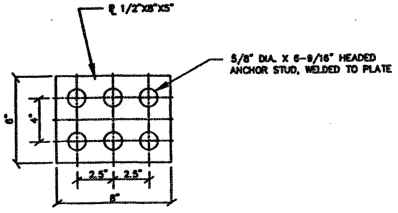

1 / S1 ANCHORAGE DETAIL
SCALE: 3" = 1'-0"

DRAWN BY: JH
CHK'D. BY: LM
APPR. BY: JS
DATE: 9/6/02
C.A. ENGINEER
BY:
DATE: 9/11/02

PILE CAP CONNECTION-- UNIT # 1
(1/2 SCALE CONTROL OF TIMBER CR. BRIDGE, BENT NO. 2)

MONTANA STATE UNIVERSITY
MONTANA DEPT. OF TRANSPORTATION

PROJECT NO.

DRAWING NUMBER
S-1